



**QUEEN'S
UNIVERSITY
BELFAST**

Advancing mycotoxin detection in food and feed: novel insights from Surface-Enhanced Raman Spectroscopy (SERS)

Logan, N., Cao, C., Freitag, S., Haughey, S. A., Krska, R., & Elliott, C. T. (2024). Advancing mycotoxin detection in food and feed: novel insights from Surface-Enhanced Raman Spectroscopy (SERS). *Advanced Materials*, Article 2309625. Advance online publication. <https://doi.org/10.1002/adma.202309625>

Published in:
Advanced Materials

Document Version:
Publisher's PDF, also known as Version of record

Queen's University Belfast - Research Portal:
[Link to publication record in Queen's University Belfast Research Portal](#)

Publisher rights
Copyright 2024 The Authors.

This is an open access article published under a Creative Commons Attribution License (<https://creativecommons.org/licenses/by/4.0/>), which permits unrestricted use, distribution and reproduction in any medium, provided the author and source are cited.

General rights
Copyright for the publications made accessible via the Queen's University Belfast Research Portal is retained by the author(s) and / or other copyright owners and it is a condition of accessing these publications that users recognise and abide by the legal requirements associated with these rights.

Take down policy
The Research Portal is Queen's institutional repository that provides access to Queen's research output. Every effort has been made to ensure that content in the Research Portal does not infringe any person's rights, or applicable UK laws. If you discover content in the Research Portal that you believe breaches copyright or violates any law, please contact openaccess@qub.ac.uk.

Open Access
This research has been made openly available by Queen's academics and its Open Research team. We would love to hear how access to this research benefits you. – Share your feedback with us: <http://go.qub.ac.uk/oa-feedback>

Advancing Mycotoxin Detection in Food and Feed: Novel Insights from Surface-Enhanced Raman Spectroscopy (SERS)

Natasha Logan,* Cuong Cao, Stephan Freitag, Simon A. Haughey, Rudolf Krska, and Christopher T. Elliott

The implementation of low-cost and rapid technologies for the on-site detection of mycotoxin-contaminated crops is a promising solution to address the growing concerns of the agri-food industry. Recently, there have been significant developments in surface-enhanced Raman spectroscopy (SERS) for the direct detection of mycotoxins in food and feed. This review provides an overview of the most recent advancements in the utilization of SERS through the successful fabrication of novel nanostructured materials. Various bottom-up and top-down approaches have demonstrated their potential in improving sensitivity, while many applications exploit the immobilization of recognition elements and molecular imprinted polymers (MIPs) to enhance specificity and reproducibility in complex matrices. Therefore, the design and fabrication of nanomaterials is of utmost importance and are presented herein. This paper uncovers that limited studies establish detection limits or conduct validation using naturally contaminated samples. One decade on, SERS is still lacking significant progress and there is a disconnect between the technology, the European regulatory limits, and the intended end-user. Ongoing challenges and potential solutions are discussed including nanofabrication, molecular binders, and data analytics. Recommendations to assay design, portability, and substrate stability are made to help improve the potential and feasibility of SERS for future on-site agri-food applications.

1. Introduction

Mycotoxins are toxic secondary metabolites mainly produced by filamentous fungi, commonly referred to as molds. Toxicogenic molds are known to produce one or more toxic secondary metabolites, however it is well known that not all molds are toxigenic and not all secondary metabolites from molds are toxic^[1] More than 300 different mycotoxins have been discovered, however, those found in food are mainly synthesized by fungi of the genera *Aspergillus*, *Fusarium*, *Penicillium*, *Claviceps*, *Alternari* or *Monascus* (only citrinin).^[2,3] Currently, aflatoxins (AFs), deoxynivalenol (DON), T-2 toxin (T-2), HT-2 toxin (HT-2), zearalenone (referred to as ZEN or ZEA), fumonisins (FMBs), ochratoxin A (OTA), ergot alkaloids (EAs), patulin (PAT), and citrinin (CIT) are considered the mycotoxins of greatest importance from a food safety and regulatory perspective.^[4] These naturally occurring compounds contaminate agricultural commodities including cereals, dried fruits, and nuts, and their level of

N. Logan, C. Cao, S. A. Haughey, R. Krska, C. T. Elliott
 National Measurement Laboratory, Centre of Excellence in Agriculture and Food Integrity
 Institute for Global Food Security
 School of Biological Sciences
 Queen's University Belfast
 19 Chlorine Gardens, Belfast BT9 5DL, UK
 E-mail: n.logan@qub.ac.uk

C. Cao
 Material and Advanced Technologies for Healthcare
 Queen's University Belfast
 18-30 Malone Road, Belfast BT9 5BN, UK

S. Freitag, R. Krska
 Department of Agrobiotechnology IFA-Tulln
 Institute of Bioanalytics and Agro-Metabolomics
 University of Natural Resources and Life Sciences
 Konrad-Lorenz-Str. 20, Tulln 3430, Vienna, Austria

S. Freitag, R. Krska
 FFoQSI GmbH – Austrian Competence Centre for Feed and Food Quality, Safety and Innovation
 Technopark 1C, Tulln 3430, Austria

C. T. Elliott
 School of Food Science and Technology
 Faculty of Science and Technology
 Thammasat University
 99 Mhu 18, Khong Luang, Pathum Thani 12120, Thailand

 The ORCID identification number(s) for the author(s) of this article can be found under <https://doi.org/10.1002/adma.202309625>

© 2024 The Authors. Advanced Materials published by Wiley-VCH GmbH. This is an open access article under the terms of the [Creative Commons Attribution](https://creativecommons.org/licenses/by/4.0/) License, which permits use, distribution and reproduction in any medium, provided the original work is properly cited.

DOI: [10.1002/adma.202309625](https://doi.org/10.1002/adma.202309625)

mycotoxin contamination is relative to both regional and climatic conditions.^[5,6] A recent global report on mycotoxin occurrence in grains and animal feed revealed that, in Northern temperate regions with humid and cool conditions for example, Europe and North America, the presence of trichothecenes (e.g., DON, T-2, and HT-2) are most common, followed by FMBs and ZEN, while the level of OTA and AFs are still relatively low.^[7] However, higher levels of AFs and FMBs are more likely to be found in tropical and subtropical regions, such as Southeast Asia and Africa.^[2]

Climate change will greatly influence global mycotoxin occurrence, whilst also encouraging the emergence of new toxins. Calculations by the University of Exeter in the United Kingdom (UK) show that pathogenic microorganisms have been migrating toward the polar ice caps at a rate of several kilometers per year since 1960.^[8] This also includes crop pests and fungi including *Aspergillus*, which form AFs. These carcinogenic mycotoxins have commonly been a health concern within southern Europe, Africa, and Southeast Asia but will become problematic for Central Europe in the near future.^[9] A recent report by EFSA in 2020, highlighted that climate change will increase the presence of AFs from low to moderate in food from Europe particularly France, Italy, and Romania and should be monitored continuously.^[10,11] These climatic events have already been witnessed in Serbia at the beginning of 2013, which became known as the Serbian maize scandal due to unprecedentedly high aflatoxin B₁ (AFB₁) concentrations, caused by extremely low precipitation combined with high temperatures.^[12] These types of events and outbreaks will become more apparent in the future as the planet continues to warm.

Exposure to mycotoxins can lead to reduced productivity, fertility issues, reduced metabolic activities, reduced feed intake, and stunted growth in animals. Whilst exposure in humans can lead to numerous health issues including liver cancer, estrogenic problems, reduced immunity, and kidney problems.^[13] According to the Food and Agriculture Organization of the United Nations (FAO), an estimated 25% of grain worldwide is contaminated with mycotoxins.^[14] However, this figure may greatly underestimate the number of mycotoxin contamination occurrences found above detectable levels. As reported by Eskola et al., the true value is more likely to be ≈60–80% due to the improved sensitivity of analytical techniques and the impact of climate change.^[4] The Rapid Alert System for Food and Feed (RASFF) also reports an annual loss of ≈1 billion metric tons of food and food products as a direct result.^[15] Since mycotoxins are omnipresent, strict contamination limits for regulated mycotoxins, adequate surveillance, and frequent checks are crucial to ensure the quality and safety of food and feed. To meet these requirements, industry, food and feed manufacturers, and researchers in the field are continuously faced with the evolution of regulations both at a European and national level.^[16]

Despite decades of research, the rapid and on-site determination of mycotoxins in food and feed crops remains a challenge. Moreover, constant monitoring of regulated and especially carcinogenic mycotoxins is more important than ever considering the effects of climate change and globalization. The main technological challenge for the in-field testing of mycotoxins is that for many years analytical techniques, including thin-layer chromatography (TLC) and high-performance TLC, high-

performance liquid chromatography (HPLC) coupled with fluorescence, ultraviolet (UV) or diode array detectors, liquid chromatography (LC), gas chromatography coupled with electron capture, flame ionization, or mass spectrometry (MS) detectors have dominated.^[17,18] More recently, liquid chromatography-tandem mass spectrometric (LC-MS/MS) methods have become the gold-standard and gained much attention for the quantification of multiple mycotoxins simultaneously within various food and feed matrices.^[19,20] Whilst these techniques are highly sensitive and accurate, they are not applicable outside of the laboratory and require highly skilled operators and expensive instrumentation.

Immunoassay-based, DNA-based, and biosensor-based techniques have also been applied to detect mycotoxins and have been reviewed previously.^[21] In the real world, immunological tests and confirmatory analysis both play a crucial role in routine testing, however, they do also come with drawbacks from an industry perspective. The reliability of some immunological tests is often questionable due to antibody cross reactivity and matrix interferences, particularly when determining low-levels of multiple analytes in complex matrices.^[22] Additionally, some level of expertise in terms of sample preparation and equipment including pipettes are required, which may not be considered as “field-deployable” depending on the end-user. On the other hand, the sophisticated instrumentation and laboratory environment required for confirmatory analysis leads to high analysis costs per sample and lengthy turnaround times due to complex procedures (i.e., sampling, extraction, clean-up, and analysis). As a result, samples are often held in storage for significant periods, which can result in distribution delays and increased risk of further contamination, due to prolonged exposure with the natural environment. Therefore, the development and incorporation of screening techniques to help eliminate these financial and safety concerns is a crucial requirement. To tackle the challenge moving forward, relying on rapid but inconsistent immunological tests or accurate but expensive and time-consuming confirmatory analysis will not be a sufficient solution for the fast-paced global food supply chain.

Spectroscopy-based techniques, particularly infrared (IR) methods, have shown their potential and applicability for the rapid, routine screening of mycotoxins in food crops.^[23] In recent years, IR techniques have been applied to various food matrices including, rice,^[24] maize,^[25] corn,^[25,26] wheat,^[27] raisins,^[28] and peanut oil.^[29] During the years 2010 to 2023, spectroscopy techniques including, near-infrared (NIR),^[24,30,31] mid-infrared (MIR),^[28,29,32–34] Raman spectroscopy,^[35] surface-enhanced Raman spectroscopy (SERS),^[36] UV-fluorescence,^[25] and hyperspectral imaging (HSI) (including shortwave-IR, visible to near infrared, and UV-fluorescence)^[26,27,37] have been reported.

Despite the increase in SERS-based approaches over the past decade, the trend analysis graph would suggest that MIR spectroscopy still heavily dominates the research area (**Figure 1**). A further search into the literature highlighted that, of those publications that mentioned MIR, 31% of these also mentioned portability, compared to only 13% of published SERS papers. However, this is difficult to accurately measure as some of the earlier dated publications may have considered compact instruments or those which could be moved out of the laboratory as portable. Nonetheless many of these instruments still required bulky parts, numerous components, hardware, controlled environments or had to be dismantled and reassembled at the point of need. Due to

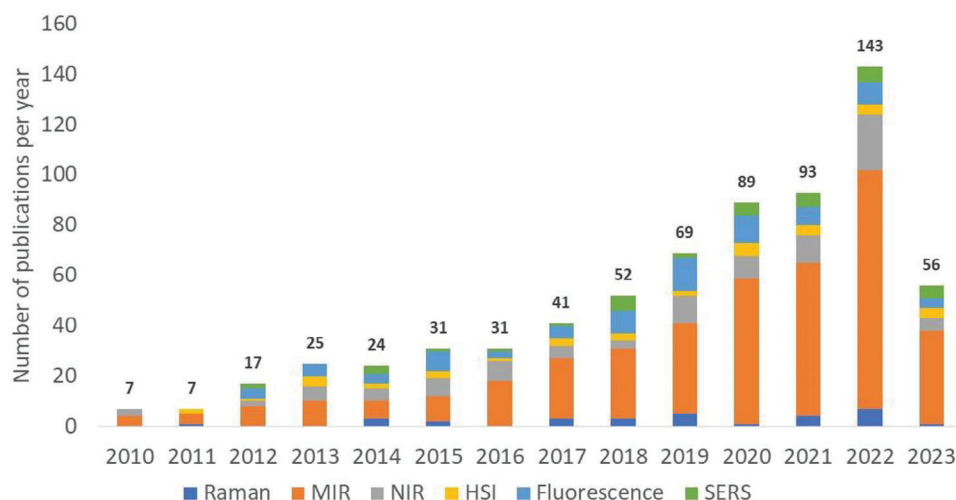


Figure 1. Trend analysis obtained using keyword search in Scopus database between the years 2010 to 2023 (as of April 2023). Number of publications published per year for mycotoxin determination using different infrared (IR), scattering, and imaging spectroscopy techniques. (N.B.: trend values are prior to full text screening and are based on the number of mentions only. SERS papers were full text screened for eligibility and readers are referred to the publication by Freitag et al.,^[23] for a comprehensive review of IR and imaging techniques for mycotoxin determination).

extensive technological advances to hardware, software design, and miniaturization of spectroscopic devices, it is therefore difficult to class these earlier technologies as “portable” in the same way as handheld spectrometers today.^[38] As a result of these advancements, various areas of the food industry (i.e., food and feed manufacturers, stakeholders, government bodies, etc.) are keen to adopt field-deployable spectroscopy techniques for food and feed screening.

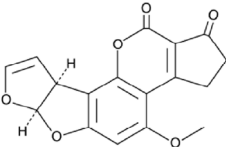
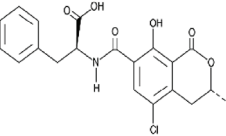
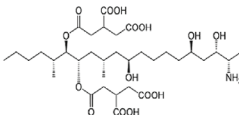
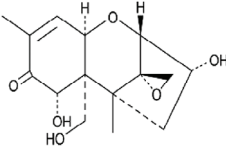
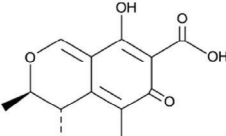
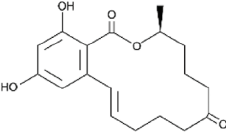
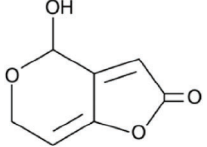
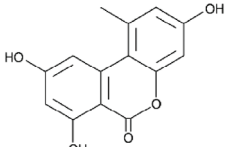
Currently, IR techniques (e.g., NIR or MIR) and conventional Raman are employed within many industrial sectors including the pharmaceutical and agri-food sector to monitor authenticity and quality. The use of IR techniques and conventional Raman spectroscopy for food safety applications is still quite challenging due to poor sensitivity, which often cannot meet strict regulatory limits, although alterations in the percentage regime are addressable. However, Raman spectroscopy as a technique may be advantageous over IR for the analysis of biological samples for several reasons. First, molecules analyzed using Raman do not need to possess a permanent dipole moment change, as with IR spectroscopy where they need to be polarizable. Second, a major problem with IR is the interference caused from the vibrational effects of water molecules. Due to its intense absorption, water often interferes during IR spectroscopy and despite the increasing popularity of ATR for aqueous applications, water can be used as a solvent in Raman spectroscopy as it possesses very weak Raman scattering. Third, as a result the sample preparation for IR can be lengthier as samples need to be dried to remove the water content. However, compared to IR, Raman alone is not very sensitive thus, techniques such as SERS and surface-enhanced resonance Raman spectroscopy (SERRS) have been developed to overcome this problem.^[39]

SERS is a surface-sensitive technique designed to improve Raman scattering through the electromagnetic and chemical enhancements provided by noble metallic substrates or particles. The technique is widely used for molecular identifica-

tion and structural characterization and has gained popularity in recent years for mycotoxin determination.^[40] SERS also has great potential to provide sensitive, quantifiable results through the direct determination of mycotoxins. This is another advantage of SERS over other vibrational spectroscopic techniques including IR, which is an indirect measurement and monitors the composition of food/feed and the changes that occur to components such as, proteins, carbohydrates, lipids, or moisture in the presence of fungal growth or toxins.^[41] Additionally, for SERS, sample extraction is often performed therefore, localized hot spot contamination can be more readily removed and detected in the extract. The Raman scattering properties of mycotoxins including their Raman cross-sections, excitation wavelength, and chemical structures have been exploited previously to determine their unique “fingerprint” spectra, molecular bonds, and Raman scattering bands (Table 1). Additionally, the possibility of conducting the technique outside of the laboratory is made more likely through the increased availability of commercial SERS substrates and handheld Raman spectrometers. The technique itself may also be particularly useful when combined with IR screening, as a final quantitative step. However, the current situation would imply that the technique itself is not ready for implementation and that it is unlikely to be considered by industry as a potential on-site test.

Conventional Raman spectroscopy was first employed by Harvey et al., in 2002 who evaluated two portable Raman instruments alongside a Hazardous Material Response Unit (HMRU) spectral library database to determine the presence of mycotoxins in-field.^[58] A total of 58 unknown matrices were analyzed using two different devices, by two users and searched against the custom hazardous materials reference library (HMRU spectral library database). Results of the study confirmed that 97% of the samples were correctly identified including the samples containing mycotoxins, T-2 toxin, and AFB₁, with no occurrences of false positives. However, using this technique no quantitative results were

Table 1. Chemical formula, molecular structure, excitation wavelength (λ), and characteristic “fingerprint” used to identify mycotoxins using SERS.

| Mycotoxin | Chemical formula | Molecular structure | $\lambda_{\text{Excitation}}/\lambda_{\text{Emission}}$ | Raman fingerprint [cm^{-1}] | Refs. |
|---|---|---|---|---|------------|
| Aflatoxin B ₁ , B ₂ Aflatoxin G ₁ , G ₂ Aflatoxin M ₁ , M ₂ | C ₁₇ H ₁₂ O ₆ , C ₁₇ H ₁₄ O ₆ C ₁₇ H ₁₂ O ₇ , C ₁₇ H ₁₄ O ₇ C ₁₇ H ₁₂ O ₇ , C ₁₇ H ₁₄ O ₇ |  | 365/425 nm | 813–818 930–934 1135–1158 1273–76 1355–1358 1438–1440 1550, 1592 1693–1698 | [42,43] |
| Ochratoxin A Ochratoxin B | C ₂₀ H ₁₈ ClNO ₆ C ₂₀ H ₁₉ NO ₆ |  | 330/460 nm | 1000 1028 1316 1503 1657 1670 | [44–46] |
| Fumonisin B ₁ Fumonisin B ₂ Fumonisin B ₃ | C ₃₄ H ₅₉ NO ₁₅ C ₃₄ H ₅₉ NO ₁₄ C ₃₄ H ₅₉ NO ₁₄ |  | 335/440 nm | 480 700 701 1128 1264 1388 1452 | [47,48] |
| Deoxynivalenol | C ₁₅ H ₂₀ O ₆ |  | 360/470 nm | 663 881 1002 1364 1553 1596 | [49,50] |
| Citrinin | C ₁₃ H ₁₄ O ₅ |  | 320/505 nm | 1382 1568 1616 | [46,51] |
| Zearalenone | C ₁₈ H ₂₂ O ₅ |  | 275/460 nm | 762 880 1448 1517 | [49,52,53] |
| Patulin | C ₇ H ₆ O ₄ |  | 275 nm | 1025 1205 1609 | [54,55] |
| Alternariol | C ₁₄ H ₁₀ O ₅ |  | 345/420 nm | 1173 1252 1298 1367 1615 | [56,57] |

obtained, only information regarding the absence or presence (Y/N) of the toxin could be confirmed. Whilst we now understand that Raman scattering may not be able to produce the sensitivity required to meet the regulatory limits for mycotoxin determination, this blind field test highlighted the importance of perform-

ing realistic studies using unknown samples to define the reliability of the portable, in-field technique. Ultimately, in the early 2000s the principle of Raman scattering was being exploited to determine mycotoxins alongside portable spectrometers and online spectral databases; technologies which are still in demand by

industry today. SERS was first applied one decade later in 2012, by Wu et al., to overcome the poor sensitivity of conventional Raman spectroscopy. In this work, the fingerprint spectra of pure AFB₁, AFB₂, AFG₁, and AFG₂ standards prepared in methanol (MeOH) were identified using silver nanorod (AgNR) array substrates.^[42] The detection limits for the technique were between 2 and 33 mg kg⁻¹. Therefore, the sensitivity of this early SERS technique could not meet the maximum regulated levels for AFs in food or feed. Within the European Union (EU), maximum limits are set at 2 µg kg⁻¹ for AFB₁ or 4 µg kg⁻¹ for total AFs (sum of B₁, B₂, G₁, G₂, M₁) in cereals and cereal-based products intended for human consumption,^[59] or between 5 and 20 µg kg⁻¹ for AFB₁ in all feed materials depending on animal size and whether the animal is bred for dairy or meat production.^[60] However, as the methodology was only tested using pure mycotoxin standards and the interferences from a food or feed matrix were not tested, this methodology could only be considered as a proof-of-concept or preliminary study and could not be implemented or commercialized without further developments.

Considering these important breakthroughs, many researchers have since strived to improve SERS-based methods for mycotoxin determination in terms of detection limits, portability, feasibility to food and feed matrices, and the level of validation performed. Whilst numerous publications exist, it is important to provide an update on the most recent technologies, but also to critically discuss the improvements made to the practicality of the technique over the last decade. Ultimately, SERS is not developing as rapidly as other portable spectroscopy techniques. This review aims to provide insights as to why after two decades of technological advancements to hardware and one decade of scientific research, the area is still slow to progress. This will be crucial information to help understand the current situation and allow for recommendations to be made to improve the potential of SERS as a field-deployable screening technique in the future.

First, the review will discuss the design and fabrication of nanomaterials with different morphologies (Section 2) using bottom-up (Section 3), self-assembly of bottom-up synthesized nanomaterials on solid surfaces (Section 4), and top-down approaches (Section 5). Second, the incorporation of recognition elements, e.g., aptamers, antibodies, molecular imprinted polymers (MIPs), etc., for the detection of mycotoxins will be presented (Section 6). Third, the use of chemometrics and machine learning will be evaluated and their role in single and multiplex applications within real samples will be assessed (Section 7). Fourth, the validation of SERS approaches will be evaluated in terms of sensitivity, reproducibility, selectivity, and feasibility for the determination of mycotoxins in food and feed samples will be assessed (Section 8). The issues and challenges around stability, portability, time to analysis, and sample preparation will also be highlighted in this section. These final sections of the review will focus on the feasibility of SERS from a scientific and industry perspective. This section will contribute most to understanding why the technique may not be the most popular spectroscopic measurement for routine analysis. Finally, the conclusion will summarize the main findings and provide opinions for future developments, to improve the potential of SERS for the quantitative screening of mycotoxins within the agri-food industry (Section 9).

2. Nanofabrication for the Detection of Mycotoxins

The fabrication and design of nanomaterials plays a crucial role in the sensitivity, selectivity, and reproducibility of SERS-based applications. Various colloidal metal particles or metallic nanostructures have been fabricated using a range of bottom-up and top-down approaches (Figure 2). Many of these structures are advantageous as SERS substrates due to their plasmonic and light scattering properties. The principle of SERS as a sensing technique relies on the inelastic scattering of molecules, which is greatly enhanced (by magnitudes of 10⁸ or even larger, enabling single-molecule detection in some cases) when the molecules of interest are adsorbed onto corrugated metal surfaces or nanoparticles.^[61] When the resulting incident wavelength of light is coupled to the localized surface plasmonic resonance (LSPR) of plasmonic particles the electromagnetic field is enhanced thus, resulting in the formation of hot spots.^[62] Silver (Ag) and gold (Au) nanostructures are the most commonly used materials in SERS applications due to their LSPRs, which cover most of the visible and near-infrared wavelength range (where most Raman measurements occur).^[63]

Consequently, spherical particles made of Au^[70,71] (illustrated in the TEM image in Figure 3a) or Ag^[51,72,73] have been exploited for the detection of AFs, OTA, and CIT mycotoxins. However, as the electromagnetic enhancement mechanism is strongly distance-dependent changing the morphology of the nanomaterials can result in a much stronger enhancement and lower detection limits. For example, the sharp tips and corners of anisotropic plasmonic nanoparticles (e.g., Au nanostars) can produce remarkable SERS enhancements as they acquire more than one LSPR peak. When excited with a laser with corresponding wavelength, the SERS intensity can be enhanced by 5 orders of magnitude in respect to Raman scattering alone^[74] and 2–3 orders of magnitude higher than that of spherical nanoparticles. Therefore, numerous shapes, sizes, and compositions of particles have also been employed for the detection of mycotoxins PAT, DON, OTA, FB₁, and AFB₁ including nanocubes^[75] (illustrated in the TEM image in Figure 3b), nanobipyramids^[76] (illustrated in the TEM image in Figure 3c), nanoprisms^[77] (illustrated in the TEM image in Figure 3d), nanostars^[78] (illustrated in the TEM image in Figure 3e), and nanorods^[79,80] (illustrated in the TEM image in Figure 3f).

Functionalized nanoparticles, core-shell nanoparticles, and magnetic nanoparticles modified with recognition elements including antibodies, aptamers, and MIPs have been exploited for mycotoxin detection. These approaches can have a positive effect on selectivity and sensitivity due to chemical enhancement, which is achieved by chemically attaching specific analytes to the surface of nanosubstrates, thus changing the Raman cross-section.^[84] Core-shell nanomaterials composed of Au and Ag can also improve the reproducibility of SERS signals as the generation of hot spots relies on target analytes adsorbing within nanogaps or forming nanobridges. Ma et al. reported a plasmonic nanogap gold@silver nanodumbbell (Au@AgND) structure to enhance the SERS effect and construct an aptasensor for the sensitive detection of OTA (Figure 4a).^[81] Additionally, core-shell Ag nanocubes functionalized with polydopamine (Ag NCs@PDA) were fabricated by Tegegne et al. for the quantitative detection of DON in pig feed (Figure 4b).^[75] The shell improved the

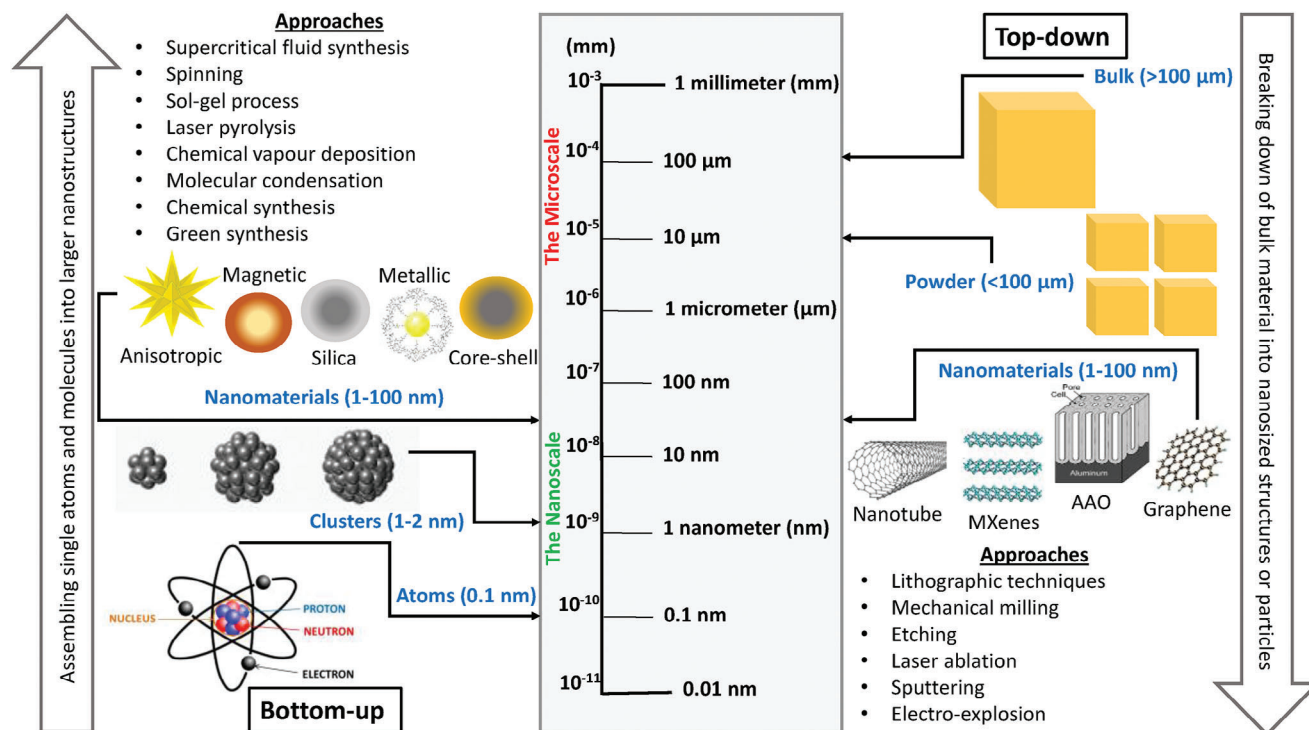


Figure 2. Synthesis of nanomaterials using bottom-up and top-down fabrication approaches.

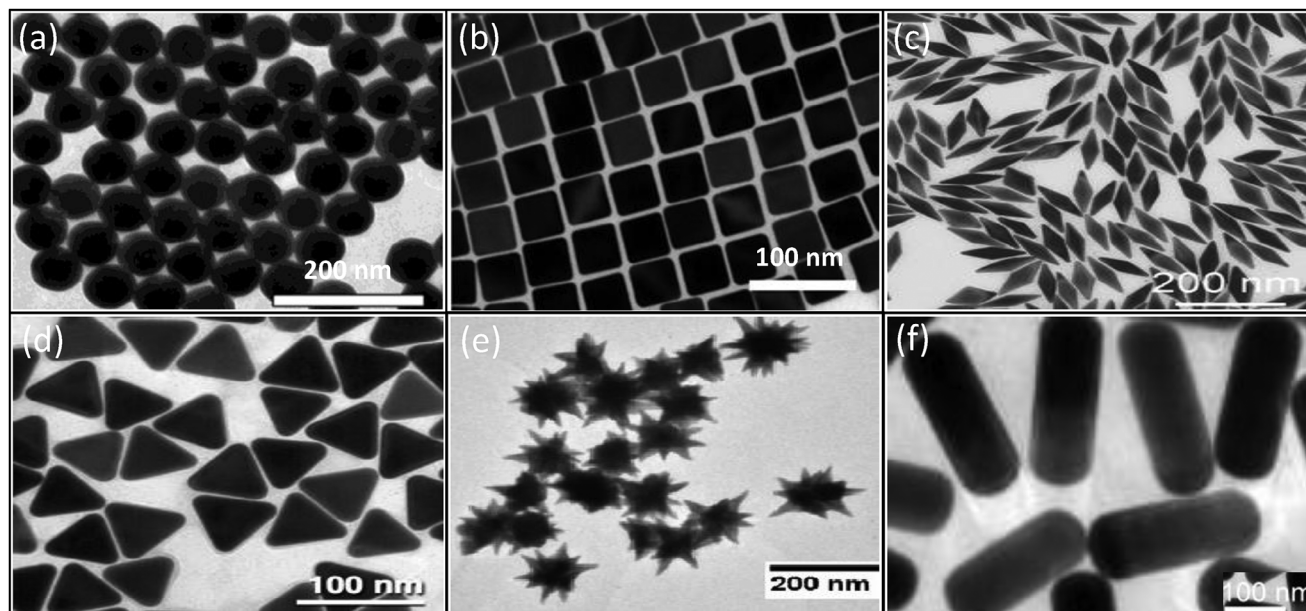
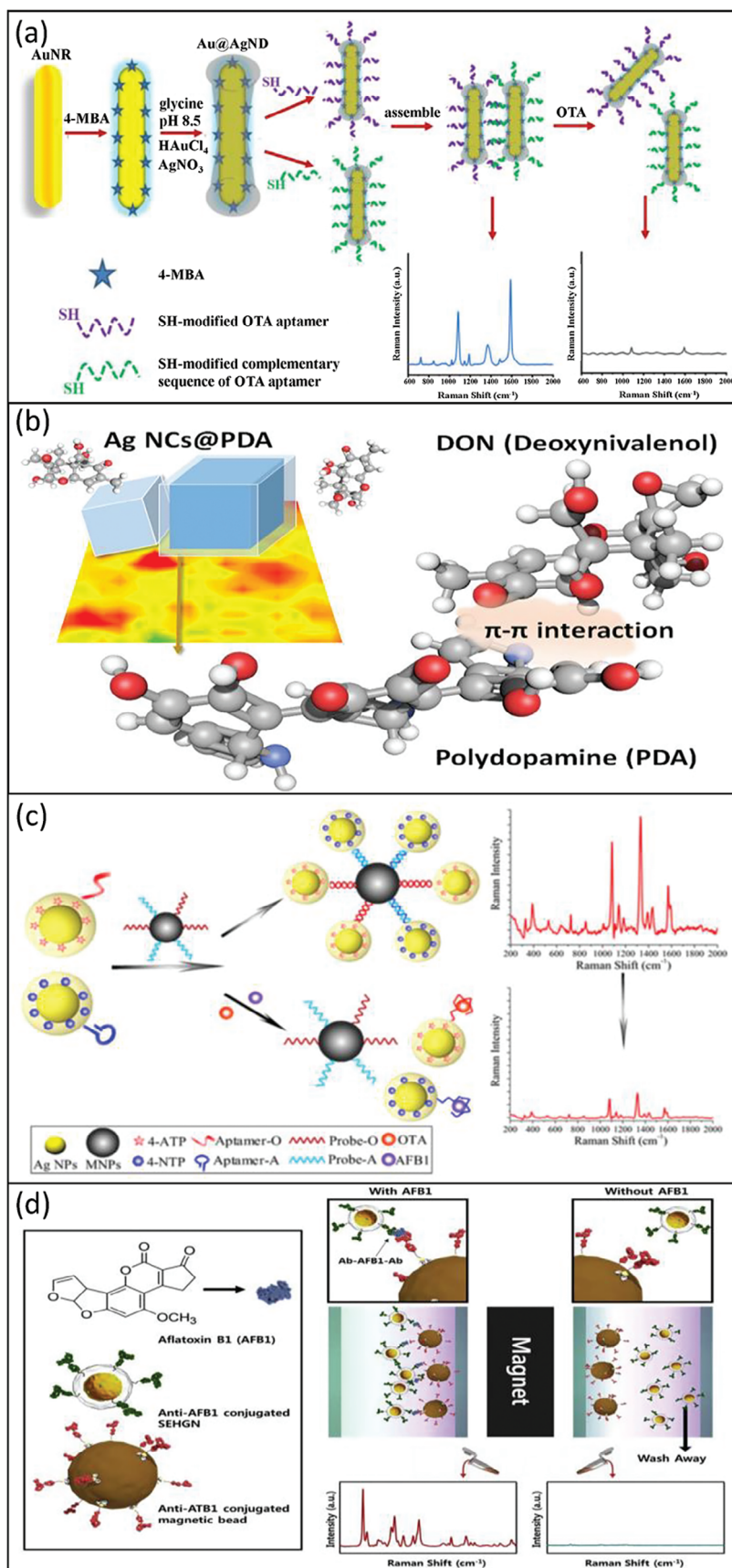


Figure 3. Transmission electron microscopy (TEM) images of nanomaterials with different shapes and sizes fabricated using bottom-up approaches. a) Au nanoparticles. Reproduced with permission.^[64] Copyright 2011, American Chemical Society. b) Au nanocubes. Reproduced with permission.^[65] Copyright 2018, American Chemical Society. c) Au nanobipyramids. Reproduced with permission.^[66] Copyright 2015, John Wiley & Sons. d) Au nanoprisms. Reproduced with permission.^[67] Copyright 2018, American Chemical Society. e) Au nanostars. Reproduced with permission.^[68] Copyright 2012, Royal Society of Chemistry. f) Au nanorods. Reproduced with permission.^[69] Copyright 2013, American Chemical Society.



stability of the substrate by protecting the Ag core from oxidation, which is also important for obtaining reproducible SERS signals. Spot-to-spot variation was examined to determine the reproducibility of the obtained SERS spectra using the same spot on the substrate and seven different Ag NCs@PDA substrates and the relative standard deviation (RSD) was calculated as 8% and 13%, respectively. Thus, the core-shell substrates are highly reproducible as the RSDs are much lower than the accepted rate of 20–30% (i.e., <10% very good, 10–20% good, and 20–30% acceptable, >30% not acceptable). The optical properties of Au and magnetic properties of iron oxide (Fe_3O_4) nanoparticles are often exploited and combined to develop aptasensing (Figure 4c)^[82] and immunosensing (Figure 4d)^[83] platforms for mycotoxin detection. During these procedures Raman reporters (e.g., DTNB, R6G, 4-NTP, 4-ATP) are commonly incorporated into the fabrication of nanoprobe for chemical SERS enhancement. Additionally, the magnetic properties of $\text{Fe}_3\text{O}_4/\text{Au}$ composites can offer rapid separation and signal enrichment using an external magnet, therefore, reducing matrix effects and helping to provide reproducible SERS signals. A summary of the bottom-up and top-down fabrication techniques and their mycotoxin applications will be discussed in the following sections.

3. Bottom-Up Approaches for the Determination of Mycotoxins

Colloidal spherical particles produced using bottom-up fabrication approaches can provide high stability and improved shelf-life owing to their homogeneity. These substrates are cost-effective and easy to both produce and functionalize. Bottom-up synthesis methods have been performed to fabricate plasmonic particles,^[47,51,72,76,85] core-shell particles,^[78,86] and magnetic particles^[82,87–90] for mycotoxin detection (Table 2). Several of these materials, typically plasmonic spherical materials, are known to provide weaker SERS enhancement than their anisotropic counterparts. Despite their heterogeneous size and shape, without functionalization their stability and shelf-life can be impacted by aggregation. Some take advantage of this detection mechanism by adding an aggregating agent such as a strong electrolyte (e.g., NaCl, KCl) or an acid (e.g., HCl, HNO_3) to modify the surrounding environment and purposely induce aggregation. This action increases the density of hot spots between aggregated particles and improves SERS enhancement. However, controlling aggregation and ensuring that the signals are reproducible is also challenging without exploiting recognition elements or chemical interactions such as, Au–thiol bonding, electrostatic or hydrophobic affinity interactions.^[91]

3.1. Metallic Nanoparticles

Metallic nanoparticles composed of Ag or Au have unique optical, electronic, catalytic, and magnetic properties in comparison

to their bulk structure. These properties can be tailored to determine their electronic, spectroscopic, scattering, and conductive properties.^[120] Ag nanomaterials offer several advantages for SERS over Au, as they exhibit a stronger and sharper plasmon response and can be excited from the UV to the IR region, while Au is restricted to IR alone due to damping induced by interband transitions. For these reasons, the scattering enhancement factor for Ag can be 10 to 100 times higher than Au.^[121,122] For the determination of mycotoxins, Lee et al. applied Ag nanospheres for the rapid detection of AFB₁, AFB₂, AFG₁, and AFG₂ in maize. The technique was one of the first to confirm its practicality in matrix alongside the development of models *k*-nearest neighbors (KNN) and multiple linear regression (MLR). The AgNS combined with MLR led to a substantial improvement in sensitivity with detection limits of 13–36 $\mu\text{g kg}^{-1}$, quantitation limits of 44–121 $\mu\text{g kg}^{-1}$ and *r* values of 0.939–0.967.^[72] Additionally, the determination of CIT was also reported by Singh et al. using AgNPs and density functional theory (DFT) calculation to estimate binding energies and determine adsorption rates of CIT on the surface of the metallic nanoparticles. Levels of CIT down to 0.25 mg kg^{-1} could be observed on the surface within a few minutes.^[51]

Furthermore, the potential of SERS was investigated by Lee et al. to detect FUM in maize using Ag dendrites. The substrates were mixed with maize extract prior to SERS analysis. Afterward, the SERS fingerprint spectra was collected and a range of classification models; KNN, linear discriminant analysis (LDA), partial least squares-discriminant analysis (PLS-DA) algorithms and quantification models; MLR, partial least-squares regression (PLSR), and principal component regression (PCR) algorithms were developed. Differences were clearly observed amongst groups of maize samples with concentrations of FUMs ranging from 1 to 209 mg kg^{-1} .^[47] Also, pre-etched Ag nanoclusters were fabricated on EP-FDU-12 as SERS substrates by Chen et al. followed by the addition of AFB₁ to the surface (Figure 5a). The respective theoretical spectrum was calculated by DFT to assign characteristic peaks. Spectral pre-processing methods were conducted followed by linear PLS and nonlinear BP-AdaBoost multivariate calibration methods. The limit of detection (LOD) was calculated as 5 $\mu\text{g kg}^{-1}$ and the applicability was confirmed in spiked peanut oil with recoveries in the range of 90–113% and an RSD of $\approx 5\%$.^[106]

Ag embedded silica nanospheres (aka SERS dots) have also been fabricated and described as having advantages including easy handling and preparation, long-term stability, high reproducibility, and strong signal generation.^[123,124] Hahm et al. reported the fabrication of Ag-embedded silica nanoparticles ($\text{SiO}_2@\text{AgNPs}$) for the detection of AOH.^[85] Thiolated SiO_2 NPs were first prepared, and AgNPs were introduced onto the surface of the $\text{SiO}_2\text{-SH}$ NPs. AOH standard solutions prepared in MeOH were incubated with $\text{SiO}_2@\text{AgNPs}$ followed by SERS analysis. Several intense bands appeared after the addition of AOH due

Figure 4. Fabrication of core-shell and magnetic nanomaterials using bottom-up approaches for the detection of mycotoxins. a) Schematic illustration for OTA detection based on Au@AgND assembly. Reproduced with permission.^[81] Copyright 2021, Elsevier. b) Preparation of core-shell Ag nanocubes coated with polydopamine (Ag NCs@PDA) for the detection of DON in pig feed. Reproduced with permission.^[75] Copyright 2020, Elsevier. c) Schematic illustration of aptasensor for double detection of OTA and AFB₁ with the use of SERS labels embedded Ag@Au CS NPs. Reproduced with permission.^[82] Copyright 2015, American Chemical Society. d) Schematic illustration of SERS-based immunoassay platform for AFB₁ detection using SEHGNs and magnetic beads. Reproduced with permission.^[83] Copyright 2015, Elsevier.

Table 2. Summary of SERS nanosubstrate fabrication using bottom-up approaches for the detection of mycotoxins.

| Bottom-up fabrication approaches | | |
|---|--|--------------------|
| Mycotoxin | SERS substrate | Refs. |
| Aflatoxin B ₁ , B ₂ , G ₁ , G ₂ , M ₁ , M ₂ | – Bipyramid gold nanocrystal-gold nanoclusters (BPGN/GNC) | [92] |
| | – Gold film over nanospheres (AuFONs) | [93,94] |
| | – Silver nanoparticles (AgNPs) | [72,95] |
| | – Gold nanoparticles (AuNPs) | [70,71,96–99] |
| | – Ag@Au core–shell nanoparticles (CSNPs) | [82,100] |
| | – Magnetic Fe ₃ O ₄ nanoparticles (MNPs) | [82,83] |
| | – Silica-encapsulated hollow gold nanoparticles (SEHGNS) | [83] |
| | – Gold nanostar (AuNS) core–silver nanoparticle (AgNP) satellites | [78] |
| | – Magnetic Ni@Au nanoparticles | [101] |
| | – Gold-DTNB@Silver-DTNB nanotriangles (GDADNTs) | [102] |
| | – Chitosan-functionalized magnetic-beads and AuNR@DTNB@AgNRs | [87] |
| | – Fe ₃ O ₄ @Au nanoflowers and Au-4MBA@Ag nanospheres | [90] |
| | – Gold nanotags on a silica photonic crystal microsphere (SPCMs) | [103] |
| | – Au@SiO ₂ core–shell NPs | [104] |
| | – Polyethyleneimine (PEI) modified ZNFe ₂ O ₄ @Ag magnetic nanoparticles | [105] |
| | – Mesoporous silica EP-FDU-12 pre-etched Ag nanocluster | [106] |
| Ochratoxin A, B | – Silver nanoparticles (AgNPs) | [73,95,107] |
| | – Gold nanoparticles (AuNPs) | [97,108–110] |
| | – Gold nanorods (AuNRs) | [79,86] |
| | – Gold nanoprism | [77] |
| | – Film over nanospheres (FONs) | [111] |
| | – Ag@Au core–shell nanoparticles (CSNPs) | [82,86,100,108] |
| | – Magnetic Fe ₃ O ₄ nanoparticles (MNP) | [82,88,89,110,112] |
| | – Au(core)@Au–Ag(shell) nanogapped nanostructures | [89] |
| | – Au-DTNB@AgNPs (GSNPs) | [88] |
| | – Upconversion nanoparticle (UCNP) | [113] |
| | – AuNanostar@4-MBA@Au core–shell nanostructures | [114] |
| | – Gold@silver nanodumbbell (Au@AgND) | [81] |
| | – Gold nanotags on a silica photonic crystal microsphere (SPCMs) | [103] |
| – AuNPs-loaded inverse opal silica photonic crystal microsphere (SIPCM) | [115] | |
| – Pd–Pt bimetallic nanocrystals (Pd–Pt NRs) | [112] | |
| – Au@SiO ₂ core–shell NPs | [104] | |
| Fumonisin B ₁ , B ₂ , B ₃ | – Ag dendrites | [47] |
| | – Platinum-coated gold nanorod (AuNR) | [80] |
| | – Upconversion nanoparticle (UCNP) | [113] |
| | – AuNPs-loaded inverse opal silica photonic crystal microsphere (SIPCM) | [115] |
| | – Ag@Au core–shell nanoparticles (CSNPs) | [100] |
| Deoxynivalenol | – Silver nanoparticles | [116] |
| | – Film over nanospheres (FONs) | [111] |
| | – Silver nanocubes@polydopamine substrate (Ag NCs@PDA) | [75] |
| | – AuNPs-loaded inverse opal silica photonic crystal microsphere (SIPCM) | [115] |
| | – Ag@Au core–shell nanoparticles (CSNPs) | [100] |
| Citrinin | – Silver nanoparticles (AgNPs) | [51] |
| Zearalenone | – Gold nanoparticles (AuNPs) | [97,117] |
| | – Upconversion nanoparticle (UCNP) | [113] |
| | – Gold nanotags on a silica photonic crystal microsphere (SPCMs) | [103] |
| | – Gold nanorod (AuNR) | [86] |
| | – Au@Ag core–shell nanoparticles (CSNPs) | [86,100,118] |
| – Fe ₃ O ₄ @Au magnetic nanoparticles (MNPs) | [118] | |
| Patulin | – Gold nanopyramids | [76] |
| | – Molecularly imprinted gold nanoparticle (MIP-ir-AuNP) | [54] |
| | – Gold nanorod (AuNR) | [119] |
| Alternariol | – Silver-embedded silica (SiO ₂ @Ag) NPs | [85] |
| | – Silver nanoparticles (AgNPs) | [57] |
| | – Gold nanorod (AuNR) | [119] |
| T-2 toxin | – Au@Ag core–shell nanoparticles (CSNPs) | [100] |

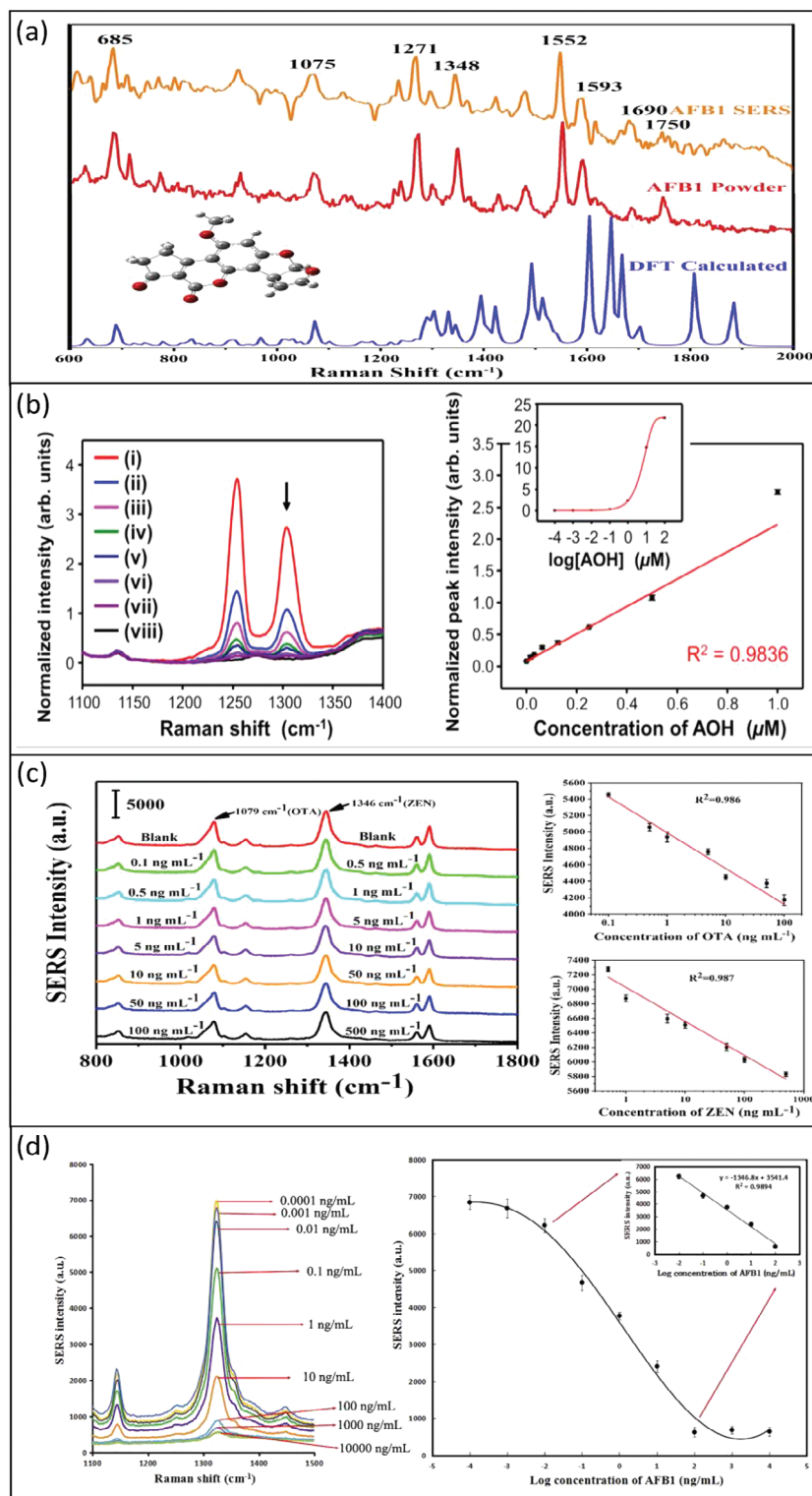


Figure 5. SERS applications exploiting bottom-up fabricated nanosubstrates to detect mycotoxins. a) The detection of AFB₁ using pre-etched metallic Ag nanoclusters as SERS substrates. Reproduced with permission.^[106] Copyright 2020, Elsevier. b) SERS spectra and intensity plot at 1304 cm⁻¹ of silver-embedded silica nanoparticles treated with various concentrations of AOH. Reproduced under the terms of the Creative Commons Attribution CC-BY license.^[85] Copyright 2020, The Authors, Licensee MDPI, Basel, Switzerland. c) SERS spectra and calibration curve obtained using a SERS-based aptasensor for the determination of OTA and ZEN with Au@Ag core-shell nanoparticles. Reproduced with permission.^[86] Copyright 2021, Springer Nature. d) Decreasing SERS spectra with increasing AFB₁ concentrations obtained using a SERS-based aptasensor using Au@DTNB@Ag core-shell nanorods and magnetic beads for signal enrichment. Reproduced with permission.^[87] Copyright 2018, Elsevier.

to the aggregation of AgNPs on the surface of SiO₂-SH NPs. The intensity of the SERS bands at 1254 and 1304 cm⁻¹ decreased with decreasing AOH concentration. Thus, the results indicated good linearity between the SERS intensity of the AOH-treated SiO₂@AgNPs and AOH concentration and an LOD of 1.25 µg kg⁻¹ for AOH was achieved (Figure 5b). The reproducibility of the SERS signal was also assessed with low RSD values of 2–6%.^[85]

Whilst Au nanomaterials are restricted to excitation within the red and near infrared regions, for some SERS applications this may be beneficial to reduce the effects of fluorescence. Other advantages of Au include its nontoxic nature and higher chemical stability than Ag.^[125] PAT for the first time was determined by Kang et al. using Au nanobipyramids as a SERS substrate. It was found that PAT could react with 4-MBA by its thiol group. Thus, 4-MBA and PAT were combined as a SERS probe and Au nanobipyramids were subsequently applied as SERS substrates. In the presence of PAT, a distinct vibrational signature at 1641 cm⁻¹ was observed which allowed PAT to be quantified in aqueous phase. The intensity ratio of two bands, 1641 and 1586 cm⁻¹ from target and 4-MBA, respectively, was calculated and an LOD for PAT of 6 µg kg⁻¹ and an RSD of 8% was achieved. Real sample analysis was conducted using the juice from rotten apples and pears with LODs of 126⁻ and 78 µg kg⁻¹, respectively.^[76] Additionally, a handheld system was developed by Qu et al. for the detection of AFs using TLC combined with SERS. AFs (AFB₁, AFB₂, AFG₁, AFG₂) were successfully separated by TLC and detected using Au colloids as the SERS substrate and a portable Raman spectrometer. Vibrational peaks were identified using DFT and the method could successfully determine LODs for AFs between 2.0 and 3.5 mg kg⁻¹. Recoveries for three AFs (AFB₁, AFG₁, AFG₂) in spiked moldy peanuts were reported between 88% and 114%, although the recovery for AFB₂ was not reported.^[70] Furthermore, SERS combined with QuEChERS (quick, easy, cheap-effective, rugged, safe) extraction was reported for the first time by Liu et al. to detect AFB₁ in feed samples. Samples were initially analyzed using a Raman microscope and the LOD for AFB₁ was calculated as 0.85 µg kg⁻¹ using standard solutions and AuNP aggregation to enhance the SERS signal. After combining potassium iodide (KI) and 50–60 nm gold nanoparticles (AuNPs), the samples were analyzed using a portable Raman spectrometer. The recoveries for spiked wheat and corn powder were between the range of 85–108% with an RSD of <10%.^[71] The rapid detection of *Aspergillus flavus* and quantitative determination of AFB₁ in maize using SERS was reported by Wang et al. who exploited AuNPs and a portable Raman spectrometer. *Aspergillus flavus* was inoculated on corn grains and the spore suspension (10²–10⁸ CFU mL⁻¹) was mixed with colloidal AuNPs to determine an LOD of 3.85 CFU mL⁻¹. The results demonstrated that the SERS signal of *Aspergillus flavus* increased after coupling with AuNPs, whereas under non-SERS conditions the signal was barely detectable using the portable instrument. HPLC analysis was conducted on the corn samples to obtain AFB₁ concentrations in parts per million (ppm). The SERS spectra of AuNPs mixed with AFB₁ standards in MeOH were collected using a portable spectrometer and the LOD for AFB₁ was 0.5 µg kg⁻¹.^[99] However, there was no correlation made between the LODs achieved for *Aspergillus flavus* and AFB₁. Additionally, the quantification of naturally occurring AFB₁ in corn was not reported and AFB₁ was

not spiked into the blank matrix for validation. Detection limits were only obtained for AFB₁ using standards prepared in MeOH, thus, interferences and reduced sensitivities in matrix conditions could not be assessed.

3.2. Core–Shell Nanomaterials

Bimetallic nanomaterials composed of Au and Ag have gained much attention due to the ability to amalgamate LSPR, i.e., plasmonic coupling. This Au–Ag alloy can offer several advantages including, enhanced SERS signal and broad band absorption of light. Furthermore, they possess the long term stability and biocompatibility of Au and the phenomenal enhancement provided by Ag.^[126] For mycotoxin detection, Li et al. applied the Au nanostar (AuNS) and AgNP satellite assembly for the ultrasensitive detection of AFB₁ in spiked peanut milk. The SERS sensor was constructed using AFB₁ aptamer (DNA1)-modified Ag satellites and a complementary sequence (DNA2)-modified AuNS. A Raman label of 4-ATP was modified on the surface of Ag satellites which attached to the AuNS leading to the formation of a core–satellite architecture with intense SERS signal. After the release of complementary DNA2 from the AuNS, in the presence of target, the SERS signal is reduced. An LOD of 500 ng kg⁻¹ was achieved whilst recoveries and RSDs for three concentrations of AFB₁ in spiked peanut milk were between 88–104% and 11–18%, respectively.^[78] Additionally, Chen et al. combined Au@Ag core–shell NPs with Au nanorods (AuNRs) for the simultaneous detection of OTA and ZEN in wheat and corn. For the sensing application, the capture and reporter probes were fabricated using SH-cDNA-modified AuNRs and SH-Apt-O-modified Au@4-MBA@Ag core–shell NPs (Au@Ag CS) or SH-Apt-Z-modified Au@DTNB@Ag CS, respectively. The reporter probe witnessed strong SERS signal when OTA and ZEN aptamers recognize complementary strands (SH-cDNA). However, binding between OTA and ZEN aptamers resulted in reduced SERS signal as reporter probes release the capture probes. The SERS intensity was indirectly proportional to increasing OTA and ZEN concentrations and linearity was observed for 4-MBA at 1079 cm⁻¹ ($R^2 = 0.986$) and DTNB at 1346 cm⁻¹ ($R^2 = 0.987$) (Figure 5c). The LOD for OTA and ZEN was calculated as 20 and 50 ng kg⁻¹ and the recovery rate for wheat and corn ranged from 96% to 111%.^[86]

3.3. Magnetic Nanomaterials

A typical advantage of using magnetic nanomaterials (MNPs) is that they are easy to separate thus, allowing the controllable formation of hot spots and enhancement.^[127,128] Additionally, magnetism allows effective extraction and separation of targets from complex samples, which greatly improves accuracy, reproducibility of detection and allows for matrix interferences to be significantly reduced.^[128] Many of the applications exploiting MNPs also commonly incorporate other highly stable and/or SERS enhancing nanosubstrates such as, Au–Ag core–shell particles. For sensing they are often functionalized with mycotoxin-specific aptamers to improve reproducibility and selectivity. For example, Zhao et al. reported MNPs fabricated by the reduction of iron salts (FeCl₃) using sodium citrate as a reducing agent for

the double detection of AFB₁ and OTA in maize. Additionally, SERS labels (4-NTP or 4-ATP) were embedded onto Ag and Au core–shelled nanoparticles (Ag@Au CS NPs). Strong SERS enhancement from Raman reporters is observed after the complexes are purified with an external magnet. However, in the presence of OTA and AFB₁, binding with aptamers induces the dissociation of Ag@Au CS NPs from the MNPs and decreased SERS is observed after the MNPs are isolated and Ag@Au CS NPs are removed. The technique could achieve detection limits of 6–30 ng kg⁻¹ and was applied to maize with recovery values between 95%–100% and an RSD of 4%.^[82] Additionally, Chen et al. also reported an SERS-based aptasensor for the ultrasensitive detection of AFB₁ in spiked peanut oil. The procedure takes advantage of chitosan magnetic beads (CS-Fe₃O₄) conjugated with amino-terminal AFB₁ aptamer (NH₂-DNA1) and thiol-terminal AFB₁ complementary aptamer (SH-DNA2) as enrichment nanoprobe and Au–Ag nanorods functionalized with Raman reporter DTNB (AuNR@DTNB@Ag nanorods or ADANRs) as reporter nanoprobe. In the presence of AFB₁, competitive binding between aptamers on CS-Fe₃O₄ and complementary aptamers on ADANRs induce dissociation and the Raman signals are reduced after washing with an external magnet to separate the unbound ADANRs nanoprobe (Figure 5d). An LOD of 4 ng kg⁻¹ and an RSD of 3% was achieved with recoveries between 91% and 106%.^[87] Furthermore, Song et al. developed an SERS-based aptasensor for OTA in red wine and coffee based on Fe₃O₄@Au magnetic nanoparticles (MGNPs) and Au@Ag nanoprobe modified with Raman reporter DTNB. Au-DTNB@AgNPs were modified with OTA aptamer (aptamer-GSNPs) and used as Raman signal probes and MGNPs were modified with complementary DNA (cDNA–MGNPs) as capture probes and reinforced substrates. After magnetic separation reduced Raman signal is observed and the LOD for OTA was determined as 500 ng kg⁻¹, with recoveries between 80% and 110% and RSDs <10%.^[88] A SERS-based aptasensor with direct correlation was developed for the detection of OTA in red wine by Shao et al. The technique applied Au core and Au–Ag shell nanogapped nanostructures (Au@Au–Ag NNSs) coupled with Fe₃O₄-MNPs by OTA aptamer and its complementary DNA sequence. Hybridization occurs without OTA and after magnetic separation the supernatant provides weaker SERS signal as 4-MBA. The assembly disassembles in the presence of OTA and, as the OTA concentration increases, more 4-MBA remains available in the supernatant after magnetic separation. Therefore, the SERS peak of 4-MBA at 1591 cm⁻¹ was directly correlated to increasing concentrations of OTA with an LOD of 4 ng kg⁻¹ and recoveries between 92% and 112%.^[89] In addition, He et al. also reported an SERS aptasensor based on multifunctional Fe₃O₄@Au nanoflowers (Fe₃O₄@Au NFs) for the ultrasensitive detection of AFB₁ in peanut oil. Hybridization between reporter and capture probes formed the basis of the SERS aptasensor, which after magnetic separation produced high Raman signal from reporter probes. In the presence of AFB₁, the AFB₁ aptamer selectively bound to AFB₁ and reporter probes (Au-4MBA@AgNNSs) were released from the capture probes (Fe₃O₄@Au NFs) causing a linear decrease in SERS intensity after magnetic separation. A detection limit of 400 ng kg⁻¹ was achieved with an RSD of 3% and satisfactory recoveries of 97–115% and RSD values from 4% to 12%.^[90]

Reproducibility and uniformity in the assembly of hot spots remains to be one of the major challenges for SERS detection. The great potential of metallic nanomaterials using bottom-up approaches has been demonstrated for the detection of mycotoxins; however, the reproducibility of SERS signals and long-term stability of substrates acquired through top-down fabrication, or a combination of approaches may be preferred. Bottom-up fabrication methods tend to be readily scalable to large batches but typically offer limited control over size, homogeneity, and shape.^[129] Commonly, there have been three approaches reported for the immobilization of nanostructures on solid substrates including 1) self-assembly of bottom-up nanomaterials on solid surfaces and 2) top-down fabrication of roughened Ag and Au surfaces and 3) a combination of these techniques.^[91] These approaches and their applications will be discussed in the following sections.

4. Self-Assembly of Colloidal Nanomaterials on Solid Surfaces

Self-assembly of chemically synthesized nanoparticles is one of the most widely used bottom-up approaches due to the lower cost and fabrication time compared to those produced using top-down approaches. Detection can be performed through the addition of sample material directly onto a roughened surface which can be composed of a Raman active material, or another low-cost, readily available material. The detection of mycotoxins has previously been performed using the self-assembly approach of metallic nanosubstrates on solid surfaces fabricated of glass,^[95,119] paper,^[75] Au,^[73] and aluminum (Al) foil.^[81] To control self-assembly and improve reproducibility, bifunctional linker molecules have been employed to chemically immobilize or electrostatically attach nanomaterials onto the solid surface. Through this approach, one available functional group can be anchored onto the solid support whilst the second one remains free to bind to the metal nanostructure.^[91,130] Thus, the production of hot spots and SERS signal can be obtained in a more accurate and reproducible manner.

4.1. Silica

Silica (or glass) is commonly used for the self-assembly of nanomaterials as it is highly stable, robust, and easy to functionalize. For the determination of PAT and AOH, Guo et al. demonstrated a coffee-ring effect on glass slides using AuNRs dried onto the surface of a silicon (Si) chip (Figure 6a). A stable coffee ring was formed by optimizing the droplet volume, drying temperature, and evaporation rates at the edge of the droplet, prior to analyzing mycotoxins at varying concentrations. The characteristic peak of Rhodamine B (RB) was used to capture a pseudo color image and the signal intensity was used to optimize and characterize the coffee ring. The color image shows that the signal intensity of RB in the coffee-ring region is significantly higher than the central region, indicating that the coffee ring can enrich and capture the detection molecules and enhance the Raman signal of the measured molecules. Afterward, PAT and AOH standards and

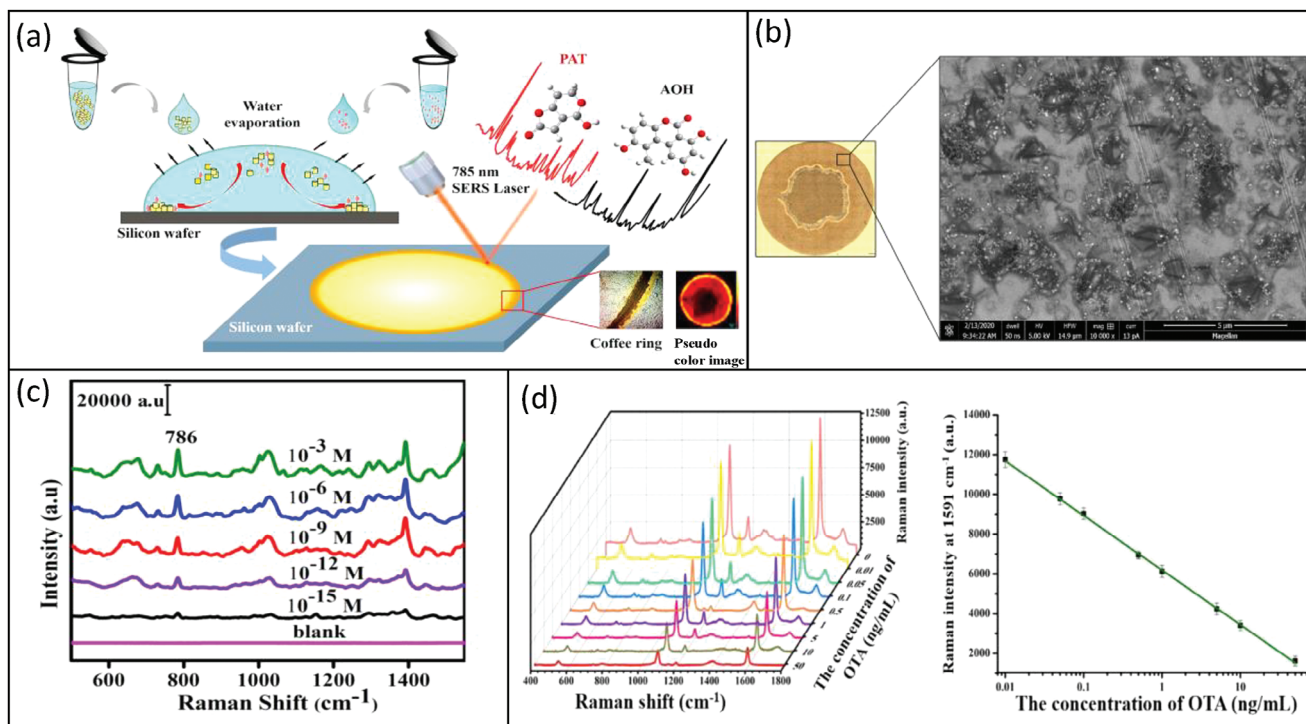


Figure 6. Self-assembly of bottom-up fabricated nanomaterials on solid surfaces for the detection of mycotoxins. a) Schematic illustration of the SERS detection of PAT and AOH based on the coffee-ring effect using AuNRs assembled on a silicon chip. Reproduced with permission.^[119] Copyright 2021, Elsevier. b) SEM image of donut-like structure created using acidified chloroform extraction to remove OTA residues from wine before drying on a Au film. Reproduced with permission.^[73] Copyright 2021, Elsevier. c) SERS spectra of DON in pig feed using Ag NCs@PDA substrate dried on filter paper. Reproduced with permission.^[75] Copyright 2020, Elsevier. d) SERS spectra of 4-MBA embedded on Au@AgND assembly upon addition and drying of different OTA concentrations on tin foil. Reproduced with permission.^[81] Copyright 2021, Elsevier.

spiked apple juice extracts were premixed with AuNRs and dried onto the Si wafer. The SERS spectra from the edge of the coffee ring were analyzed and DFT was employed to determine the theoretical distribution of Raman peaks. The spectra were pre-processed prior to the development of algorithms; synergy interval (Si)-PLS, genetic algorithm (GA)-PLS, and uninformative variable elimination (UVE)-PLS and detection limits of 1 $\mu\text{g kg}^{-1}$ were obtained. PAT and AOH were extracted from apple juice using solid phase extraction (SPE) and the LOD was calculated as 1 mg kg^{-1} with recoveries between 82% and 108%.^[119] Additionally, a Si platform was exploited by Kutsanedzie et al. for the detection of OTA and AFB₁. After optimizing pH, AgNPs were dried onto the Si platform, followed by the independent addition of two mycotoxins and NaCl to induce aggregation and increase signal intensity from SERS hot spots. Acquired spectra were independently pre-processed and two feature selection algorithms paired with PLS; GA-PLS and competitive adaptive reweighted sampling-PLS (CARS-PLS) were used for model development. The LODs for OTA and AFB₁ in spiked cocoa beans were calculated using the linear range of 0.1–10 $\mu\text{g kg}^{-1}$ for all established models, predicted concentrations and computations based on the IUPAC definition as 3 and 4 ng kg^{-1} , respectively. Additionally, recoveries and coefficient of variation (CV) values were determined for OTA and AFB₁ in spiked cocoa beans ranging between 97–105% and 1–7%, respectively.^[95]

4.2. Gold

Whilst Au SERS substrates are more expensive than those made of Al, a major advantage is that Au can strongly absorb mercaptans and other sulfur-containing compounds.^[131] To detect OTA, Rojas et al. exploited Au-coated glass slides as solid supports to dry sample extracts from wine and wheat mixed with colloidal AgNPs. During this procedure Au slides play a role in facilitating and enhancing SERS measurements. The formation of a donut-like structure was observed after performing three different extraction procedures. For extraction 1 and 3, a coffee-ring effect was observed, which was attributed to the presence of NaCl causing particle aggregation. The coffee ring disappeared after extraction 2 and a donut-like structure was observed when sample acidification was performed using chloroform as a separation solvent. Further investigation using SEM revealed AgNPs spread around bigger crystal-like structures, which were homogeneously distributed to form one thick ring (Figure 6b). Compared to the coffee-ring structure, the nanoparticles had a much lower degree of aggregation. Although nanoparticle aggregation is required to form the coffee ring and enhance SERS sensitivity, this process is often difficult to control and leads to non-reproducible results. Therefore, the donut structure demonstrated a more homogeneous distribution and reproducible SERS signals. The authors also speculate that the formation of crystal-like structures in the donut involves proteins but requires further investigation.

Table 3. Summary of SERS nanosubstrate fabrication using top-down approaches for the detection of mycotoxins.

| Top-down fabrication approaches | | |
|---|---|-------|
| Mycotoxin | SERS substrate | Refs. |
| Aflatoxin B ₁ , B ₂ , G ₁ , G ₂ , M ₁ , M ₂ | <ul style="list-style-type: none"> – Silver nanorod (AgNR) array [42] – Graphene oxide–Au@Ag core–shell nanoparticle complex [134] – Carbon nanostructures by plasma-enhanced chemical vapor deposition [135] – PDMS@AAO complex sputtered with Au (3D-nanocauliflower substrate) [49] – Gold nanobipyramids (AuNBPs) in nanoholes of anodic aluminum oxide (AAO) (Au NBPs-AAO) [136] – 3D nanopillar arrays [137] – Porous anodized aluminum (PAA) membrane (two-step anodization) and AgNPs [138] – CuO@Ag microbowl array (lithography combined with chemical oxidation and Ag sputtering) [139] – Graphene oxide-based 3D Au nanofilm (GO@Au–Au) [140] – MXene (Ti₃C₂T_x) nanosheets loaded with AuNP dimers [141] – MXenes and Au nanorod (AuNR) substrates [142] | |
| Ochratoxin A, B | <ul style="list-style-type: none"> – Gold nanotriangle structures fabricated by electron beam lithography [44] – Au–Ag Janus NPs-MXenes nanosheet assemblies [143] – 3D nanopillar arrays [137] – Thermal evaporation of Au on glass [144] – Ag-capped silicon nanopillars using reactive ion etching [145] | |
| Fumonisin B ₁ , B ₂ , B ₃ | <ul style="list-style-type: none"> – 3D nanopillar arrays [137] – Nano-pillar arrays fabricated by two-photon polymerization [146] – Carbon nanostructures by plasma-enhanced chemical vapor deposition [135] – Metal–organic framework (MOF-5) coated SERS active gold gratings [147] – Graphene oxide-based 3D Au nanofilm (GO@Au–Au) [140] | |
| Deoxyvalenol | <ul style="list-style-type: none"> – Nano-pillar arrays fabricated by two-photon polymerization [146] – PDMS@AAO complex sputtered with Au (3D-nanocauliflower substrate) [49] | |
| Zearalenone | <ul style="list-style-type: none"> – Carbon nanostructures by plasma-enhanced chemical vapor deposition [135] – PDMS@AAO complex sputtered with Au (3D-nanocauliflower substrate) [49] – Graphene oxide-based 3D Au nanofilm (GO@Au–Au) [140] | |
| Patulin | <ul style="list-style-type: none"> – MIP on AuNP sputtered PDMS–AAO nanoarray [148] | |
| Alternariol | <ul style="list-style-type: none"> – Carbon nanostructures by plasma-enhanced chemical vapor deposition [135] | |

During extraction 2, five different concentrations of OTA (0.01–1 mg kg⁻¹) were spiked into wine and wheat samples and acidified with H₃PO₄ followed by extraction with chloroform. Extracts were mixed 1:1 with AgNPs for 3 min and dropped onto a Au slide to dry prior to analysis. PLS regression analysis showed good linearity between OTA concentration and the Raman intensity at 1030 and 1003 cm⁻¹ for wine and wheat.^[73] However, the perhaps unnecessary use and the associated health and environmental risks of using chlorinated extraction solvents make this procedure unlikely to be performed outside of the laboratory.

4.3. Paper

Filter paper serves as a suitable support for noble metal nanoparticles due to the combination of hydroxyl groups on the fibers surface making it ideal for loading with AgNPs. Additionally, filter paper as SERS substrates can afford more hot spots than planar substrates thus, decorating with sharp edged Ag nano-materials is ideal for ultrasensitive detection.^[132] Taking advantage of this, Tegegne et al. fabricated core–shell Ag nanocubes (Ag NCs) coated with polydopamine (PDA), which were loaded onto the surface of filter paper by ultrasonication for 30 min. The Ag NCs@PDA substrates are composed of an ultrathin (1.6 nm) PDA shell which promotes the adsorption of DON via hydrogen bonding and π – π stacking interactions. Pig feed extract and DON

at varying concentrations were added to the surface and dried at room temperature prior to SERS analysis. The quantitative analysis of DON was studied by analysing the characteristic SERS peak at 786 cm⁻¹ with increasing DON concentrations (Figure 6c). A linear calibration curve was obtained within the range from 0.3 ng kg⁻¹ to 296 mg kg⁻¹ and the LOD for Ag NCs@PDA was determined as 0.2 pg kg⁻¹ with the sensitivity attributed to affinity interactions between PDA and DON.^[75]

4.4. Aluminum Foil

Aluminum (Al) foil is one of the most widely available household materials and a cost-effective metallic material that is often used for SERS. As a result, Ma et al. successfully applied tin foil as an SERS substrate combined with a plasmonic nanogap gold@silver nanodumbbell (Au@AgND) structure for the detection of OTA. The Au@AgND structure was prepared by reducing Ag onto the surface of AuNRs in the presence of glycine. Ag preferred to grow at both ends of the AuNR to create a nanodumbbell structure. Thiolated OTA aptamer and its complementary sequence were modified on Au@AgND respectively using Ag-SH bonds. Analysis was performed by reacting Au@AgND with OTA solutions for 30 min and drying the sample on tin foil prior to analysis. Complementary pairing of the two probes reduced the inter-nanogap enhancing the Raman signal from 4-MBA Raman

reporter immobilized on Au@AgND. However, in the presence of OTA the aptamer preferentially binds to the target and the assembly was disintegrated therefore, decreasing the signal of 4-MBA. The OTA concentration was inversely proportional to the SERS signal and the LOD was 7 ng kg^{-1} . The recoveries in spiked beer and peanut oil were calculated as 92–102% and 94–104%, respectively (Figure 6d).^[81]

5. Top-Down Fabrication of Roughened Ag and Au Surfaces for Mycotoxin Detection

Roughened Ag and Au surfaces can be fabricated using several methods including chemical etching, mechanical deformation, electroplating, and oblique angle deposition. Electron beam lithography is also a popular technique for creating well defined metallic-coated Si nanostructures however, fabrication costs are higher than their non-lithographic counterparts.^[133] The fabrication of these nanostructures using lithographic and non-lithographic techniques and their mycotoxin applications will be discussed in the following sections and are summarized in Table 3.

5.1. 3D Nanofabrication Using Lithographic Techniques

Lithography is the process of transferring patterns from one medium to another using different forms of radiation including traditional optical or UV photolithography, or those which provide higher resolution including X-ray, electron or ion beam lithography.^[149] Fischer's patterns composed of a hexagonal array of Au triangles have been well documented in the literature (Figure 7). To fabricate glass slides are spin-coated with a photoresist thin film, followed by the deposition of chromium (Cr) using magnetic sputtering. The electron beam system is then used to write the Fischer's pattern and the size, distance, and resolution can be tailored by modifying the dose.^[150] Using this nanofabrication method, a metallic platform was prepared by Galarreta et al. consisting of an assembly of Au nanotriangles organized

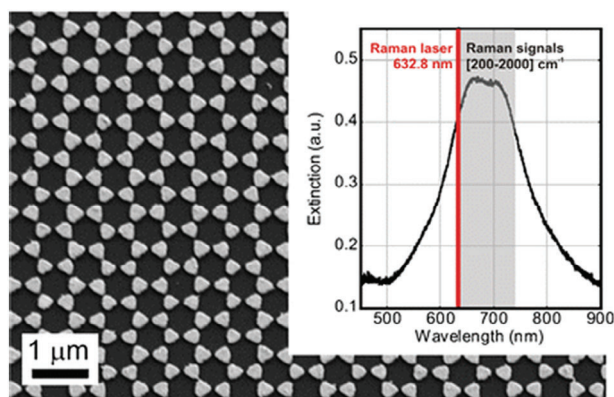


Figure 7. Scanning electron microscopy image of the SERS substrate consisting of arrays of Au nanotriangles organized in a hexagonal lattice (Fischer's pattern) inscribed by electron beam lithography on a microscope glass coverslip. Reproduced with permission.^[44] Copyright 2012, Springer Nature.

in a hexagonal lattice inscribed by electron beam lithography on a glass coverslip. The SERS platform was embedded with a microfluidic channel layer sputtered with polydimethylsiloxane (PDMS) followed by the functionalization of aptamers to the Au surface through covalent Au–S bonds. The substrate was applied to capture and enhance the SERS fingerprint recognition of OTA with detection limits of $20 \text{ } \mu\text{g kg}^{-1}$.^[44]

Additionally, excimer laser patterning of poly(methyl methacrylate) followed by the evaporation of Ag or Au has been explored for the creation of reproducible SERS-active gratings.^[151,152] Guselnikova et al. took advantage of spin-coating Su-8 thin films patterned by excimer laser. Au was deposited onto the patterned polymer surface by vacuum sputtering to create metal-organic framework (MOF-5)-coated SERS active Au gratings. The substrate was applied to analyze organic contaminants in soil (a mixture of FB₁, Sudan III, and paraoxon) using a portable Raman spectrometer. The LOD for FB₁ was determined after extracting from soil using water or chloroform as $0.072 \text{ } \mu\text{g kg}^{-1}$.^[147] Furthermore, Meng et al. employed colloidal lithography on copper (Cu) and subsequent chemical oxidation on Cu foils to form a quasi-2D CuO microbowl array film, which was sputtered with Ag to achieve CuO@Ag microbowl array substrate (Figure 8a). The SERS-active substrate with enhanced SERS sensitivity, reproducibility, and recyclability (photocatalytic degradation under visible illumination aids its self-cleaning and reusable properties) was applied to detect AFB₁ in maize samples and an LOD of 4 pg kg^{-1} was achieved.^[139]

Two-photon polymerization (TPP) nanolithography is a powerful and useful manufacturing tool using direct laser writing to fabricate 3D nanostructures of various materials.^[153] It allows the transferring of any desirable pattern in polymer, by exposing a photopolymer to laser pulses at a certain power, resulting in photo-polymerization within a smaller region of the photopolymer due to two-photon absorption. The unexposed regions of the photopolymer are washed away leaving behind the solidified polymer.^[154] TPP-based fabrication has a unique set of advantages including high-resolution nanostructures with greater precision, 3D printing in a single exposure step and fabrication of complex features with high accuracy and repeatability over conventional microfabrication techniques.^[155] For the determination of mycotoxins DON and FB₁, an additive manufacturing method employing TPP to fabricate nanopillar arrays ranging from 200 to 600 nm was reported by Liu et al. followed by sputtering the nanostructures with a 20 nm layer of Au (Figure 8b). The complexity and time of nanostructure fabrication was reduced using computer aided design/manufacturing (CAD/CAM). The SERS substrates were fabricated using a 3D printer and the electric field enhancement simulation of nanopillar arrays was performed using the finite-difference time-domain (FDTD) method. The 200 nm nanopillar arrays had the highest enhancement factor in the presence of Rhodamine 6G (R6G) and were applied to detect DON and FB₁ in acetonitrile (ACN) combined with principal component analysis (PCA). The LOD for DON and FB₁ were 1 and 1.25 mg kg^{-1} , respectively however these were the only concentrations analyzed and validation in matrix was not performed.^[146]

Oblique angle deposition (OAD), or often referred to as glancing angle deposition (GLAD), is a deposition process,

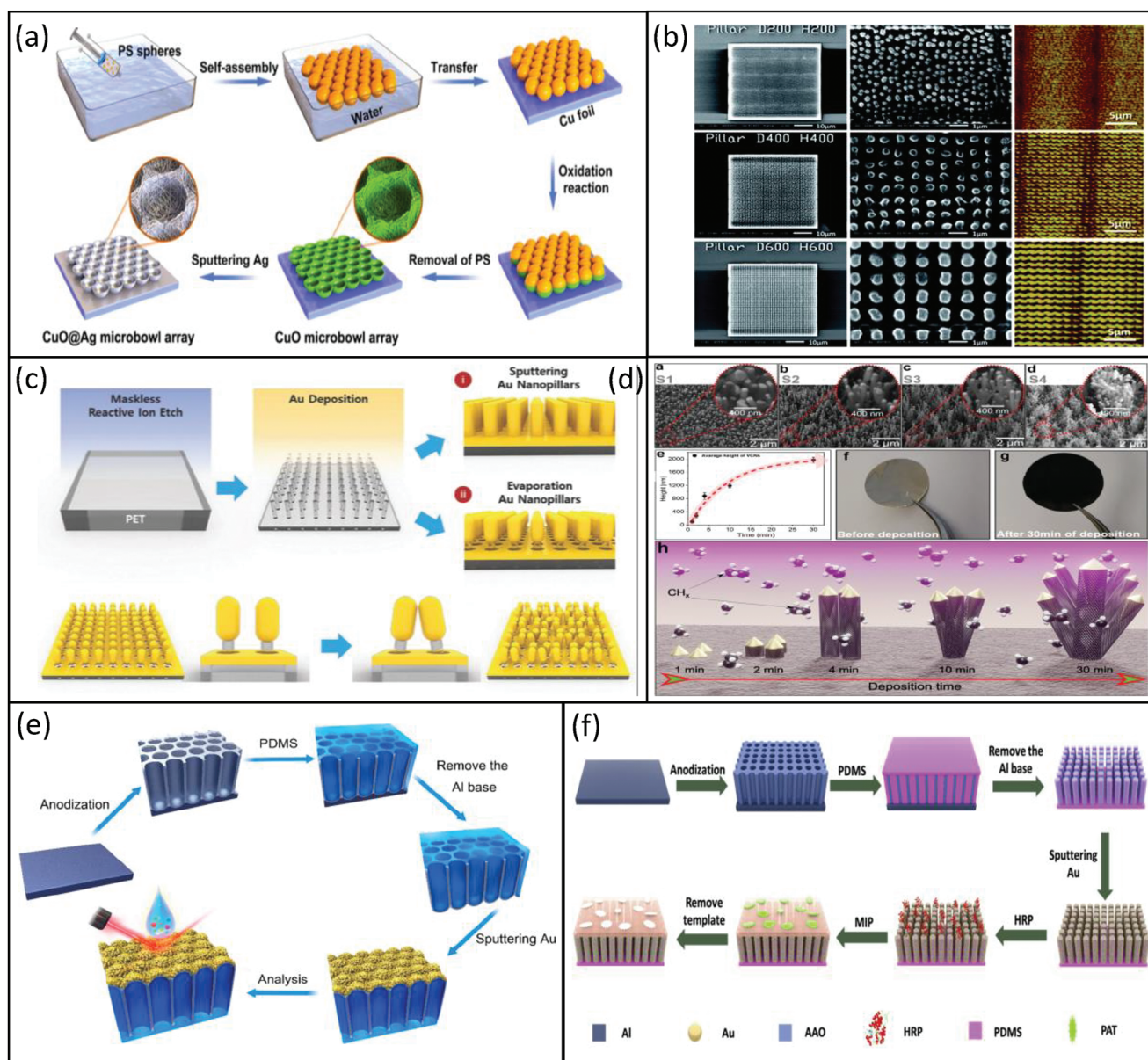


Figure 8. Fabrication of 3D nanosubstrates using top-down lithographic and non-lithographic approaches for the detection of mycotoxins using SERS. a) Schematic diagram for the preparation of CuO@Ag microbowl array substrate using colloidal lithography and chemical oxidation reaction. Reproduced with permission.^[139] Copyright 2021, Royal Society of Chemistry. b) Morphologies of 200, 400, and 600 nm nanopillar arrays fabricated using TPP photolithography and characterized using SEM and AFM. Reproduced with permission.^[146] Copyright 2020, Royal Society of Chemistry. c) Schematic illustration for the fabrication of 3D nanopillar substrates by i) sputtering and ii) thermal evaporation methods and the leaning effects of adjacent nanopillars after solution evaporation. Reproduced with permission.^[137] Copyright 2018, John Wiley & Sons. d) Morphology of carbon nanostructures synthesized by plasma-enhanced chemical vapor deposition. Reproduced with permission.^[135] Copyright 2021, John Wiley & Sons. e) Schematic demonstration of the preparation of 3D-nanocauliflower substrate using two-step anodization. Reproduced with permission.^[49] Copyright 2019, American Chemical Society. f) Illustration of the preparation process of enzyme induced MIP-SERS substrate (MIP-ir-Au/PDMS/AAO) using two-step anodization. Reproduced with permission.^[148] Copyright 2020, Elsevier.

which uses a highly directional vapor flux source to produce an array of 3D nanostructures with excellent controllability in geometrical shape, reproducibility, and low-cost. By controlling deposition parameters during OAD, a variety of nanostructures and self-organized nanoporous films can be fabricated including nanorods and nanohelices.^[156] One of the earliest reports by Wu et al. acquired SERS spectra with AuNR array substrates fabri-

cated using an OAD technique using a custom-designed electron beam/sputtering evaporation (e-beam) system. Briefly, the fabrication relied on a 20 nm titanium (Ti) film followed by a 500 nm Au film being evaporated onto glass microscopic slides using the e-beam deposition system, whilst being held perpendicular. The substrates were then rotated 86° and AuNRs were successfully grown at this oblique angle, which were later applied

to determine the SERS fingerprint of AFB₁, AFB₂, AFG₁, and AFG₂.^[42]

Maskless or grayscale lithography and reactive ion etching have been described as simple, fast, and cost-effective processes used to fabricate flexible freestanding nanopillars composed of Si by omitting the conventional lithographic process.^[133] During the approach, the system does not require any hard masks but instead uses digital image pattern data designed in CAD, which are then transferred into Si substrates using reactive ion etching (RIE).^[157] These leaning nanopillars provide stable and reproducible SERS enhancement as they trap analyte molecules at the hot spots formed within the 20 nm inter-nanopillar gaps, which can be abridged to 10 nm by sputtering with a metallic coating such as Ag, producing higher reproducibility and an enhancement factor up to 10⁷ (nearly two orders larger than that of the bare Au nanopillar arrays).^[158,159] Taking advantage of this, Rostami et al. developed a Ag-capped Si nanopillar SERS substrate for the determination of OTA in wine. The fabrication was conducted using RIE over a 4-in. Si wafer and the Ag coating was deposited using e-beam evaporation, before placing the SERS chips into a custom-made measurement chamber on a glass slide. The SERS procedure was used in combination with high throughput supported liquid membrane (SLM) extraction to separate two aqueous phases with different pH. For SERS detection, OTA in ammonium acidified ammonium hydroxide (AW-AA) (pH 3 using acetic acid) had good affinity toward the Ag-capped silicon nanopillars and could anchor to the surface through coordination or electrostatic interactions. Linearity between increasing Raman intensity and OTA peak at 1003 cm⁻¹ was achieved within the concentration range of 0.02–1 mg kg⁻¹. The LOD of the SERS sensor for detecting OTA spiked in white and red wine was calculated as 155 and 306 µg kg⁻¹, respectively.^[145]

5.2. 3D Nanofabrication using Non-lithographic Techniques

Non-lithographic techniques including deposition (inc. sputtering, thermal evaporation, and chemical vapor) and electrochemical oxidation (inc. anodization) have also been explored to produce 3D substrates with high reproducibility. These methods and have been described as cost-effective and high throughput methods compared to other lithography processes for fabricating wafer-scale plasmonic substrates.^[137] It was reported by Wang et al. that the high uniformity of densely packed leaning 3D nanopillars minimized spot-to-spot variations in Raman signal when Raman mapping is performed. To produce these substrates Au was deposited using sputtering or thermal evaporation to fabricate 80 nm thick Au nanopillar structures (Figure 8c). Multiple mycotoxins were detected using SERS mapping on 3D plasmonic nanopillar arrays. A carboxylic self-assembled monolayer on the 3D Au nanopillar substrate was prepared and immobilized with mycotoxin-BSA for the detection of three mycotoxins: OTA, FMB, and AFB₁. The competitive immunoassay reported decreasing Raman intensities with increasing mycotoxin concentrations and LODs for OTA, FMB, and AFB₁ were determined between 5% and 6 ng kg⁻¹. The selectivity was also determined by exposing the technique to three cocktail solutions with different ratios of the three mycotoxins and the recoveries were between 86% and 129%.^[137] Additionally, thermal evap-

oration methods were conducted by Gillibert et al. to produce glass slides coated with 6 nm of Au. Surface functionalization with OTA-specific aptamer was conducted and blocking of the Au surface with 6-mercaptohexanol (MOH) to develop a fast and highly sensitive SERS approach for detecting OTA. By incorporating chemometric algorithms, PCA, PLS, orthogonal partial least squares (OPLS), and a quantitative PLSR, OTA concentrations could be predicted down to 4 ng kg⁻¹.^[144]

Plasma-enhanced chemical vapor deposition (PECVD) is a fast, facile, and highly controllable method for the deposition of various carbon (C) nanostructures on solid substrates by dissociating the precursor gases at relatively low temperatures.^[135] During PECVD, morphology and growth rate can be controlled by plasma discharge parameters including gas selection, power density, substrate material and temperate selection, substrate position, and treatment time.^[160] Using this technique, high-performing plasmonic substrates (EF SPE = 5 × 10⁷) based on plasma-grown vertical hollow C nanotubes (CNTs) were fabricated by Santhosh et al. The C structures were grown on nickel (Ni) film and after 30 min branched nanotubes were transformed smoothly to a nanoforest-like texture that continued to grow vertically with more intense pillar branching (Figure 8d). The multiwalled CNTs had an average diameter of 50 nm and were terminated by faceted single metallic Ni particles of ≈30 nm. As Ni crystals were located at the tip of the C tubes, it is proposed that the nanostructures were formed by the tip-growth mechanism. The substrate was employed as a label-free platform to investigate the vibrational features of pure AFB₁, FB₁, AOH, and ZEN. Fingerprint spectra were obtained for all four mycotoxins and a parabolic fit was performed using standard least-squares regression (LSR), followed by OPLS and PCA to develop statistical models. The LOD for the technique was determined to be between 1.0 and 3.6 µg kg⁻¹.^[135]

Anodic aluminum oxide (AAO) films are formed by the electrochemical oxidation (or anodization) of Al by anodizing in acids such as, sulfuric, chromic, oxalic, and phosphoric at potentials ranging from 25 to 500 V. Additionally, a two-step anodization to produce layers of Al sheets can be conducted using a range of conditions or repeating the same anodization process.^[161] For example, Li et al. conducted a two-step anodization of Al foils using oxalic acid at 40 V for 4 h and repeated the same conditions for 30 min after washing to fabricate an AAO array. PDMS was poured onto the surface to form PDMS@AAO and AuNPs were sputtered onto the surface of PDMS-AAO after the removal of the Al base, contributing to noticeable SERS hot spots and strong enhancement of Raman signals (Figure 8e). The 3D nanocauliflower-inspired substrate was prepared for the simultaneous detection of AFB₁, ZEN, and DON with LODs between 2 and 48 µg kg⁻¹. Additionally, spiking different concentrations into maize samples lead to recovery rates between 93% and 120% and PCA was applied to effectively differentiate between the three mycotoxins.^[49] A similar method was also reported by Zhu et al. to obtain Au/PDMS/AAO functionalized with polymers and the MIP-SERS substrate was applied to detect PAT in blueberry jam, grapefruit and orange juice^[148] (Figure 8f). Additionally, commercially available AAO was obtained by Lin et al. to fabricate an SERS substrate based on the self-assembly of Au nanobipyramids (Au NBPs) in the nanoholes of AAO (Au NBPs-AAO substrate). Probe molecules (4-ATP and R6G) were added to the

developed Au NBPs–AAO substrates and analyzed using a hand-held Raman spectrometer to examine uniformity, reproducibility, and SERS intensity using different nanohole depths. The hand-held spectrometer was used to detect AFB₁ concentrations between 1.5 and 1500 μg kg⁻¹ within 1 min by referencing the –H bending peak at 1442 cm⁻¹ and the LOD was calculated to be 0.5 μg kg⁻¹. Additionally, the technique could distinguish four AFs (AFB₁, AFB₂, AFG₁, and AFG₂) by examining the difference in maximum peak intensities and was applied to determine AFB₁ in spiked peanut samples (300⁻, 30⁻, and 3 μg kg⁻¹) with recoveries between 106% and 126% and an RSD <10%.^[136] Furthermore, Feng et al. carried out the anodization of Al foils under a constant cell potential of 27 V in sulfuric acid solution for 2 h at 2 °C, followed by a second anodization using the same conditions to obtain the porous anodized aluminum (PAA) membrane. Raman reporter 4-ATP and DNA partially complementary to AFB₁ were attached to the surface of AgNPs by chemical bonding to form a 4-ATP–AgNPs–DNA complex and PAA membrane was functionalized with AFB₁ aptamer. The PAA surface was modified with 4-ATP–AgNPs–DNA through complementary base pairing to form a AgNPs–PAA sensor with strong Raman signal from reporter 4-ATP. The SERS signal of 4-ATP at 1080 cm⁻¹ was indirectly proportional to AFB₁ concentration and the LOD for AFB₁ standard solution and in walnut was 83 ng kg⁻¹ and 9 ng kg⁻¹ using a portable spectrometer, respectively.^[138]

5.3. Assembly of 3D Nanosubstrates Using 2D Materials

Graphene oxide (GO) is a 2D honeycomb-like sheet which consists of a single layer of graphite oxide.^[140] The properties of GO are strongly dependent on the synthesis method which influences the number of oxygen-containing groups and number of GO layers contained within the structure.^[162] Graphite oxide can be prepared by the oxidation of graphite (a crystalline form of C) using concentrated acids and strong oxidants using several methods including the Hummers method^[163,164] and the Marciano-Tour's method.^[165,166] The dispersion and exfoliation of graphite oxide in water or suitable organic solvent is then conducted producing GO.^[167] Advantages of GO include a large surface-area to volume ratio, high electronic conductivity, stability, and dispersion and abundant surface functionalities (e.g., carboxyl, epoxy, hydroxyl groups) for biomolecular conjugation.^[140] Thus, GO can be applied as a practical support to anchor nanomaterials and has been functionalized previously with metallic nanoparticles, metal oxide nanoparticles, and quantum dots for numerous applications.^[167]

For the determination of ZEN, AFB₁, and FB₁, Zheng et al. developed a GO-based 3D Au nanofilm (GO@Au–Au) consisting of three parts: a thin GO@Au nanofilm (400–800 nm) that serves as uniform inner substrate, a precisely controlled 0.5 nm polyethyleneimine (PEI) interlayer that acts as a built-in nanogap, and numerous externally assembled 30 nm AuNPs to provide a greater surface area and multiple SERS hotspots (Figure 9a). The properties of the film-type GO@Au–Au tags include excellent stability, monodispersity, superior SERS activity, and huge reaction interface. The materials were demonstrated for the multiplexed detection of three mycotoxins with LODs within the range of 0.5–6 ng kg⁻¹. Recoveries and RSDs for spiked maize, peanut, lake

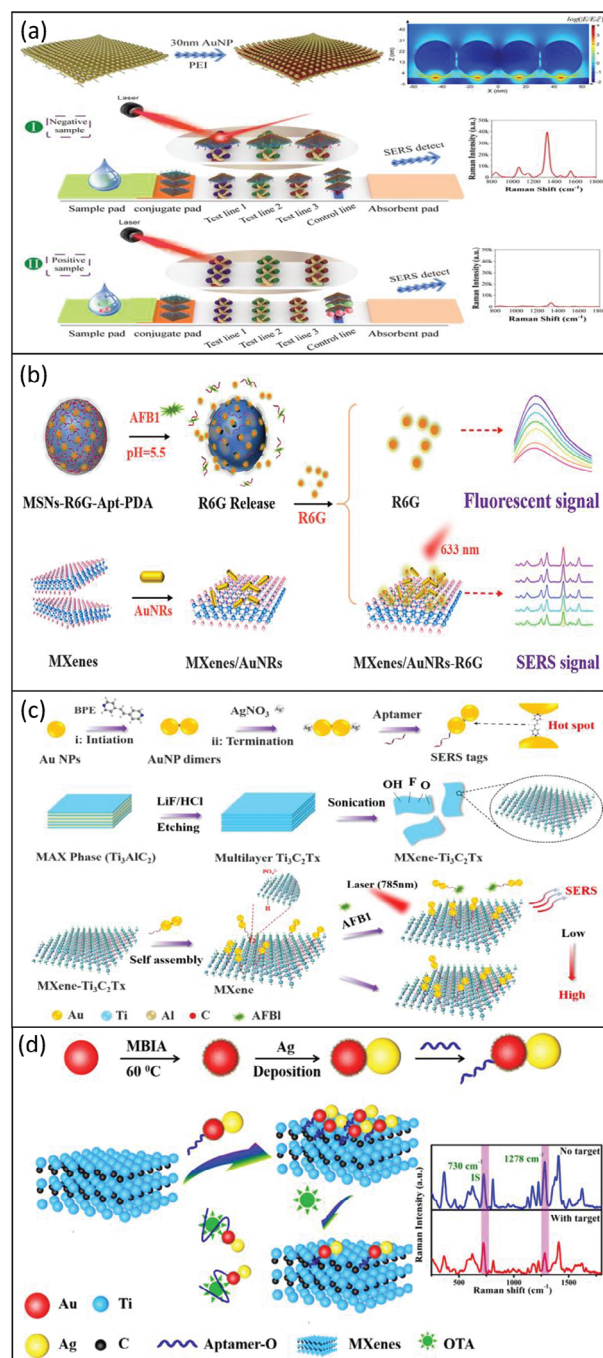


Figure 9. Fabrication of 2D materials using oxidation and etching techniques and their application to mycotoxin detection. a) Schematic diagram of the fabrication of film-type graphene oxide (GO)@Au–Au SERS nanotags and ICA strips for the multiplex detection of AFB₁, FB₁, and ZEN. Reproduced with permission.^[140] Copyright 2022, Elsevier. b) Graphical abstract of the dual signal-on biosensor based on 2D MXenes functionalized with AuNRs for the detection of AFB₁ using SERS and fluorescence. Reproduced with permission.^[142] Copyright 2023, Elsevier. c) Schematic illustration of SERS aptasensor based on MXenes/AuNP dimer assemblies for AFB₁ detection. Reproduced under the terms of the Creative Commons CC-BY license.^[141] Copyright 2021, The Authors, published by Elsevier Ltd. d) Schematic illustration of the fabrication of Raman IS-aptasensor based on MXenes Au–Ag Janus NPs for the detection of OTA. Reproduced with permission.^[143] Copyright 2019, American Chemical Society.

and river water samples were within the range of 90–114% and <13.5%, respectively.^[140] Additionally, Chen et al. developed a ratiometric SERS internal standard (IS)-aptasensor for AFB₁ detection in peanuts based on a GO–Au@Ag core–shell nanoparticle complex. Raman reporter 4-MBA was embedded in Au@Ag core–shell nanoparticles and AFB₁ aptamer conjugated to the Ag shell acted as the signal probe (Au-4MBA@AgNPs-AFB₁apt). AFB₁apt was attached to GO modified AuNPs/Indium tin oxide glass (GO/AuNPs/ITO) via π – π stacking interaction as a corrective IS and signal amplifier. A decrease in 4-MBA intensity at 1078 cm⁻¹ and unchanged GO intensity at 1330 cm⁻¹ provided a negative correlation in the ratiometric value ($I_{4\text{-MBA}}/I_{\text{GO}}$) and an LOD of 100 ng kg⁻¹. The recoveries of the sensor when applied to peanut samples were within the range of 92–103% with an RSD of 6–9%.^[134]

Although graphene has attracted more attention than any other 2D material, its simple chemistry and weak van der Waals bonding between layers in multilayer structures limit its use. Therefore, using complex or layered structures which contain two or more elements can offer new tunable properties arising from their compositional diversity and structural flexibility.^[168] Currently the number of non-oxide materials that have been exfoliated is limited to two groups, hexagonal van der Waals bonded structures (e.g., graphene and boron nitride) and layered metal chalcogenides (e.g., MoS₂, WS₂, etc.).^[169] One of the most promising classes of 2D materials under investigation is the MXenes, which are the denomination of several transition metal carbides, nitrides or carbonides typically obtained by chemical delamination of 3D ternary (or quaternary) compounds known as MAX phases.^[170] MXenes, with surface-exposed transition metal sheets, are synthesized by selective etching of A-group elements from Al components in the MAX phase, using strong acids and exfoliation techniques. For example, Ti₃C₂ layers and conical scrolls have been used to produce MXenes by exfoliating Ti₃AlC₂ in hydrofluoric acid at room temperature.^[168,169] MXenes have a unique combination of properties derived from their complex bonding (a mixture of metallic and covalent bonds) and electronic structures, atomic stacking, synthesis routes, and surface terminal groups.^[170] These include the high electrical conductivity and mechanical properties of transition metal carbides/nitrides; functionalized surfaces that make MXenes hydrophilic in nature and ready to bond to various species; high negative zeta-potential enabling stable colloidal solutions in water; efficient absorption of electromagnetic waves, high thermal stability, and surface area, which have led to numerous applications.^[171]

For the determination of AFB₁, Wu et al. combined both top-down and bottom-up synthesis techniques. First, MXenes were obtained by etching the Al component of Ti₃AlC₂ powders in hydrochloric acid (HCl). This was followed by the functionalization of MXenes with AuNR substrates through electrostatic interactions for SERS signal amplification (Figure 9b). AFB₁ was quantified with a detection limit of 0.13 ng kg⁻¹ by integrating Raman and fluorescence and recovery values of 89–107% were obtained in peanut, maize, and badam (aka almond kernel) using the approach.^[142] Additionally, Wu et al. exploited AuNP dimers and MXenes (Ti₃C₂T_x) SERS substrates obtained via selectively etching the Al component of Ti₃AlC₂ powders. The substrates were applied for detecting AFB₁ using a ratiometric SERS-based aptasensor (Figure 9c). During the procedure, 1,2-bis(4-pyridyl)

ethylene (BPE) interacted with AuNPs through Au–N bonding to trigger the assembly of AuNP dimers to form intense hot spots. Thiol-modified aptamers were immobilized onto the surface of AuNP dimers through Au–S bonds and MXenes nanosheets could bind to the aptamer-modified AuNP dimers due to hydrogen bonding and chelation between the phosphate groups of aptamers and the Ti ion of MXenes. The quantitative analysis of AFB₁ was based on the SERS ratio between AuNP dimers and MXenes (I_{1608}/I_{723}), which was negatively correlated to the AFB₁ concentration. An LOD was calculated as 600 ng kg⁻¹ with an average RSD of 6% and the recovery rates in spiked peanut samples ranged from 89% to 102% with RSD values of 4–9%.^[141] A ratiometric SERS aptasensor based on IS methods was developed for the detection of OTA by Zheng et al. who fabricated Au–Ag Janus nanoparticles assemblies with MXenes nanosheets to generate unique and stable Raman signals (Figure 9d). The assembly formation relies on hydrogen bonding and the chelation reaction between MXenes nanosheets and OTA aptamers. In the presence of OTA, Au–Ag Janus NPs are dissociated from the MXenes nanosheets due to the formation of aptamer/OTA complexes. This concentration-dependent behavior achieved an LOD of 500 ng kg⁻¹ for OTA and recovery rates in red wine between 93% and 97% with an RSD of 3%.^[143]

6. Application of Molecular Binders for the Detection of Mycotoxins

Detection limits and selectivity of SERS can also be modified or tuned by functionalizing substrates with mycotoxin specific molecular binders, such as antibodies or aptamers. Aptamer-based detection or aptasensors are commonly employed to minimize matrix interferences and improve selectivity due to the highly specific binding that can be achieved with target mycotoxins. Despite the complex design of aptamers, they may be preferable for SERS due to their high stability, longer shelf-life, and their inexpensive, rapid production in comparison to antibodies.^[172] Additionally, in contrast to commercialized colorimetric or enzymatic-based approaches, SERS can already offer several advantages including an unique spectral fingerprint for each analyte, multiplex detection capability with a single excitation laser, high sensitivity, rapidity, and accuracy.^[40,173] Therefore, SERS-based tests have the potential to become a significant upgrade on the traditional commercialized tests including enzyme-linked immunosorbent assays (ELISAs) and lateral flow tests (LFTs). The methods exploiting recognition elements (inc., aptamers and antibodies) for mycotoxin detection will be discussed in the following sections.

6.1. Aptamers

Thiolated aptamers are short synthetic oligonucleotides (\approx 20–100 nucleotide bases) designed to interact strongly with the surface of nanomaterials through Au–S bonds and can bind to a target molecule by their unique 3D structure with high affinity and specificity.^[174] For the detection of mycotoxins, AuNRs have been previously functionalized with CTAB and thiolated aptamers (ssDNA) to detect OTA. First, CTAB–AuNRs and aptamers were incubated for 1 h and second mixed with OTA solutions for 2 h, prior to SERS analysis. Uand an LOD for OTA

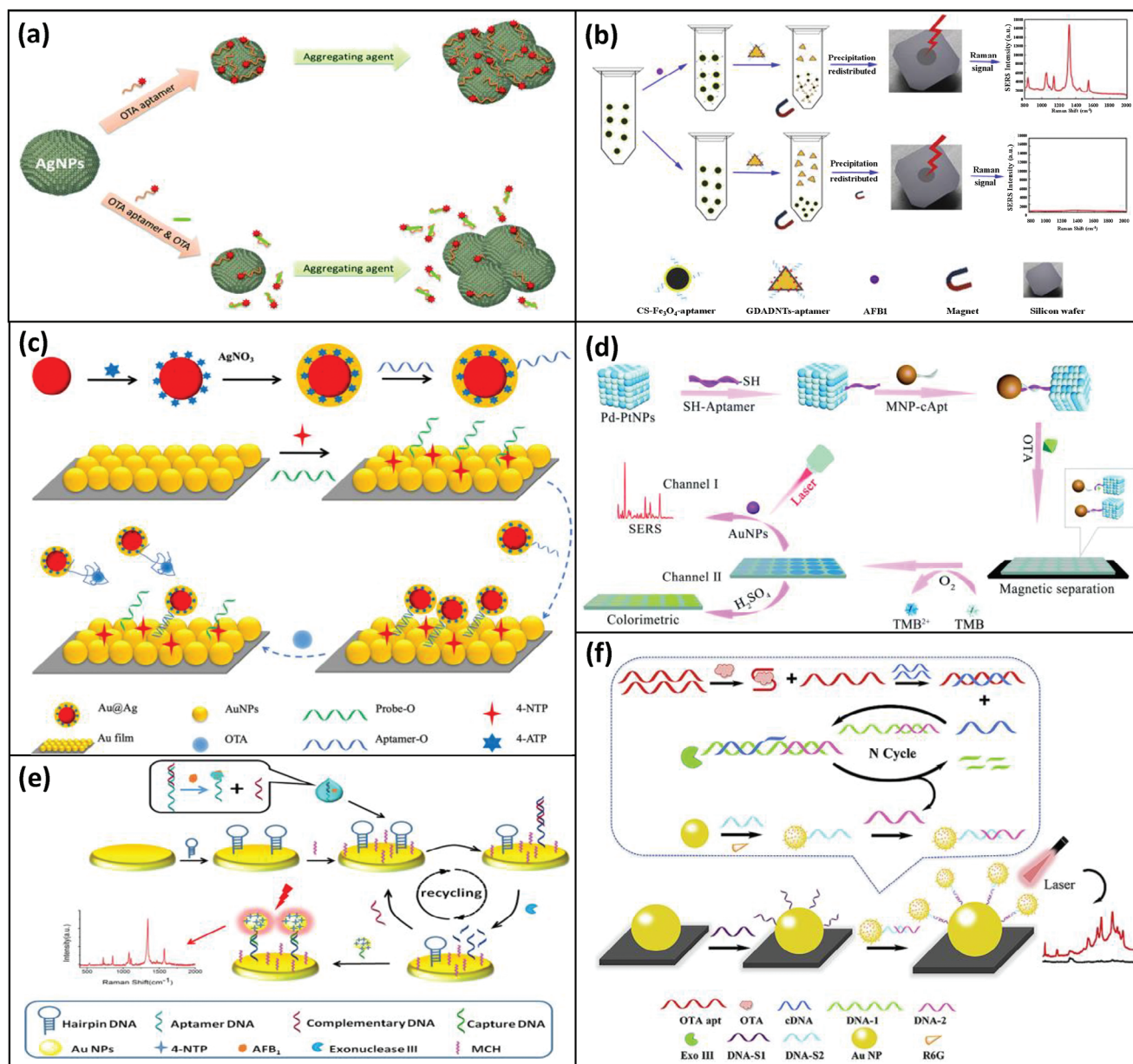


Figure 10. SERS aptasensing assays for the determination of mycotoxins in solvent and food matrices. a) Schematic diagram of SERS detection of OTA standards using Cy5-labeled aptamer on AgNPs. Reproduced with permission.^[107] Copyright 2014, Royal Society of Chemistry. b) Schematic representation of the universal SERS aptasensor designed for the trace level detection of AFB₁ in peanut oil. Reproduced with permission.^[102] Copyright 2017, Elsevier. c) Fabrication of a Au film–Au@Ag Raman IS aptasensor for the determination of OTA in red wine. Reproduced with permission.^[108] Copyright 2020, American Chemical Society. d) Schematic of nanozyme-linked apta-sorbent assay (NLASA) for the detection of OTA in red wine and grapes. Reproduced with permission.^[112] Copyright 2022, Royal Society of Chemistry. e) Schematic illustration of an SERS aptasensor based on the exonuclease-assisted recycling amplification of DNA for the detection of AFB₁ in peanuts. Reproduced with permission.^[96] Copyright 2017, Elsevier. f) Schematic illustration showing the working principle of SERS sensor based on Exo III assisted double amplification strategy for target related-signal amplification and the detection of OTA in red wine. Reproduced with permission.^[109] Copyright 2020, Elsevier.

was determined as 0.40 mg kg⁻¹.^[79] Aptamers have also been modified with Raman active dyes to indirectly monitor changes to the signal intensity acquired using SERS. As aptamer-specific recognition interactions occur with increasing mycotoxin concentrations the dye is released from the nanomaterial surface thus, leading to reduced Raman signals. Using this inverse approach, a simple and low-cost SERS-based technique was devel-

oped for the detection of OTA using AgNPs functionalized with aptamers (Figure 10a). In the absence of mycotoxin, AgNPs functionalized with Raman reporter Cy5-tagged OTA aptamers produce strong SERS signals. However, in the presence of OTA, binding is hampered leading to a decrease in SERS intensity by ≈40% and detection limits for OTA standards of 40 μg kg⁻¹ could be obtained. Although the approach was not tested in

matrix conditions thus, binding interferences could not be assessed.^[107]

For real samples, an aptasensor was first developed for the detection of AFB₁ in peanut oil. SERS substrates were based on amino-terminal aptamer conjugated magnetic beads (CS-Fe₃O₄) and DTNB-labeled Au nanotriangles (GNTs)/Ag core-shell nanotriangles (GDADNTs) and applied as capture and reporter probes for AFB₁, respectively (Figure 10b). Detection was performed in solution and afterward dried onto a Si wafer for analysis. Under optimized conditions the assay showed good sensitivity with an LOD of 500 ng kg⁻¹. The spiked recoveries for AFB₁ (1–100 ng kg⁻¹) from real peanut oil samples varied between 95% and 109%.^[102] Additionally, the same research group synthesized an IS aptasensor to further enhance the sensitivity of OTA detection in red wine (Figure 10c). Substrates were formed through the hybridization of modified aptamers on Au@Ag core-shell nanoparticles and Au films on a Si surface. The procedure took advantage of 4-ATP and 4-NTP as a Raman reporter and IS, resulting in strong SERS signals at 1078 and 1335 cm⁻¹, respectively. The intensity ratio of 1078 and 1335 cm⁻¹ was taken to quantify the OTA concentration in a ratiometric manner (I_{1078}/I_{1335}). The detection of OTA was reported with an LOD of 2 ng kg⁻¹, recoveries in red wine within the range of 96–97% and a SD within 2%.^[108]

Dual-mode assays employing aptamers have been reported as a more reliable and accurate approach compared to applying a single-mode or SERS-based assay alone, as two techniques can be used for quantification. An aptamer-based assay combining both SERS and fluorometry was developed for the determination of FB₁ in corn. The surface of platinum (Pt)-coated AuNRs is immobilized with complementary aptamer DNA (cDNA). In the absence of FB₁ the aptamer of FB₁ modified with the fluorescent dye Cy5.5, hybridizes with cDNA resulting in strong SERS and weak fluorescence. As the concentration of FB₁ increases the opposite effect occurs and the SERS and fluorescence signals begin to decrease and increase, respectively. The LOD for FB₁ was 3 ng kg⁻¹ using SERS and 5 ng kg⁻¹ for fluorescence and the recoveries in corn ranged from 92% to 107%, which were comparable to the LC-MS/MS recoveries of 91–106%.^[80] The same research group also reported a triple-mode aptasensor for the simultaneous detection of ZEN, OTA, and FB₁ in spiked corn based on SERS and fluorimetry. For the sensor, ZEN aptamer-modified upconversion nanoparticles, Cy5-modified OTA aptamer, and AuNPs were modified with Raman reporter 4-MBA and cDNA, or FB₁ aptamer. In the presence of FB₁, FB₁ aptamer modified AuNP separated from the trimer assembly leading to a decrease in SERS signal. The LOD of the developed aptasensor for ZEN, FB₁, and OTA was calculated as 30, 0.02, and 10 ng kg⁻¹, respectively, and the recoveries in corn were within the range of 90–107%.^[113] Furthermore, a dual-mode sensor based on colorimetry, and SERS was reported using a nanozyme-linked aptasorbent assay (NLASA) for the detection of OTA in red wine and grapes using a portable Raman spectrometer (Figure 10d). The NLASA system consisted of palladium (Pd)-Pt bimetallic nanocrystals, which could catalyze the conversion of substrate 3,3',5,5'-tetramethylbenzidine (TMB) to an oxidized blue colored product. The Pd-Pt nanocrystals and MNPs were functionalized with aptamers as recognition and capture probes, respectively. After mixing, the probes were washed using an external magnet and incubated with OTA at varying concentrations, followed by

TMB and AuNPs to initiate the catalytic reaction. The LOD for OTA using the colorimetric and SERS approach was 0.039 and 0.017 μg kg⁻¹, respectively. Recoveries and RSDs for red wine and grapes were in the range of 83–95% and 1.3–9.5% for the SERS method, respectively.

Exonuclease III (Exo III) is a sequence-independent nuclease that specifically hydrolyses mononucleotides from its blunt end (5'-overhangs or nicks of duplex DNA),^[175] gradually catalyzing the stepwise removal of mononucleotide from the 3' hydroxyl termini of duplex DNAs and releasing the complementary strand intact.^[176] The advantage of incorporating Exo III is that the selective nucleotide digestion may be utilized as a catalytic tool for DNA amplification thus, leading to the recycling of recognition events, significant enhancement of detectable signals and higher sensitivity.^[96] An SERS-based aptasensor was developed based on the exonuclease-assisted recycling amplification for the determination of AFB₁ in spiked peanut samples (Figure 10e). On recognition of AFB₁, the aptamer was released and immediately hybridized with hairpin DNA on the surface of Au coated glass slides. Exonuclease III hydrolyzed the dsDNA, leaving short ssDNA on the Au surface and releasing complementary DNA for the next ring opening and digestion. SERS tags prepared using AuNPs and 4-NTP were captured on the Au surface by hybridization, thus high selectivity, and sensitivity for AFB₁ was achieved. The LOD for the aptasensor was 0.4 pg kg⁻¹ and the recoveries for peanut samples were in the range of 89–121%.^[96] Additionally, Exo III was also employed in an assisted double amplification strategy for the detection of OTA in spiked red wine samples (Figure 10f). The procedure was based on target related-signal amplification, combined with core-satellite assemblies for the formation of “hot-spot” induced signal amplification. Core-satellite assemblies were fabricated by modifying 100 nm quasi-spherical AuNPs with DNA-S1 on a Si substrate to produce SERS substrates. The SERS nanotag was produced by functionalizing AuNPs with DNA-S2 and R6G. Exo III digests cDNA-DNA from DNA-1 thus, releasing cDNA and DNA-2, which is used to link the core-satellite assemblies. In the presence of OTA, the distance between the nanoprobe and substrate is increased thus, the SERS intensity of R6G at 613 cm⁻¹ is reduced due to decreasing hot spots. An LOD of 0.8 pg kg⁻¹ was reported and recoveries in red wine were within the range of 96–106% with an RSD between 6% and 9%.^[109]

Furthermore, Exo III-assisted target cycle amplification combined with the SERS enhancement of Au nanostar-Au core-shell nanostructures led to a remarkable increase in sensitivity for the detection of OTA in spiked red wine samples. The “turn-on” mode SERS aptasensor was developed by fabricating 4-MBA-labeled AuNS as the core, followed by the growth of a Au layer using ascorbic acid (AA). The structure was employed as a Raman reporter and the SERS nanoprobe was prepared by immobilizing signal DNA (sDNA) to the surface of the AuNS@4-MBA@Au core-shell nanostructure (sDNA-modified AuNS@4-MBA@Au) and hairpin DNA (HpDNA) to streptavidin magnisphere paramagnetic particles (PMPs) (HpDNA-modified PMPs). The procedure involves the hybridization of OTA-aptamer with cDNA to form a dsDNA complex. In the presence of OTA standards or a spiked sample solution, the cDNA is released and hybridized to form dsDNA in the presence of HpDNA-modified PMPs. The 3' end of HpDNA is digested by Exo III releasing cDNA and leaving

short ssDNA on the surface of PMPs. The released cDNA would further hybridize with HpDNA to achieve target cycle amplification. Finally, the short ssDNA on the surface of PMPs would hybridize with sDNA on the surface of AuNS@4-MBA@Au to form assemblies which are analyzed after magnetic separation and the SERS signal is observed. The intensity could be positively correlated to the concentration of OTA and the LOD of the “turn-on” aptasensor was determined to be 0.25 pg kg⁻¹. The recoveries and RSDs in wine samples were within the range of 95–111% and 11–14%, respectively.^[114]

6.2. Antibodies

The immobilization of antibodies on the surface of nanomaterials is conducted through noncovalent (e.g., electrostatic, hydrophobic or van der Waals forces) or covalent interactions. Different chemistries can be used to form covalent bonds due to the presence of free amines (NH₂) and thiol (–SH) groups in the antibody chain. Commonly carbodiimide chemistry following the widely used EDC/NHS coupling method is performed. During this procedure, an amide bond is formed between the carboxylic group (–COOH) and the free NH₂ groups in the antibody and maleimide conjugation with –SH groups. The sensitivity and overall performance of the immunosensor depends on the correct orientation of the antibody to ensure recognition sites are accessible. Additionally, a high density of grafted moieties per unit of nanoparticle surface area will help to prevent nonspecific interactions.^[177] Exploiting EDC/NHS chemistry, antibodies were functionalized with bipyramid Au nanocrystal–Au nanoclusters (BPGN/GNC) as a dual-mode optical probe. The SERS-fluorescence spectral encoding was used for the simultaneous detection of AFB₁, AFB₂, AFG₁, AFG₂, AFM₁, and AFM₂. The technique describes an immunoassay conducted on glass slides prepared in poly(ethyleneimine) and 2% glutaraldehyde solution. The sandwich immunoassay was conducted using antibodies specific to each AF, antibody-conjugated BPGN/GNC, and 4-ATP as a Raman reporter. An LOD of 3 pg kg⁻¹ was reported using AF standards and no matrix was tested during the procedure.^[92]

For the detection in real matrix, a competitive SERS-based immunoassay was developed for the detection of ZEA in animal feed samples (Figure 11a). For the assay, AuNPs were labeled with Raman reporter 4,4'-dipyridyl and conjugated with ZEA antibodies (ZEA-mAb) and capture substrates were modified with ZEA-BSA. In the presence of free ZEA, binding with ZEA-mAbs labeled on AuNPs resulted in enhanced SERS intensity and detection limits of 1 ng kg⁻¹ were achieved with an RSD of 7–13%.^[117] For multiplexed detection of mycotoxins, a microarray SERS-based immunosensor was developed to simultaneously detect AFB₁, ZEA, and OTA in corn, rice, and wheat. AuNPs were labeled with Raman reporter dithiobis(succinimidyl-2-nitrobenzoate) (DSNB) and covalently linked with anti-AFB₁, anti-ZEA, and anti-OTA as SERS nanoprobables. Additionally, AFB₁-BSA, ZEA-BSA, and OTA-BSA were covalently linked onto a microarray Au-coated glass slide as capture substrates (Figure 11b). The assay design allowed for three independent immunoreactions multiplexed on a single Au chip and after optimization the LODs for AFB₁, ZEA, and OTA were between 0.053

and 0.29 μg kg⁻¹ and recoveries in matrix ranged from 84% to 108% with a CV below 15%.^[97] Additionally, a multiplex SERS array based on AuNPs-loaded inverse opal silica photonic crystal microsphere was fabricated for the detection of three mycotoxins: OTA, FB₁, and DON in corn, rice, and wheat. The principle of this technique relied on three Raman nanotags synthesized by covalently drafting mycotoxin specific antibodies and noncovalently loading different organic dyes NBA, crystal violet or methylene blue onto the AuNPs as labels to code for corresponding mycotoxins (Figure 11c). The LOD was calculated to be 2 μg kg⁻¹ for OTA, 0.2 μg kg⁻¹ for FB₁, and 70 μg kg⁻¹ for DON and the recoveries were between 71% and 118% and intra- and intervariation coefficients were calculated between 5% and 14%.^[115]

The portable detection of two mycotoxins, AFB₁ and OTA in corn, wheat, and rice was reported by Chen et al. who fabricated Au@SiO₂ SERS nanotags encoded with Raman reporters (4MBA and DTNB). The nanotags were functionalized with mycotoxin specific antibodies to develop an LFA with a single test line (T line) (Figure 11d). During the competitive immunoassay the color change of the T line indicates the presence of target analytes through visual inspection. Additionally, SERS could quantify both mycotoxins by measuring the peak intensity from the T line using a portable Raman spectrometer. The LOD for AFB₁ and OTA was 0.24 and 0.37 ng kg⁻¹ using the approach and recoveries from spiked agricultural samples were within the range of 87–112%.^[104] Furthermore, the multiplexed, portable analysis of six mycotoxins: AFB₁, DON, ZEA, FB₁, OTA, and T-2 in maize samples was developed by Zhang et al. using an SERS-based lateral flow immunosensor, which utilized dual Raman labels and triple test lines (Figure 11e). In this approach, two Raman reporter molecules, DTNB and 4-MBA, were used to label Au@Ag core-shell nanoparticles for the preparation of SERS nanoprobables. Monoclonal antibodies for each mycotoxin were conjugated to the DTNB-Au@AgNP (anti-AFB₁ mAb, anti-FB₁ mAb, and anti-OTA mAb) or to the MBA-Au@AgNP (anti-ZEA mAb, anti-DON mAb, and anti-T2 mAb). To prepare the LFT strip, antigens and secondary antibodies were dissolved and immobilized onto nitrocellulose membrane as capture elements. Three combinations of antigens (1: AFB₁-BSA and ZEA-BSA, 2: OTA-BSA and T2-BSA, 3: FB₁-BSA and DON-BSA) were applied to create three test lines on the nitrocellulose membrane and goat anti-mouse secondary antibody was applied to the control line. The LOD for AFB₁, ZEA, FB₁, DON, OTA, and T-2 were between 1 and 260 ng kg⁻¹. Additionally, the recovery values were between 79% and 106% and the CV was <16%, highlighting the accuracy of the immunosensor for analysing real maize samples.^[100]

6.3. Molecularly Imprinted Polymers

Molecular imprinting allows the creation of artificial recognition sites in synthetic polymers, tailor-made in situ by co-polymerization of functional monomers and cross-linkers around the template molecule. The print molecules are extracted from the polymer, leaving accessible complementary binding sites within the polymeric network, and have the advantages of high selectivity, good predictability, and versatility.^[148,178] The

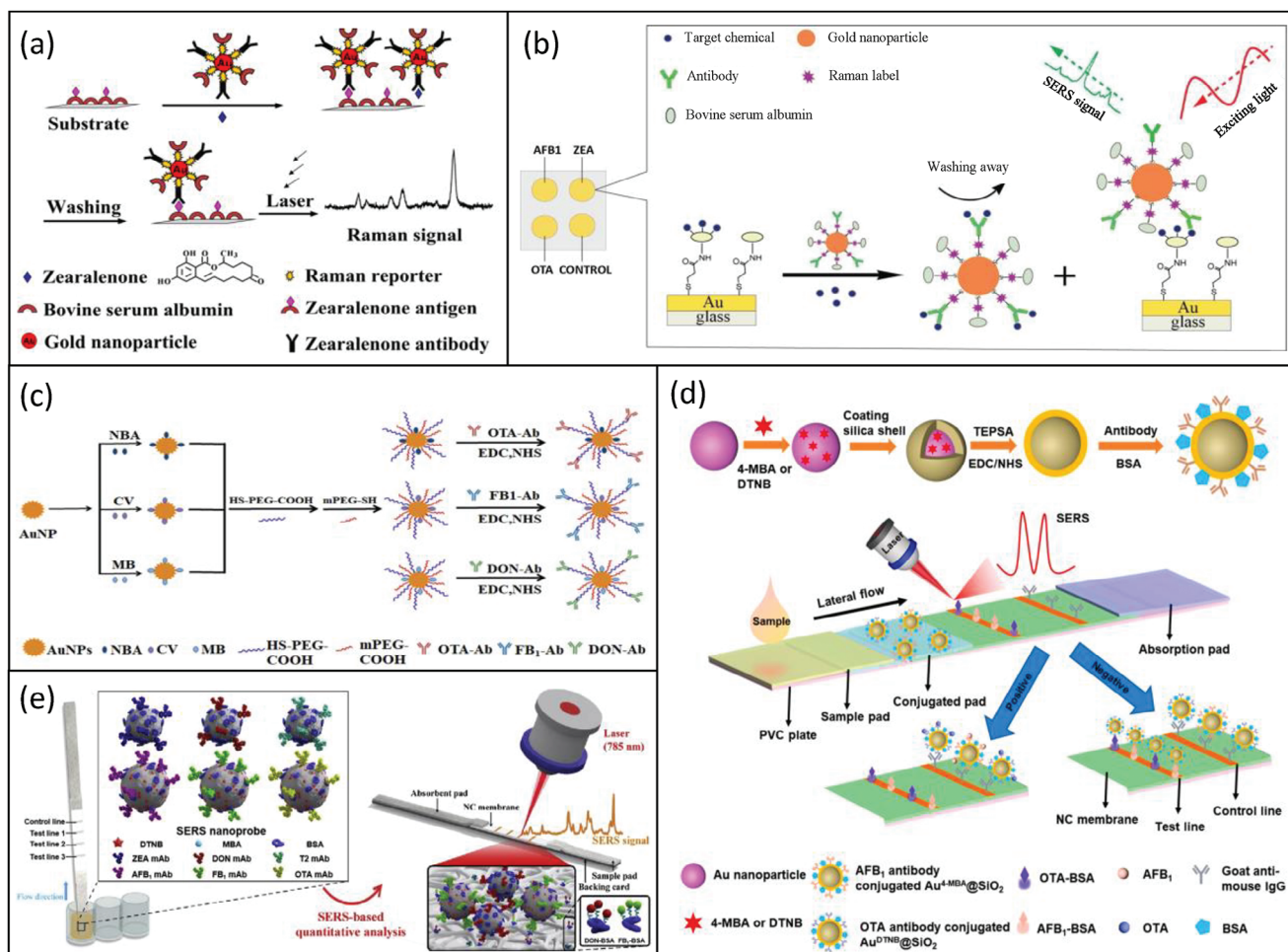


Figure 11. SERS-based immunosensors for the determination of mycotoxins in food and feed samples. a) Preparation of SERS nanoprobes and a competitive SERS immunoassay for the detection of ZEA in feed samples. Reproduced with permission.^[117] Copyright 2014, American Chemical Society. b) Schematic illustration of multiplex SERS-based immunosensor for the detection of AFB₁, ZEA, and OTA in corn, wheat, and rice. Reproduced with permission.^[97] Copyright 2018, Elsevier. c) Preparation of SERS nanotags for the immunological detection of OTA, FB₁, and DON in wheat, corn, and rice. Reproduced with permission.^[115] Copyright 2022, Elsevier. d) Schematic illustration of the preparation of antibody conjugated nanotags and the competitive SERS lateral flow assay (LFA) assembly for the simultaneous detection of AFB₁ and OTA in corn, rice, and wheat. Reproduced with permission.^[104] Copyright 2023, Elsevier. e) Illustration of multiplex SERS-based lateral flow immunosensor for the detection of six mycotoxins (ZEA, AFB₁, DON, FB₁, T-2, and OTA) in maize. Reproduced with permission.^[100] Copyright 2020, Elsevier.

detection of PAT was achieved using a molecular imprinted AuNP (MIP-ir-AuNPs) SERS sensor. To obtain the MIP-ir-AuNP SERS substrate, AuNPs were first modified with horseradish peroxidase enzyme (HRP) (AuNPs-HRP), and the imprinted polymer was synthesized by combining 4-vinylpyridine (4-VP), 1,4-diacryloylpiperazine (PDA) followed by the addition of AuNPs-HRP. After the addition of PAT, the Raman intensity at 1205 cm⁻¹ increased with increasing concentrations, which could be attributed to the recognition cavities within the polymer shell offering functional groups to bind with the PAT molecule. The LOD of MIP-ir-AuNPs for PAT detection was calculated as 800 ng kg⁻¹ demonstrating high sensitivity. Blueberry sauce, grapefruit sauce, and orange juice were spiked to determine the feasibility of the MIP-ir-AuNPs in real samples and recoveries were between 96% and 101%.^[54] Additionally, an enzyme-induced MIP SERS substrate for the determination of PAT was developed. The solid substrate was prepared using PDMS solidified

on AAO to form a flexible transparent elastomeric polymer. After removal of Al, the template was sputtered with AuNPs to obtain Au/PDMS/AAO SERS substrate and HRP was immobilized on the surface. The MIP-SERS substrate was prepared using 4-VP as a functional monomer, PDA as a cross-linker, and PAT as a template. After the optimization of solvent, pH and incubation time the LOD for PAT using the MIP-SERS substrate was 10 ng kg⁻¹. Reproducibility and stability tests were performed using SERS signals from five different batches of the MIP-SERS substrate and the RSD was ≈5%. The applicability of the SERS substrate was confirmed using spiked blueberry jam, grapefruit jam, and orange juice with recoveries between 96% and 113% and an RSD of 5–8%.^[148] In both works, the MIP-SERS substrate also demonstrated high selectivity for PAT by testing in the presence of interferences including 2-oxindole (OXD) and 5-hydroxymethylfurfural (5-HMF).

6.4. Other Affinitive Binders

The surface functionalization of nanomaterials applies to the use of covalent and noncovalent bonds to integrate organic (e.g., citrates, phosphates, amines, thiols, and polymers including chitosan, PEG, dextran, streptavidin) and inorganic (e.g., silica, metals, and metal oxides) molecules at the nanoscale.^[179] For the first time, AOH concentrations were determined in pear fruit using AgNP substrates modified with pyridine to improve affinity interactions between AOH molecules and the surface of the Ag-NPs. The SERS method performed satisfactorily with an LOD of $1.3 \mu\text{g kg}^{-1}$ within the concentration range of $3\text{--}316 \mu\text{g kg}^{-1}$. Additionally, the approach was applied to detect AOH residues in pear fruit purchased from markets and pear fruits that were artificially inoculated with *Alternaria alternata*. AOH was not found in any of the analyzed fresh fruit but resided in both the rotten and inoculated fruits. The recoveries ranged from 70% to 111% while RSDs were assessed using five replicates of the same spiked samples and were between 14% and 18%.^[57]

The functionalization of SERS substrates with polymer affinity agents (PAA), poly(*N*-(2-aminoethyl methacrylamide) (pAEMA) and poly(2-hydroxyethyl methacrylate) (pHEMA) have been explored alongside isothermal titration calorimetry (ITC) as an affinity screening method for AFB₁. Different polymer chain lengths were studied as AFB₁ capture agents using both ITC and SERS. Au film over nanospheres (FONs) were applied as stable SERS substrates and were functionalized with PAAs. Intrinsic vibrational bands attributable to AFB₁ upon interaction with substrate-bound affinity agents were examined. DFT and PCA were also performed to determine clustering and separation and to identify spectral differences between the polymer, polymer in solvent, and the polymer exposed to 50 mg kg^{-1} of AFB₁. The results also determined that pHEMA performed better than pAEMA as an SERS capture substrate.^[93] Further work by the same group explored the use of a new PAA, poly(*N*-acryloyl glycylamide) to directly detect AFB₁ using a FON wafer as an SERS substrate. The FON was fabricated using nanosphere lithography and serves as anchoring substrates for PAA with different chain lengths to capture AFB₁. It was hypothesized that a surface-bound polymer may lack sufficient conformational mobility to enable optimal target binding. Therefore, the interactions were first applied in solution prior to adding to the Au FON surface. Coupling capture agents combined with ITC and computational analysis (one-way ANOVA and Tukey post hoc) allowed an LOD of $10 \mu\text{g kg}^{-1}$ to be determined.^[94] Additionally, the detection of DON and OTA was explored by capturing mycotoxins on a linear methacrylamide PAA. The advantage of applying PAA interactions in solution, is that it is more flexible thus, enabling optimal polymer–target binding. DFT was exploited to predict the vibrational information of the mycotoxins and the association between polymer, target, and FON. DON and OTA were detected at 1 mg kg^{-1} and $5 \mu\text{g kg}^{-1}$, respectively, both individually and simultaneously and were visibly distinguishable without chemometric analysis.^[111] This work highlights the importance of surface functionalization to help facilitate binding interactions with the nanomaterial surface and improve detection sensitivity, selectivity, and reproducibility, particularly when chemometrics are not being exploited.

7. Chemometrics and Machine Learning for the Detection of Mycotoxins

It can often be difficult to decipher differences in sample spectra by eye, particularly when analysing complex food or feed matrices, where interfering compounds may also mask the SERS signal from target mycotoxins. This becomes even more challenging when multiple contaminants share similar structures or when the target contaminant is present at extremely low levels. Additionally, variations in the orientation and proximity between the target molecules and the SERS substrates further complicate the detection process. Chemometrics use multivariate statistical methods to extract chemical information from high dimensional data. For example, observing differences in sample spectra or detecting contaminants at trace levels. Sensitivity and sample handling procedures often receive much attention from researchers and industry alike. However, the implementation of novel data processing methods including chemometrics (e.g., PCA, PLS, and MCR) and machine learning techniques (e.g., support vector machine (SVM), artificial neural network (ANN), random forest (RF), convolutional neural network (KNN)) are now at the forefront of research to overcome some of the common challenges faced during SERS-based procedures. The most common artifacts in SERS are baseline deviations, fluorescence, misalignment, and noise resulting from spectral overlap, suppressed SERS signal in complex matrices, and poor sensitivity at trace levels.^[180] Powerful statistical methods are often required to distinguish minimal key differences and features in spectral information that cannot be ascertained through visual inspection. There are several key stages to developing robust chemometric models including data preprocessing, generation of qualitative or quantitative models and validation of models using external datasets (those which have not been required to build the model).^[181] Those studies which have investigated SERS combined with chemometrics for the determination and differentiation of mycotoxins are highlighted in **Table 4**.

For the determination of mycotoxins, spectral pre-processing methods such as multiple scattering correction (MSC), Savitzky–Golay (S–G), standard normal variate (SNV), and 1st and 2nd derivatives, followed by unsupervised (e.g., PCA) and supervised (e.g., OPLS, PLS and BP-AdaBoost, KNN, LDA) classification modeling or regression/quantification modeling (e.g., MLR, PLSR, and PCR) have all been explored. The typical experimental procedure for SERS and the process for developing statistical models using chemometrics or machine learning are summarized in **Figure 12**. The pre-processing of spectral information prior to the development of models normally involves smoothing, light-scattering correction, spectral baseline correction and normalization.^[182] S–G filtering can help to smooth Raman spectral information and improve signal-to-noise ratio thus, helping to retain useful spectral information.^[183] MSC and SNV are two light-scattering correction techniques conducted to amplify desirable information in the spectra, whilst also reducing undesirable information, thus differences relating to the chemical nature of the sample can be observed clearly.^[184] Spectral differentiation methods including, 1st and 2nd derivatives can help to eliminate baseline drift and other background interferences thus, strengthening characteristic bands and improving overlapping

Table 4. SERS approaches exploiting chemometrics and machine learning algorithms for mycotoxin determination.

| Mycotoxin | SERS substrate | Chemometric analysis | Matrix | Validation | Portable (Y/N) | Refs. |
|---|--|------------------------------------|---|---|----------------|-------|
| AFB ₁ , AFB ₂ , AFG ₁ , AFG ₂ | Ag nanosphere | PCA, PLS, KNN, LDA, MLR, PCR, PLSR | Maize | LOD = 13–36 µg kg ⁻¹ | N | [72] |
| FUMs | Ag dendrites | KNN, LDA, PLSDA, PCA, MLR, PLSR | Maize (naturally contaminated) | LOD = 1–209 mg kg ⁻¹ | N | [47] |
| AFB ₁ , DON, ZEN | AuNPs and polydimethylsiloxane coated AAO (PDMA@AAO) complex | PCA | Maize | LOD = 2–48 µg kg ⁻¹ RSD = 5% Recovery = 93–120% | N | [49] |
| OTA, AFB ₁ | AgNPs with different pH | GA-PLS, CARS-PLS | Cocoa beans | LOD = 3–4 ng kg ⁻¹ Recovery = 97–119% CV = 1–7% | N | [95] |
| OTA | AgNPs and Au slide | PLS | Wine, wheat | LOD = 0.01–1 mg kg ⁻¹ CV = 2–4% | N | [73] |
| AFB ₁ | Pre-etched Ag nanocluster | DFT, PLS, BP-AdaBoost | Peanut oil | LOD = 5 µg kg ⁻¹ Recovery = 90–113% RSD = ≈5% | Y | [106] |
| PAT, AOH | Gold nanorod (AuNR) | DFT, PLS | Apple juice | LOD = 1 µg kg ⁻¹ LOD matrix = 1 mg kg ⁻¹ Recovery = 82–115% | N | [119] |
| DON | AgNPs | DFT | Corn, oats, kidney beans (naturally contaminated) | LOD = 30 µg kg ⁻¹ LOD matrix = 0.3–30 mg kg ⁻¹ | Y | [116] |
| AFB ₁ , AFB ₂ , AFG ₁ , AFG ₂ | Gold nanoparticles (AuNPs) | DFT | Peanuts | LOD = 2–4 mg kg ⁻¹ Recovery = 88–114% | Y | [70] |
| AFB ₁ , AFB ₂ , AFG ₁ , AFG ₂ | Silver nanorod (AgNR) array | PCA, DFT | Solvent | LOD = 1.6–33 mg kg ⁻¹ | N | [42] |
| Citrinin | AgNPs | DFT | Solvent | LOD = 0.25 mg kg ⁻¹ | N | [51] |
| AFB ₁ | Au film over nanospheres (AuFONs)-anchored polymer affinity agents | PCA, DFT | Solvent | LOD = 50 mg kg ⁻¹ | N | [93] |
| OTA | Thermal evaporation of Au on glass slide | PCA, OPLS, PLS | Solvent | LOD = 4 ng kg ⁻¹ | N | [144] |
| AFB ₁ | Film over nanosphere (FON) wafer and linear polymer affinity agent | DFT | Solvent | LOD = 10 µg kg ⁻¹ | N | [94] |
| DON, FB ₁ | Nanopillar arrays fabricated by two-photon polymerization | PCA | Solvent | LOD = 1–1.25 mg kg ⁻¹ | N | [146] |
| DON, OTA | Film over nanospheres (FONs) and linear polymer affinity agents | DFT | Solvent | LOD = 0.005–1 mg kg ⁻¹ | N | [111] |
| AFB ₁ , ZEN, AOH, FB ₁ | Carbon nanostructures | PCA | Solvent | LOD = 1–3 µg kg ⁻¹ | N | [135] |
| OTA | Label-free Au nanoprism aptasensor (AuNT@Apt@MPA) | PLS | Coffee, wheat | 10 µg kg ⁻¹ | Y | [77] |

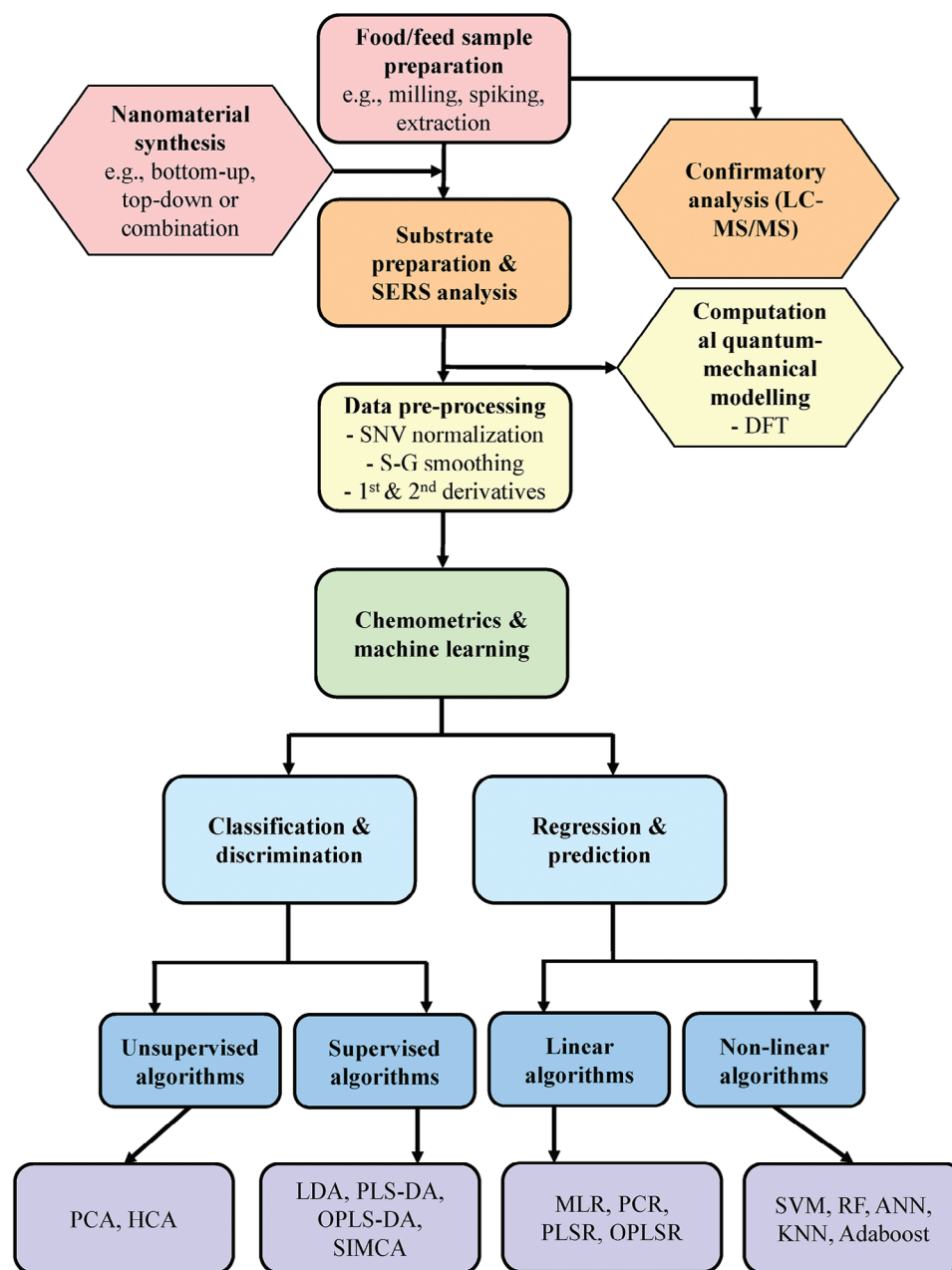


Figure 12. Summary of the overall SERS experimental procedure and development of models using classification and regression algorithms to determine mycotoxins in food and feed.

bands, which is crucial to find the distinctive features amongst the Raman spectra of a complex sample.^[183]

Supervised models can be split into either classification techniques or regression models, which are required to make qualitative and quantitative predictions, respectively.^[185] Classification modeling can be further split into unsupervised or supervised methods. Unsupervised methods are based on the identification of sample interrelationships without prior information about class membership.^[186] PCA reduces the dimensionality of the data by identifying the principal components (PC) with the most variance (e.g., PC1 and PC2). It does not utilize labels

or user-defined information but can be used as an exploratory type of analysis to visualize similarities and differences between groups of data. Thus, allowing relationships, structure, grouping, separation, and outliers to be easily detected.^[185,187] However, as PCA can only be used to explore original trends in the data it cannot be used to make predictions on new external observations. Supervised techniques including LDA, PLS-DA, and orthogonal partial least squares-discriminant analysis (OPLS-DA) consider information about the membership of samples to a certain group (class or category), with all samples labeled prior to the generation of prediction models. Thus, unknown samples can

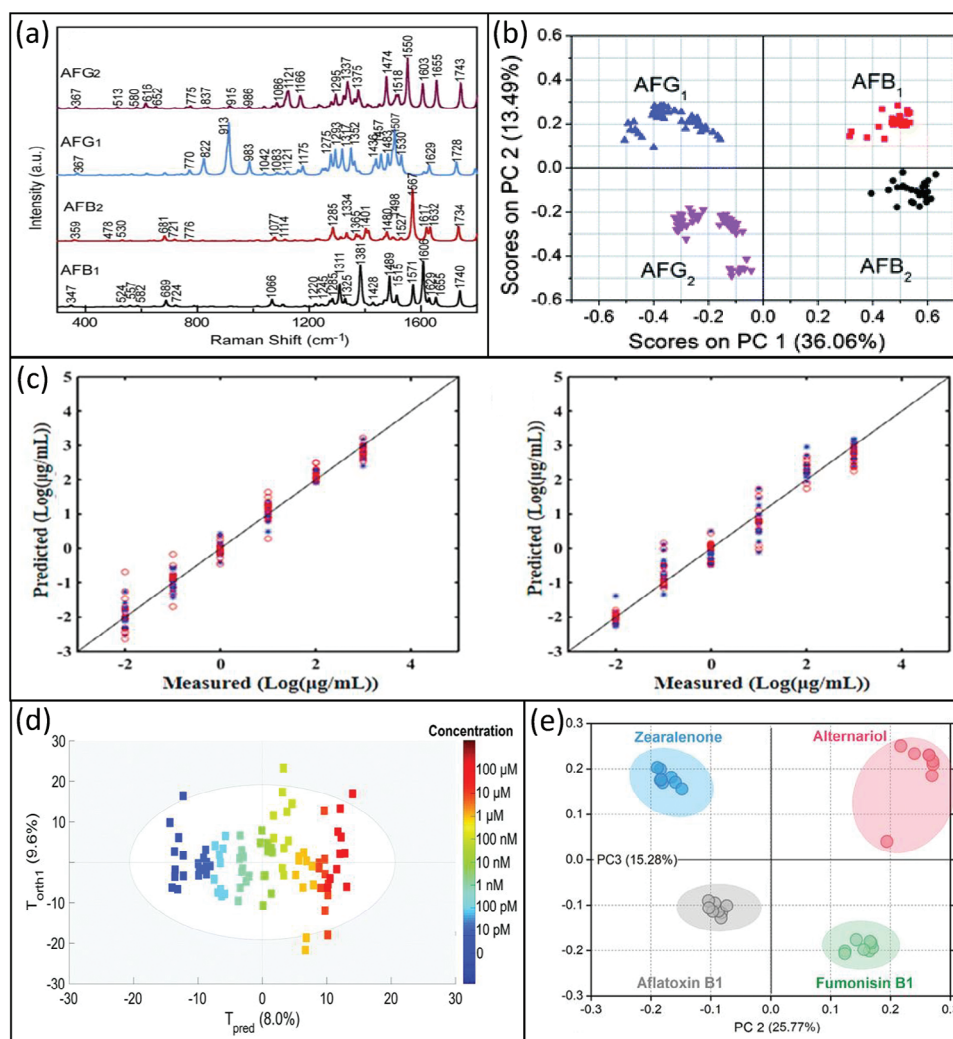


Figure 13. Computational and chemometric modeling techniques exploited for the determination of mycotoxins using SERS. a) DFT calculated Raman spectra of AFs. Reproduced with permission.^[70] Copyright 2018, Elsevier. b) PCA score plot of four AFs. Reproduced with permission.^[42] Copyright 2012, Royal Society of Chemistry. c) SiPLS and GA-PLS modeling for the quantitative detection of PAT and AOH, respectively. Reproduced with permission.^[119] Copyright 2021, Elsevier. d) OPLS score plot for the determination of OTA at different concentrations. Reproduced with permission.^[144] Copyright 2017, Royal Society of Chemistry. e) PCA of mathematically produced vibrational spectra of ZEN, ALT, FB₁, and AFB₁. Reproduced with permission.^[133] Copyright 2021, John Wiley & Sons.

be classified as one of the known classes based on their chemical composition.^[188] Predictions on external or unknown datasets can be obtained through cross-validation strategies. Additionally, regression models including MLR, PCR, and PLSR are used to study the linear relationship between a group of independent variables and a dependent variable, or set of dependent variables, and are intended to facilitate the quantitative analysis of target analytes.^[189]

DFT is a computational quantum mechanical modeling procedure used to determine the theoretical distribution of Raman scattering peaks. It allows important information to be obtained regarding spectral positions, spectral shifts in respect to normal Raman bands, intensities of the observed bands, identification of molecular sites involved with specific interactions and information on the nature of the surface active sites.^[190] DFT has previously been exploited to investigate the theoretical spec-

trum of mycotoxins; CIT,^[51] AFs^[70] (Figure 13a), DON,^[111,116] and OTA.^[111] DFT has also been applied alongside unsupervised chemometric modeling techniques such as PCA for the determination of AFB₁, AFB₂, AFG₁, and AFG₂^[42,93] (Figure 13b). Separation and clustering could be observed using either 1st and 2nd, or 2nd and 3rd PCs of the PCA score plot thus, highlighting spectral differences between the toxins. Additionally, DFT was employed to determine PAT and AOH in apple juice. The spectra was pre-processed using MSC, S–G smoothing, SNV, 1st and 2nd derivative prior to the development of algorithms synergy interval (Si)-PLS, genetic algorithm (GA)-PLS, and UVE-PLS. Comparing PLS models, the best performance was obtained using Si-PLS ($R_c = 0.9905$, $R_p = 0.9759$) and GA-PLS ($R_c = 0.9829$, $R_p = 0.9808$) for PAT and AOH, respectively^[119] (Figure 13c). Furthermore, the SERS spectra of peanut oil were recorded, and its respective theoretical spectrum was calculated by DFT to assign characteristic

peaks to AFB₁. Spectral pre-processing methods SNV, 1st derivative and 2nd derivative were conducted to eliminate or minimize interferences within the raw spectra, followed by multivariate calibration methods linear PLS and nonlinear BP-AdaBoost for chemometric modeling. The PLS model gave a high RMSEP leading to low prediction accuracy. BP-AdaBoost exhibited optimum prediction ability ($R_p = 0.9283$ and 0.9332) within the concentration range of 5–100 and 100–1000 $\mu\text{g mL}^{-1}$.^[106] Those which have exploited DFT and statistical models have typically used less complicated SERS substrates mainly fabricated of Au^[70,119] or Ag^[51,116] using bottom-up approaches. These substrates can be more prone to interferences from nontargeted compounds, matrix effects, and reduced sensitivities as the particles are left bare or unfunctionalized. Therefore, to help determine the spectral features of target analytes within a complex matrix, theoretical modeling techniques are advantageous.

For singleplex applications, OTA in solvent was not distinguishable by eye but could be determined using statistical models PCA, PLS, and OPLS^[144] (Figure 13d). The R^2 and Q^2 values for the developed OPLS model were 0.990 and 0.897, respectively, indicating that the model is robust and does not depend on the dataset. Additionally, OTA could be determined in wine and wheat by employing PLS regression models to analyze results and decipher the obtained spectral information, with a correlation factor and CV between $R = 0.9257$ – 0.9938 and 2–4%, respectively.^[73] Additionally, OTA was determined in coffee and wheat samples by pre-processing the spectra using S–G and 2nd derivative smoothing, MSC normalization and GLSW de-cluttering, followed by the development of a calibration curve using PLS regression. Acceptable predicted values ($R^2 \text{ cal} = 0.999$) and blind cross-validation ($R^2 \text{ CV} = 0.917$) were obtainable using these modeling techniques.^[77] Furthermore, DON and FB₁ could be determined in ACN using unsupervised PCA modeling with 86% variance and the two mycotoxins could be identified using the 2nd and 3rd PCs.^[146] However, a common issue for SERS is spectral overlap within complex mixtures. Therefore, multiplex applications requiring the identification of two or more mycotoxins within a mixture may benefit further by exploiting statistical algorithms.

The rapid detection of four mycotoxins AFB₁, AFB₂, AFG₁, and AFG₂ in maize was one of the first methods to confirm its practicality in matrix conditions alongside the development of models KNN, PCR, PLSR, and MLR.^[72] For classification, KNN alongside four pre-processing techniques was applied to the Raman shift region 400–1800 cm^{-1} . KNN was selected as it outperformed other chemometric methods including LDA, PLS, and PCA in other studies performed by the authors. The KNN models which offered the highest level of classification accuracy in determining AF contaminated samples were obtained using normalized (82.9%) and deconvolution (91.4%) spectral data. While those developed using 1st (74.3%) and 2nd (71.4%) derivatives experienced higher error rates in terms of misclassification rate. To quantify levels of AF, MLR led to a substantial improvement in regression quality, predictive accuracy, and lower error rate than other chemometric models, while PCR demonstrated less satisfactory results compared to MLR and PLSR models. The MLR models demonstrated higher p values and stronger correlation coefficients ($r = 0.906$ – 0.967) with the HPLC reference values than PLSR and PCR models, indicating that the MLR models

produced more comparable results to the HPLC method at the AF levels tested. The LOD and LOQ of the MLR model were within the range of 13–36 and 44–121 $\mu\text{g kg}^{-1}$, respectively, indicating that the models are more sensitive for the quantification of AFs in maize. Additionally, two chemometric algorithms were developed for the prediction of OTA and AFB₁ in spiked cocoa bean samples. The acquired spectra were pre-processed using SNV, MSC, and 1st derivative followed by GA-PLS and CARS-PLS for model development. All GA-PLS and CARS-PLS models achieved high-prediction performance for OTA and AFB₁ in standards and real samples with RPD values above 3. However, CARS-PLS was determined as a better alternative due to its faster data processing speed (4.07 s) compared to GA-PLS (2.5 min).^[95] Furthermore, the fingerprint spectra for AFB₁, ZEA, ALT, and FB₁ were obtained mathematically and exposed to pre-processing to smooth and subtract the baseline, followed by a parabolic fit using standard LSR, OPLS, and PCA to develop statistical models^[135] (Figure 13e). Unsupervised PCA models have been successfully applied to identify and differentiate AFB₁, ZEN, and DON in maize.^[49] In addition, an accelerated spectroscopic method to detect FB₁, FB₂, and FB₃ in maize was developed using a range of classification algorithms including KNN, LDA, PLS-DA, and quantification algorithms MLR, PLSR, and PCR. Chemometric classification exhibited moderately acceptable correct classification rates of 68–100% for the training set and 59–85% for the validation dataset. However, the authors highlighted how challenging it is to improve the models predictive accuracy and error rate amongst samples with low toxin concentrations.^[47]

Today this remains a challenging area for SERS, however, this review also highlights the importance of developing advanced statistical models to improve detection limits and accuracy within food and feed matrices. Machine learning algorithms including RF, SVM, and ANN or CNN have not yet been reported for SERS and may be the focus of future work to improve model classification and prediction. To-date, classification and regression modeling using machine learning algorithms already have the edge over traditional chemometrics and will undoubtedly progress further in the future for low-level toxin detection using spectroscopy. In addition, the integration of large datasets using several or different techniques (aka “data fusion”) may provide more robust and accurate models when combined with machine learning, than those which are generated using only one analytical technique.^[191]

8. Challenges for the Detection and Validation of Mycotoxins in Food and Feed

A major advantage of SERS is the rapid analysis time compared to other analytical techniques. To obtain the spectral information of mycotoxins, procedures are normally conducted in a rapid and straightforward manner by mixing or drying a volume of standard or sample extract with a previously fabricated SERS substrate (via bottom-up or top-down approaches, respectively). A major benefit of using the self-assembly or top-down approach is the additional SERS enhancement that can be achieved by incorporating two or more metallic substrates. Crucially, the first step of any SERS procedure is to confirm the sensitivity, selectivity, and reproducibility of the technique using mycotoxin

standards, before the technique is applied to a food or feed matrix. A summary of validation parameters and their performance is highlighted in **Table 5** (Table 4 also summarizes validation parameters for those which have performed chemometrics and/or machine learning) and will be discussed in the following sections.

8.1. Sensitivity and Reproducibility

Detection limits were reported by all methods however, the sensitivity is strongly influenced by assay design and the choice of fabricated substrate. Sensitivity or LOD is defined as the lowest concentration of an analyte in a sample that can be consistently detected with a stated probability (typically at >95% certainty).^[192] Arguably detection limits are the most important and controversial parameter when developing or validating any analytical method. Many researchers strive to develop techniques, which rival and improve upon those which already report low LODs. A challenge is that the maximum limits set by regulatory bodies for mycotoxins within food and feed are extremely low, therefore the analytical techniques must be capable of detecting trace levels. Sensitivities ranging from parts per million (mg kg^{-1}),^[73,111] parts per billion ($\mu\text{g kg}^{-1}$),^[83,136] parts per trillion (ng kg^{-1}),^[113,134] and parts per quadrillion (pg kg^{-1})^[75,101] have been reported using SERS, underlining the potential of the technique to detect extremely low levels of mycotoxins (Table 5). However, unless these impressive LODs are reported within a food or feed matrix the relationship between LOD, and regulatory maximum limits is negligible. Additionally, if the LOD obtained in aqueous or solvent conditions does not meet the maximum limits, the potential for implementation in a food or feed matrix is also highly unlikely.^[42,44]

Methods exploiting particle aggregation to increase localized hot spot formation and improve sensitivity have been reported in various formats. For example, the addition of electrolytes such as sodium chloride (NaCl) increases the number, strength, and location of hot spots by shielding the repulsive electrostatic forces and reducing interparticle distance.^[193] Mycotoxins can become trapped between adjacent particles more effectively thus, providing electromagnetic field enhancements. As a result, unique fingerprint spectra can clearly be obtained and these procedural steps have been reported for the detection of OTA and AFB₁.^[95] However, exploiting aggregation-based enhancement commonly involves using bare or uncoated nanomaterials, which can also result in reduced sensitivity in matrix conditions. For example, Yuan et al. incorporated salt-induced aggregation of AgNPs to determine DON in naturally contaminated corn, kidney beans and oats.^[116] The LOD for DON-contaminated corn and kidney beans was 3 mg kg^{-1} and for DON-contaminated oats was 300 mg kg^{-1} , compared to $30 \mu\text{g kg}^{-1}$ using only DON standard solutions. Therefore, although detection limits in matrix were reported they cannot meet the regulatory limits for DON in unprocessed cereals within the EU (limits set at 1.25–1.75 mg kg^{-1}). However, the main advantage of this technique is that the procedure is straightforward and involves mixing only AgNPs with DON solutions in ultrapure water and drying on Al foil, or adding AgNPs directly to the surface of agricultural products after spiking with DON solutions (to imitate a naturally contaminated sample). Additionally,

the analysis is rapid and conducted using a portable instrument making it feasible for on-site use. However, limitations need to be addressed including improving the reduced accuracies and sensitivities in matrix conditions caused by environmental influences, and the nonreproducible SERS enhancement witnessed by bare or uncoated nanomaterials.

In addition to stability issues, SERS applications can often suffer from weak interactions and low affinity between the metallic surface and target molecules. To overcome this, various functionalization techniques have been applied to improve detection limits. For example, Pan et al. functionalized AgNP SERS substrates with pyridine as an attempt to circumvent the weak affinity of AOH molecules with the AgNPs surface.^[57] By functionalizing the substrate with pyridine, affinity interactions were improved. In addition, the selectivity of the interactions, the reproducibility of SERS signals and the stability of the SERS substrate could also be improved. As mentioned previously, hot spots formed by particle-induced aggregation can cause issues in terms of reproducibility. Batch-to-batch variation can also occur between nanomaterial syntheses, which can be difficult to control thus, fabrication requires skilled personnel to ensure consistency.

Numerous studies also report highly specific interactions with recognition elements to improve sensitivity and reproducibility. Commonly the functionalization of core-shell structures with aptamers have been applied for the detection of mycotoxins in SERS-based aptasensing applications.^[86] Chen et al. developed an SERS-based aptasensor by fabricating Au@Ag core-shell NPs and AuNRs for the detection of ZEN and OTA. The reproducibility was performed using 20 SERS measurements from the same spot on the substrate and the RSD was $\approx 4\%$. Additionally, Zhao et al. embedded Raman reporters and aptamers specific to AFB₁ and OTA onto Ag and Au core-shelled nanoparticles (Ag@Au CS NPs) and modified MNPs with complementary DNA.^[82] Despite this being the first report to mention multiplexing during a SERS-based aptasensor, one drawback of the method is the 2-h analysis time required to ensure complete recognition between aptamers and mycotoxins. However, this may be an acceptable improvement considering the time taken for confirmatory analysis. Antibodies have been reported to improve the sensitivity, selectivity, and reproducibility of SERS approaches. Ko et al. reported the first SERS-based sandwich immunoassay for the detection of AFB₁ with an analysis time of only 30 min.^[83] However, for these techniques laboratory equipment and skills held by the end-user are still required to conduct the immunoassay and produce reliable, repeatable, and accurate results.

8.2. Selectivity

Within a real food or feed sample, the release of nontargeted compounds from the matrix (i.e., proteins, carbohydrates, sugars, fats, other contaminants) will impact sensitivity. Due to spectral overlap, SERS can often struggle to decipher the spectral fingerprints of several analytes in an aqueous or solvent-based mixture, particularly those with similar chemical structures. Therefore, it is important to first confirm the selectivity of the method in the presence of interfering compounds or contaminants before analysing in a matrix. An example of reduced sensitivities as a result of matrix effects were previously reported by Guo et al.

Table 5. Validation parameters and performance achieved using SERS for the determination of mycotoxins in solvent, food or feed matrices.

| Target | SERS substrate | LOD | Matrix | Sample preparation, extraction and detection | Validation | Instrumentation | Laser wavelength [nm] | Refs. |
|----------------|--|--------------------------------------|--------------|--|------------------------------------|---|-----------------------|-------|
| ZEA | AuNP-4,4'-dipyridyl-ZEAmAb and ZEA-BSA capture substrates | 1 ng kg ⁻¹ | Feed samples | <ul style="list-style-type: none"> Dispersive liquid-liquid extraction performed using MeOH, NaCl, and chloroform Competitive SERS immunoassay using 4,4'-dipyridyl as a label | RSD = 7–13% | Microscopic Raman spectrometer (Nippon Optical System Co., Tokyo) | 623.8 nm | [117] |
| OTA, AFB1 | Ag@Au core-shell (CS) nanoparticles (NPs) and functionalized magnetic nanoparticles (MNPs) | 6–30 ng kg ⁻¹ | Maize | <ul style="list-style-type: none"> Aptasensor performed in solution using 4-ATP and 4-NTP as labels Magnetic separation performed to purify | Recovery = 95–100% RSD = 4% | Renishaw inVia Raman spectrometer | 785 nm | [82] |
| OTA, FB1, AFB1 | 3D nanopillar arrays, antibody conjugated SERS nanotags | 5–6 ng kg ⁻¹ | Solvent | <ul style="list-style-type: none"> Competitive immunoassay performed on Au/PET nanopillar substrates using MGITC as a Raman reporter | Recovery = 93–129% | Renishaw inVia Raman microscope system | 632.8 nm | [137] |
| AOH | Silver-embedded silica (SiO ₂ @Ag) NPs | 1 µg kg ⁻¹ | Solvent | <ul style="list-style-type: none"> Standards prepared in MeOH Label-free detection performed in solution | RSD = 2–6% | Thermo Scientific DXR Raman microscope | 532 nm | [85] |
| AFB1 | Gold nanostar (AuNS) core-silver nanoparticle (AgNP) satellites | 0.5 ng kg ⁻¹ | Peanut milk | <ul style="list-style-type: none"> Matrix prepared by centrifugation and dilution in PBS buffer (pH 7.4) prior to spiking Aptasensor performed in solution using 4-ATP as a Raman label | Recovery = 88–104% RSD = 11–18% | LabRam-HR800 micro-Raman spectrometer | 632.8 nm | [78] |
| AFB1 | Magnetic Ni@Au nanoparticles | 0.05 pg kg ⁻¹ | Maize | <ul style="list-style-type: none"> Standards prepared in phosphate buffer (PB, 2 mM, pH 7.4) Magnetic sandwich immunoassay using 4-MBA as a label Magnetic separation performed to enrich immunocomplexes | Recovery = 87–112% RSD = <5% | HR800 confocal micro-Raman spectrometer | 632.8 nm | [101] |
| AFB1 | AuNPs-DNA | 0.4 pg kg ⁻¹ | Peanut | <ul style="list-style-type: none"> Extraction performed using MeOH/H₂O (vol ratio 80:20) Competitive aptasensor performed on Au coated glass slides using 4-NTP as a Raman label | Recovery = 89–121% | Renishaw inVia Raman spectrometer | 633 nm | [96] |
| AFB1 | DTNB-labeled GNPs/Ag core-shell nanotriangles (GDADNTs) | 0.5 ng kg ⁻¹ RSD = ≈5% | Peanut oil | <ul style="list-style-type: none"> Standards prepared in PBS buffer (10 mM, pH 7.4) Aptasensor performed using DTNB as a Raman reporter molecule Extraction performed using NaCl and MeOH/H₂O (7:3, v/v) Sample solution dropped onto wafer prior to measurement Magnetic separation performed to purify | Recovery = 95–109% | SPLD-RAMAN spectrometer | 785 nm | [102] |

(Continued)

Table 5. (Continued).

| Target | SERS substrate | LOD | Matrix | Sample preparation, extraction and detection | Validation | Instrumentation | Laser wavelength [nm] | Refs. |
|----------------|---|--------------------------------------|-------------------|--|------------------------------------|---|-----------------------|-------|
| AFB1, ZEA, OTA | AuNPs-DSNB-anti-mycotoxin antibody nanoprobes | 6–570 ng kg ⁻¹ | Corn, rice, wheat | <ul style="list-style-type: none"> Competitive immunoassay performed on Au-coated glass slide using DSNB as a Raman reporter Extraction performed using 70% MeOH (v/v) | Recovery = 84–108% CV = <15% | Thermo Fisher Scientific SmartRaman Spectrometer | 632.8 nm | [97] |
| AOH | Pyridine-modified AgNPs | 1.3 µg kg ⁻¹ | Pear fruit | <ul style="list-style-type: none"> Standards prepared in MeOH Extraction performed using NaCl, H₂O and CAN (1% HAC) Samples reconstituted in MeOH:H₂O (1:9) prior to analysis in solution | Recovery = 70–111% RSD = 14–18% | Raman microscope (LabRAM HR, Horiba Scientific) | 633 nm | [57] |
| AFB1 | Chitosan-functionalized magnetic-beads and AuNR@DTNB@AgNRs | 4 ng kg ⁻¹ RSD = 3% | Peanut oil | <ul style="list-style-type: none"> Standards prepared in MeOH and diluted in phosphate buffer solution Aptasensor performed using DTNB as a Raman reporter Sample solution dropped onto silicon wafer prior to measurement Magnetic separation performed to purify | Recovery = 91–106% | SPLD-RAMAN Spectrometer (Hangzhou SPL photonics) | 785 nm | [87] |
| OTA | Au _(core) @Au-Ag _(shell) nanogapped nanostructures (NINS) coupled with Fe ₃ O ₄ magnetic nanoparticles by OTA aptamer | 4 ng kg ⁻¹ | Red wine | <ul style="list-style-type: none"> Standards dissolved in substrate solution Residual assemblies separated from mixture using an external magnet Aptasensor performed using 4-MBA as a Raman reporter Samples distilled, spiked, and analyzed in solution | Recovery = 92–112% | LabRam-HR800 Micro-Raman spectrometer (HORIBA Jobin Yvon) | 633 nm | [89] |
| OTA | Fe ₃ O ₄ @Au magnetic nanoparticles (MGNPs) and aptamer-modified Au-DTNB@AgNPs (GSNPs) | 0.5 ng kg ⁻¹ RSD = <9% | Wine, coffee | <ul style="list-style-type: none"> Standards prepared in 0.01 M PBS pH 7.4 Aptasensor performed using DTNB as a Raman reporter Samples dried onto a Si-plate prior to analysis Magnetic separation performed to enhance signal | Recovery = 80–110% RSD = <10% | inVia confocal Raman microscope | 633 nm | [88] |
| OTA | IS-Aptasensor based on Au-Ag Janus NPs-MXenes nanosheet assemblies | 0.5 ng kg ⁻¹ | Red wine | <ul style="list-style-type: none"> Standards prepared in H₂O Ratiometric IS-aptasensor applied in solution using MBIA as a Raman reporter Samples distilled and spiked prior to analysis | Recovery = 93–97% RSD = <3% | Micro-Raman spectrometer (Renishaw inVia) | 785 nm | [143] |

(Continued)

Table 5. (Continued).

| Target | SERS substrate | LOD | Matrix | Sample preparation, extraction and detection | Validation | Instrumentation | Laser wavelength [nm] | Refs. |
|---------------|---|---------------------------------------|---|--|---|---|-----------------------|-------|
| PAT | Gold nanobipyramids | 6 $\mu\text{g kg}^{-1}$ RSD = 8% | Apple juice, pear juice (naturally occurring) | <ul style="list-style-type: none"> Standards prepared in H_2O Extraction performed using H_2O, NaCl, and ethyl acetate Reaction between PAT and 4-MBA formed an SERS active molecule, with 4-MBA used as a label | LOD apple juice = 12.6 $\mu\text{g kg}^{-1}$ LOD pear juice = 78 $\mu\text{g kg}^{-1}$ Recovery = 93–97% RSD = <3% | inVia Reflex confocal microscope | 785 nm | [76] |
| PAT | Molecularly imprinted gold nanoparticle (MIP-ir-AuNP) sensor | 0.8 ng kg^{-1} | Blueberry sauce, grapefruit sauce, orange juice | <ul style="list-style-type: none"> Extraction performed using ethyl acetate:n-hexane (95:5, v/v) and Na_2SO_4 Label-free detection performed and analyzed in solution | Recovery = 96–108% | inVia Raman spectrometer | 633 nm | [54] |
| FBI | cDNA-modified platinum-coated gold nanorod (AuNR) | 3 ng kg^{-1} | Corn | <ul style="list-style-type: none"> Standards prepared in MeOH Extraction performed using MeOH:H_2O (2:8, v/v) Aptasensor analyzed in solution using Cy5.5 as an SERS and fluorescent label | Recovery = 92–97% | LabRAM HR Evolution system | 785 nm | [80] |
| AFBI | DNA functionalized Fe_3O_4 @Au nanoflowers and Au-4MBA@Ag nanospheres | 0.4 ng kg^{-1} (RSD = 3%) | Peanut oil | <ul style="list-style-type: none"> Aptasensor performed using 4-MBA as a Raman reporter Extraction performed using MeOH:H_2O (80:20, v/v) Magnetic separation performed to obtain complexes, enhance signal, and enrich binding sites | Recovery = 97–115% RSD = 4–12% | LabRAM HR Evolution microscope Raman system | 633 nm | [90] |
| OTA | Ag-capped silicon nanopillars | 0.02–1 mg kg^{-1} | White wine, red wine | <ul style="list-style-type: none"> Standard prepared in EtOH and diluted in ammonium H_2O (25 mM) (AW), 0.2 M AA or acidified ammonium hydroxide (AW-AA) Extraction performed using a supported liquid membrane (SLM) procedure Samples analyzed utilizing a custom-made SERS chip and multiwell measurement chamber | LOD = 115 $\mu\text{g kg}^{-1}$ white wine, 306 $\mu\text{g kg}^{-1}$ red wine | Thermo Fisher Scientific DXRxi Raman Imaging Microscope | 780 nm | [145] |
| ZEN, OTA, FBI | Upconversion nanoparticle (UCNP) and trimer-based aptasensor | 0.02–30 ng kg^{-1} | Corn | <ul style="list-style-type: none"> Trimer-based aptasensor analyzed in solution using Cy5.5 and 4-MBA as SERS and fluorescent labels | Recovery = 90–107% | F-7000 fluorescence spectrophotometer (Hitachi) | 785 nm | [113] |

(Continued)

Table 5. (Continued).

| Target | SERS substrate | LOD | Matrix | Sample preparation, extraction and detection | Validation | Instrumentation | Laser wavelength [nm] | Refs. |
|--------|--|---------------------------------------|---|---|------------------------------------|--|-----------------------|-------|
| OTA | Au film-Au@Ag core-shell NP (CMS NP) | 2 ng kg ⁻¹ | Red wine | <ul style="list-style-type: none"> IS-Aptasensor performed by linking CMS NP to Si-wafer Ratiometric detection utilizes 4-NTP as an internal standard (IS) and 4-ATP as the Raman reporter | Recovery = 96–97% SD = 2% | Horiba LabRAM HR Evolution using labspec6 software | 785 nm | [108] |
| OTA | AuNanostar@4-MBA@Au core-shell nanostructures (AuNS@4-MBA@Au) | 0.25 pg kg ⁻¹ (RSD = 9%) | Wine | <ul style="list-style-type: none"> Aptasensor performed using 4-MBA as a Raman signal molecule Assemblies enriched and separated using an external magnet Extraction performed using ethyl acetate | Recovery = 95–111% RSD = 11–14% | Renishaw inVia reflex Raman spectrometer | 632.8 nm | [114] |
| OTA | Quasi spherical AuNPs-DNA | 0.8 pg kg ⁻¹ | Red wine | <ul style="list-style-type: none"> Samples were analyzed on a Si wafer modified with AuNP-DNA Aptasensor conducted using R6G as a Raman reporter | Recovery = 96–106% RSD = 6–9% | Renishaw in Via-reflex micro-Raman spectrometer | 633 nm | [109] |
| PAT | Molecularly imprinted polymer (MIP) on Au/PDMS/AAO nanoarray | 10 ng kg ⁻¹ | Blueberry jam, grapefruit jam, orange juice | <ul style="list-style-type: none"> Standards were prepared in H₂O after testing a range of solvents Substrates are incubated with sample, washed and dried prior to analysis Real samples required no pretreatment Label free detection | Recovery = 96–113% RSD = 6% | Renishaw inVia Raman spectrometer | 785 nm | [148] |
| DON | Silver nanocubes@polydopamine substrate (Ag NCs@PDA) | 0.2 pg kg ⁻¹ (RSD = 8–13%) | Pig feed | <ul style="list-style-type: none"> Standards were prepared in EtOH:H₂O (1:1, v/v) Samples were dried onto filter paper prior to analysis Extraction performed using MeOH:H₂O (50%, v/v) Label-free detection, based on interactions between PDA and DON | LOD = 0.3 pg/kg | UniDRON Raman spectrometer | 633 nm | [75] |
| OTA | OTA-BSA-AuNPs (nanotags) and antibody-conjugated (anti-OTA)-magnetic beads | 0.6 ng kg ⁻¹ | Wine | <ul style="list-style-type: none"> Competitive immunoassay performed in solution using MGITC as a Raman reporter Samples diluted five times with PBS buffered solution and filtered prior to spiking Immunocomplexes were isolated using a magnetic bar | Recovery = 91–103% RSD = 2–3% | Renishaw inVia Raman microscope system | Not specified | [110] |

(Continued)

Table 5. (Continued).

| Target | SERS substrate | LOD | Matrix | Sample preparation, extraction and detection | Validation | Instrumentation | Laser wavelength [nm] | Refs. |
|-------------------------------------|--|------------------------------------|-------------------|--|----------------------------------|---|-----------------------|-------|
| OTA | Gold@silver nanodumbbell (Au@AgND) | 7 ng kg ⁻¹ | Beer, peanut oil | <ul style="list-style-type: none"> Standards prepared in Tris-HCl buffer Aptasensor performed using 4-MBA as a Raman reporter Samples were analyzed after drying on tin foil Extraction on peanut oil was performed using NaCl and MeOH:H₂O (80:20) | Recovery = 92–104% | LabRAM HR 800 microscopy confocal Raman spectrometer (Japan HORIBA Corporation) | 633 nm | [81] |
| AFB1, OTA, ZEN | Gold nanotags on a silica photonic crystal microsphere (SPCMs) | 0.8–1 ng kg ⁻¹ | Corn, wheat, rice | <ul style="list-style-type: none"> Standards prepared in MeOH Competitive immunoassay performed on fabricated biochip using Nile blue A (NBA) as a label Extraction performed using chloroform | Recovery = 70–118% CV = 7–11% | Confocal micro-Raman spectrometer LabRam HR Evolution (HORIBA Jobin Yvon) | 785 nm | [103] |
| OTA, ZEN | SH-cDNA-modified gold nanorods and SH-Apt-modified Au@Ag core-shell nanoparticles | 18–54 ng kg ⁻¹ | Wheat, corn | <ul style="list-style-type: none"> Aptasensor performed using 4-MBA and DTNB as Raman reporters Samples analyzed in solution Extractions performed using MeOH:H₂O (7:1, v/v) | Recovery = 96–111% RSD = <4% | SPLD-RAMAN-785-Q spectrometer | 785 nm | [86] |
| OTA, FB1, DON | Gold nanoparticles (AuNPs)-loaded inverse opal silica photonic crystal microsphere (SIPCM) | 0.2–70 ng kg ⁻¹ | Wheat, corn, rice | <ul style="list-style-type: none"> Competitive immunoassay using NBA, crystalline violet (CV) or methylene blue (MB) as nanotags Extraction performed using chloroform | Recovery = 71–118% CV = 5–14% | Horiba LabRAM HR Evolution (Horiba Jobin Yvon) | 785 nm | [115] |
| AFB1 | Au-4MBA@AgNPs-AFB1 apt and GO/AuNPs/ITO substrates | 0.1 ng kg ⁻¹ | Peanuts | <ul style="list-style-type: none"> Ratiometric IS-aptasensor performed using 4-MBA used as a Raman label Samples analyzed on ITO glass substrates modified with AuNP, graphene oxide (GO) and SERS probes Extraction performed using MeOH:H₂O (70:30) | Recovery = 92–104% RSD = 6–9% | Thermo Electron DXR2xi Raman microscope | 633 nm | [134] |
| AFB1 | MXene (Ti ₃ C ₂ T _x) nanosheets loaded with AuNP dimers | 0.6 ng kg ⁻¹ (RSD = 6%) | Peanuts | <ul style="list-style-type: none"> Ratiometric IS-aptasensor performed in solution using BPE and MXenes nanosheets as the IS Samples analyzed after incubating on AuNP dime/MXenes assemblies Extraction performed using MeOH:H₂O (80:20, v/v) | Recovery = 89–102% RSD = 4–9% | LabRAM HR confocal microscope Raman system | 785 nm | [141] |
| AFB1, DON, ZEA, FB1, OTA, T-2 toxin | Au@Ag core-shell mAb-functionalized SERS nanoprobe | 1–260 ng kg ⁻¹ | Maize | <ul style="list-style-type: none"> Extraction performed using MeOH–H₂O (7:3 v/v) Target detected using a lateral flow device Detection using DTNB and MBA as labels | Recovery = 79–106% CV = <16% | Portable i-Raman Plus Raman System (B&W Tek) | 785 nm | [100] |

(Continued)

Table 5. (Continued).

| Target | SERS substrate | LOD | Matrix | Sample preparation, extraction and detection | Validation | Instrumentation | Laser wavelength [nm] | Refs. |
|-----------------------------|---|-----------------------------|--|---|---|---|-----------------------|-------|
| AFB1 | Gold nanopipyramids (Au NBPs) within nanoholes of anodic aluminum oxide (AAO) (Au NBPs-AAO) | 0.5 $\mu\text{g kg}^{-1}$ | Peanuts | <ul style="list-style-type: none"> Extraction performed using 60% MeOH Samples drop cast on preprepared Au NBPs-AAO substrate Label-free detection | Recovery = 106–126% RSD = <10% | Portable Ocean optics, HRS-30 Raman spectrometer | 785 nm | [136] |
| AFB1 | AuNPs | 0.85 $\mu\text{g kg}^{-1}$ | Wheat powder, corn powder | <ul style="list-style-type: none"> Standards prepared in MeOH Extractions performed using water, DCM and QueChERS Label-free detection | Recovery = 85–108% RSD = <10% | Portable Raman spectrometer (Xiamen Spec Technology) | 785 nm | [71] |
| AFB1 | 4-ATP-AgNPs-DNA assembly on porous anodized aluminum (PAA) membrane | 80 ng kg^{-1} | Walnut | <ul style="list-style-type: none"> Standards prepared in MeOH Extraction performed using MeOH/H₂O (8:2) AF detected on PAA membrane Detection using 4-ATP as a label | LOD = 9 ng kg^{-1} RSD = <10% | Portable Raman spectrometer (Ocean Optics, SR-510 Pro) | 785 nm | [138] |
| ZEN | Fe ₃ O ₄ @Au MNPs coupled to Au@DTNB@Ag core-shell (CS) NPs | 1 ng kg^{-1} | Beer, wine | <ul style="list-style-type: none"> Samples filtered and diluted prior to spiking Detection using DTNB as a label Magnetic separation performed to purify | Recovery = 96–111% | Portable SPLD-RAMAN-785-Q spectrometer (Hangzhou SPL photonics) | 785 nm | [118] |
| OTA | Aptamer-functionalized Pd-Pt bimetallic nanocrystals (Pd-Pt NPs) and magnetic nanoparticles (MNPs) | 0.017 $\mu\text{g kg}^{-1}$ | Wine and grapes | <ul style="list-style-type: none"> Wine mixed with OTA standards and diluted 100 times Grapes crushed prior to spiking Extraction performed using MeOH:H₂O (70:30) Aptamers used to prepare recognition and capture probes oxTMB used as Raman reporter | Recovery = 83–95% RSDs = 1.3–9.5% | Portable RT5000 Portable Raman spectrometer (Tinghua Tongfang, Beijing, China) | 785 nm | [112] |
| FB1, AFB ₁ , ZEN | Graphene oxide-based 3D Au nanofilm (GO@Au-Au) | 0.5–6 ng kg^{-1} | Maize, peanut, lake water, river water | <ul style="list-style-type: none"> Food samples weighed and extracted with MeOH:H₂O (70:30) Water samples used directly without pretreatment | Recovery = 90–114% RSD < 13.5% | Portable Remishaw InVia Qontor Raman spectrometer | 633 nm | [140] |
| AFB ₁ , OTA | Antibody-conjugated Au-4-MBA@SiO ₂ and Au-DTNB@SiO ₂ nanotags on LFA test strip | 0.2–0.4 ng kg^{-1} | Corn, rice, wheat | <ul style="list-style-type: none"> Extraction performed using MeOH and ACN (v/v, 3:1) 4-MBA and DTNB used as Raman reporters for AFB₁ and OTA, respectively | Recovery = 87–112% | Portable RS 2000 Raman microscope system (Beijing JINSP Technology Co., Ltd., Beijing, China) | 785 nm | [104] |
| AFB ₁ | MNP@Ag-PEI microspheres | 0.45 ng kg^{-1} | Peanuts, walnuts, almonds | <ul style="list-style-type: none"> Apt-Cy5 used as a Raman reporter and fluorophore Extraction performed using MeOH:dH₂O (4:1) | Recovery = 95–109% RSDs \leq 9.7% | LabRAM HR Evolution (Horiba France SAS, Villeneuve, d'Ascq, France) | 785 nm | [105] |

(Continued)

Table 5. (Continued).

| Target | SERS substrate | LOD | Matrix | Sample preparation, extraction and detection | Validation | Instrumentation | Laser wavelength [nm] | Refs. |
|------------------|--|--------------------------|----------------------------|---|--------------------|---|-----------------------|-------|
| AFB ₁ | Mesoporous silica nanoparticles (MSNs) and MXenes with gold nanorods | 0.13 ng kg ⁻¹ | Peanut, maize, badam | <ul style="list-style-type: none"> • MSNs were loaded with R6G as a Raman reporter • Aptamers and PDA were assembled on the surface of MSNs • Extraction performed using MeOH:H₂O (70:30) | Recovery = 89–107% | LabRAM HR Evolution (Horiba France SAS, Villeneuve, d'Ascq, France) | 633 nm | [142] |
| AFB ₁ | AuNPs | 3.1 µg kg ⁻¹ | Corn, peanut flour, sesame | <ul style="list-style-type: none"> • Standards prepared in ACN • RG6 used as a Raman reporter • Samples were extracted in water, followed by spiking of supernatant with standard solutions | Recovery 95–119% | DXR Smart Raman spectrometer (Thermo Fisher Scientific, Waltham, MS, USA) | 780 nm 785 nm | [98] |
| AFB ₁ | AuNPs | 0.5 µg kg ⁻¹ | Corn | <ul style="list-style-type: none"> • Standards prepared in MeOH • No extraction performed • SERS conducted on corn inoculated with <i>Aspergillus flavus</i> | x | Raman spectrometer (Renishaw, UK) Portable RamTracer-200 (Suzhou OptoTrace Technologies Co. Ltd., Suzhou, China) | 785 nm | [99] |

who reported that the LOD of PAT and AOH was three orders of magnitude higher (1000×) in standard conditions than in spiked apple juice.^[119] Therefore, in this instance selectivity and matrix effects would need to be addressed as nontargeted compounds released after conducting SPE may be contributing to the reduced sensitivities observed in matrix.

The detrimental effect of sample matrix on detection limits was again highlighted by Rostami et al. who exploited a Ag-capped Si nanopillar SERS substrate placed in the bottom of a multiwell platform. The detection of OTA in spiked white and red wine was performed with LODs of 155⁻ and 306 µg kg⁻¹, respectively.^[145] The decrease in LOD for red wine was due to interferences experienced after extracting nontargeted compounds from the matrix. Therefore, the SLM extraction performed was not efficient for removal of residues from red wine. The incorporation of clean-up steps to reduce matrix effects was suggested, however this would lengthen and complicate the procedure further. A preferred option may be to redesign substrates with enhanced stability and selectivity through functionalization of the NP surface, or modification with recognition elements to help facilitate nano-toxin interactions.

Selectivity tests have been performed by introducing one to six different mycotoxins (or other potential interfering compounds) and their mixtures into the developed SERS procedure or assay. Selectivity trials are conducted and defined by IUPAC as the ability to assess “the extent to which the method can be used to determine particular analytes in mixtures or matrices without interferences from other components of similar behavior.”^[194] By doing so, this ensures that the procedure can be applied to a matrix, as it has been confirmed that the presence of other mycotoxins or contaminants in the food or feed sample will not interfere with the detection of target analyte. Works which have highlighted high selectivity are those which commonly rely on highly specific interactions between mycotoxins and recognition elements (e.g., aptamers, antibodies) or other affinity binders. The techniques which have conducted specificity tests are highlighted in Table 6.

8.3. Assessment of Applicability for Detecting Mycotoxins in Food and Feed Matrices

To ensure the developed SERS procedures are feasible for detecting mycotoxins in food and feed, their applicability is normally confirmed by spiking samples with different concentrations of mycotoxin standard solutions (ranging from mg kg⁻¹ to µg kg⁻¹ level). This is commonly performed in one of two ways: 1) by directly adding the mycotoxin into a blank food/feed sample (confirmed prior using confirmatory techniques) followed by an extraction, or 2) by directly spiking the sample extract/supernatant after conducting the extraction procedure (i.e., matrix-matched calibration). These type of analyses have been performed using SERS for the detection of mycotoxins in different commodities including, feed,^[75] maize,^[101] peanuts,^[134] peanut oil,^[102] corn, rice, and wheat,^[97] coffee and wine,^[88,145] soil,^[147] and tap water.^[83] (Figure 14). Although spiking experiments are crucial for validation purposes, spiking samples on-site would not be performed. Performing validation using naturally contaminated samples is preferred in most cases, but not one that is conducted frequently, due to the difficulties obtaining samples

Table 6. Summary of the SERS techniques performing selectivity tests and the potential interferences tested.

| Target analyte | SERS substrate | Potential interferences tested | Refs. |
|--|--|--|-------|
| OTA | Thermal evaporation of Au on glass slide | DON, BSA | [144] |
| FB ₁ | Metal–organic framework (MOF-5)-coated SERS active gold gratings | Sudan III, paraoxon | [147] |
| AFB ₁ | Gold nanobipyramids (Au NBPs) within nanoholes of anodic aluminum oxide (AAO) (Au NBPs–AAO) | AFB ₂ , AFG ₁ , and AFG ₂ | [136] |
| PAT | Molecularly imprinted polymer (MIP) on Au/PDMS/AAO nanoarray | 5-HMF, oxindole | [148] |
| AFB ₁ | 4-ATP–AgNPs–DNA assembly on porous anodized aluminum (PAA) membrane | OTA, AFB ₂ , AFG ₁ | [138] |
| PAT | Gold nanobipyramids | 5-HMF, 2-HNA, 2-Oxin, AOH | [76] |
| AFB ₁ | AuNPs | ZEN, OTA, FB ₁ , DON | [71] |
| OTA | Label-free Au nanoprism aptasensor (AuNT@Apt@MPA) | AFB ₁ | [77] |
| OTA | Gold@silver nanodumbbell (Au@AgND) | OTB, AFB ₁ , ZEN, DON, FB ₁ | [81] |
| OTA, ZEN | SH-cDNA-modified gold nanorods and SH-Apt-modified Au@Ag core–shell nanoparticles | AFB ₁ , T-2, FB ₁ , PAT | [86] |
| AFB ₁ | DTNB labeled GNTs/Ag core–shell nanotriangles (GDADNTs) | OTA, AFG ₁ | [102] |
| AFB ₁ | Chitosan-functionalized magnetic-beads and AuNR@DTNB@AgNRs | OCA, FB ₁ | [87] |
| OTA | Au _(core) @Au–Ag _(shell) nanogapped nanostructures (NNS) coupled with Fe ₃ O ₄ magnetic nanoparticles by OTA aptamer | OTB, AFB ₁ , DON, FB ₁ , ZEN | [89] |
| AFB ₁ | DNA-functionalized Fe ₃ O ₄ @Au nanoflowers and Au-4MBA@Ag nanospheres | AFB ₂ , AFG ₁ , AFG ₂ | [90] |
| ZEN | Fe ₃ O ₄ @Au MNPs coupled to Au@DTNB@Ag core–shell (CS) NPs | AFB ₁ , FB ₁ , T-2, PAT | [118] |
| OTA | IS-Aptasensor based on Au–Ag Janus NPs–MXenes assembly | BSA, AFB ₁ , FB ₁ , MC-LR | [143] |
| OTA | Au film–Au@Ag core–shell NP aptasensor | AFB ₁ , FB ₁ , MC-LR and BSA | [108] |
| FB ₁ | cDNA-modified platinum-coated gold nanorod (AuNR) | FB ₂ , FB ₃ , AFB ₁ , ZEN, PAT, OTA | [80] |
| ZEN, OTA, FB ₁ | Upconversion nanoparticle (UCNP) and trimer-based aptasensor | AFB ₁ , PAT, T-2 toxin | [113] |
| AFB ₁ | Au-4MBA@AgNPs-AFB ₁ apt and GO/AuNPs/ITO | OTA, AFM ₁ , FB ₁ | [134] |
| AFB ₁ | MXene (Ti ₃ C ₂ T _x) nanosheets loaded with AuNP dimers | AFB ₂ , AFG ₁ , AFG ₂ | [141] |
| AFB ₁ | Antibody-conjugated silica-encapsulated hollow gold nanoparticles (SEHGNs) and magnetic beads | OTA, FMB | [83] |
| OTA | OTA–BSA–AuNPs (nanotags) and antibody-conjugated (anti-OTA)-magnetic beads | ZEN, AFB ₁ | [110] |
| OTA, FB ₁ , AFB ₁ | 3D nanopillar arrays, antibody conjugated SERS nanotags | OTA, FMB, and AFB ₁ (different ratios) | [137] |
| AFB ₁ , OTA, ZEN | Gold nanotags on a silica photonic crystal microsphere biochip | AFG ₁ | [103] |
| OTA, FB ₁ , DON | Gold nanoparticles (AuNPs)-loaded inverse opal silica photonic crystal microsphere (SIPCM) | OTA, OTB, AFB ₁ , FB ₁ , ZEN, DON (mixtures) | [115] |
| PAT | Molecularly imprinted gold nanoparticle (MIP-ir-AuNP) sensor | 5-HMF, OXD | [54] |
| AFB ₁ | AuNPs–DNA | DON, ZEA, AFM ₁ , AFB ₂ , AFG ₁ , AFG ₂ | [96] |
| OTA | AuNanostar@4-MBA@Au core–shell nanostructures (AuNS@4-MBA@Au) | OTB, AFB ₁ , AFB ₂ , AFG ₁ , AFG ₂ , ZEN | [114] |
| OTA | Quasi spherical AuNPs–DNA | AFB ₁ , ZEN, OTB | [109] |
| OTA | Aptamer functionalized Pd–Pt bimetallic nanocrystals (Pd–Pt NRs) and magnetic nanoparticles (MNPs) | AFB ₁ , AFM ₁ , ZEN, DON, FB ₁ , T-2 toxin | [112] |
| FB ₁ , AFB ₁ , ZEN | Graphene oxide-based 3D Au nanofilm (GO@Au–Au) | T-2 toxin, DON, OTA, STR, CAP, OFLX | [140] |
| AFB ₁ | MNP@Ag–PEI microspheres | AFB ₂ , AFG ₁ , AFG ₂ | [105] |
| AFB ₁ | Mesoporous silica nanoparticles (MSNs) and MXenes with gold nanorods | AFB ₂ , AFG ₁ , AFG ₂ , and their mixtures (inc. AFB ₁) | [142] |

naturally contaminated with mycotoxins. Nonetheless, if naturally contaminated samples can be obtained these would be preferential from a validation perspective, to test and replicate real-life scenarios. Ideally, mycotoxin analysis should also be performed post or alongside another confirmatory technique. For example, some studies have also analyzed the same samples using LC-MS^[47,71,80,97,100,101,145] or HPLC^[54,57,72,76,81–83,114,117,119,141,148] as a benchmark to assess the performance of the developed SERS procedures. Some procedures also compare the performance of SERS methods to ELISA.^[81,86,89,103,115,118,136,137,141] These compar-

isons may be beneficial to promote SERS as part of a two-tier screening system and as a rival to those tests which are already commercially available. However, for confirmatory, LC-MS/MS will remain the gold standard due to its high sensitivity, accuracy, and multi-analyte detectability.

Only three of the reported SERS approaches validated using naturally contaminated samples of maize,^[47] corn, kidney beans, oats,^[116] and apple and pear juice^[76] contaminated with FUMs, DON, and PAT, respectively. The LODs in matrix for naturally occurring PAT in rotten apple and pear juice were

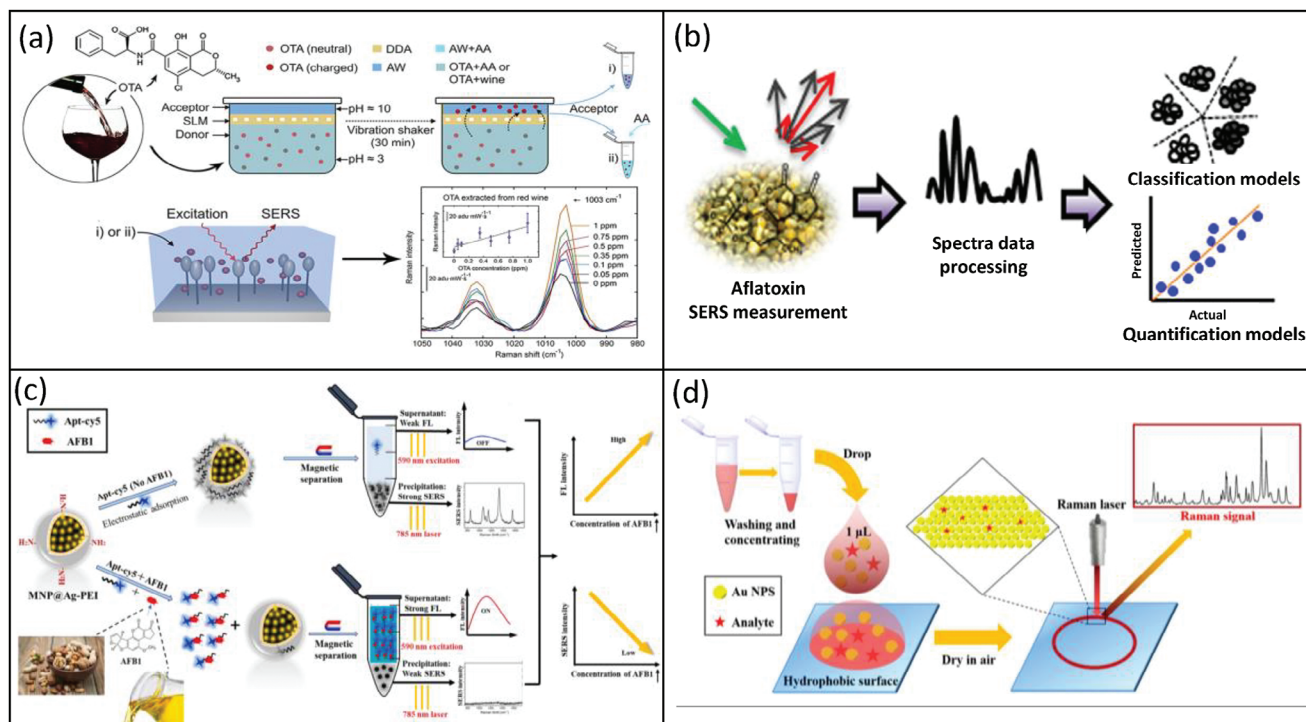


Figure 14. Determination of mycotoxins in spiked matrices using SERS. a) Schematic illustration of OTA extraction from spiked wine with SLM using the parallel artificial liquid membrane extraction (PALME) setup prior to SERS analysis. Reproduced with permission.^[145] Copyright 2020, Elsevier. b) Schematic demonstration of AFB₁, AFB₂, AFG₁, and AFG₂ detection in spiked maize using SERS. Reproduced with permission.^[72] Copyright 2014, American Chemical Society. c) Principle of a SERS-fluorescence dual-signal aptasensor for the determination of AFB₁ in spiked peanuts, walnuts, and almonds. Reproduced with permission.^[105] Copyright 2023, Elsevier. d) Schematic process of the optimization of a “coffee-ring” effect for the detection of AFB₁ in spiked corn, peanut, and sesame samples. Reproduced under the terms of the Creative Commons Attribution CC-BY license.^[98] Copyright 2020, The Authors, Licensee MDPI, Basel, Switzerland.

reported as 126⁻ and 78 $\mu\text{g kg}^{-1}$, respectively, using Au nanobipyramids as a SERS substrate, which were elevated compared to the LOD of 6 $\mu\text{g kg}^{-1}$ obtained using standards in solvent.^[76] Despite, this technique making advancements, it is not currently sensitive enough to meet the EU maximum limits of 10⁻ and 50 $\mu\text{g kg}^{-1}$ for PAT in apple and fruit juices. For corn, kidney beans and oats naturally contaminated with DON, LODs between 0.03 and 30 mg kg^{-1} were obtained using AgNPs and a portable Raman spectrometer.^[116] The EU regulatory limits for DON are 0.75⁻ and 8 mg kg^{-1} (in cereal and cereal products) for food and feed, respectively. Therefore, as the LOD for corn was reported as 0.03 mg kg^{-1} the approach may be accepted for testing corn intended as a food or feed ingredient. However, as the LOD for oats was 30 mg kg^{-1} , which is elevated above both the food and feed EU regulatory limits, the technique would not be acceptable for testing oats. Additionally, the LOD was not accompanied with validation data to address any repeatability issues, for example, CV, RSD, or measurement uncertainty (although this parameter is not commonly reported for SERS), which makes the LOD less significant. Nonetheless, it is important to consider that while detectable levels may not be sensitive enough to meet the regulatory maximum limits for food, they may be accepted for animal feed. Mycotoxin levels required for feed are generally higher than the same commodity intended for human consumption, but can also differ between animal species and the intension of animal production (i.e., for meat or dairy). For FUM contaminated maize

an LOD of 1–209 mg kg^{-1} was obtained using Ag dendrites.^[72] This approach may be considered acceptable as the EU regulatory limit is 1 mg kg^{-1} for maize or maize-based foods intended for human consumption. Overall, the SERS performance when quantifying in naturally contaminated matrices should be in sync with the regulations to be considered as truly acceptable or sensitive enough. To improve detection limits in matrix conditions it is recommended that substrate fabrication, assay design, and the incorporation of data analytics and statistical modeling are considered in the future.

8.4. Substrate Stability

For practical applications, it is important to confirm the stability of the SERS substrate and sensing platform. All techniques developed should be tested in a range of storage and atmospheric conditions to depict real life situations and ensure their feasibility for on-site applications. It has been reported that a combination of nanomaterials may either help, or hinder substrate stability in different storage conditions. For example, Zhu et al. reported that the performance of an enzyme induced molecular imprinted SERS substrates had declined to 80% after two weeks and to 70% after 30 days.^[148] Additionally, a SERS Au nanoap-tasensor composed of nanoprisms functionalized with aptamer and MPA (AuNT@Apt@MPA) only remained stable for up to 14

days.^[77] Also, the stability of three nanoprobe was evaluated every hour for only 4 h and no difference in SERS intensity was observed.^[86] As a commercialized product, the shelf-life of these substrates would be too short resulting in irreplicable results due to batch-to-batch variations and high production costs. Therefore, it would be more beneficial if substrates could be produced and remain stable for several months.

To verify the stability of GO–Au@Ag core–shell nanoparticle complex, various storage times (0–14 days), temperatures (20–60 °C) and salt ionic concentrations (10–50 mM) were assessed and had little influence on SERS intensity.^[134] Although different environmental conditions were tested, 14 days were the longest duration tested. However, Yang et al. determined that GNTs/GDADNTs could remain stable for at least three months by comparing the SERS spectrum over time.^[102] Additionally, the stability of core–shell Ag nanocubes with PDA was assessed every 15 days for 3 months with the substrate retaining 88% of its initial SERS intensity after 90 days.^[75] Furthermore, the stability of Au–Ag Janus NPs and MXenes nanosheets were determined under different pH (pH 4–8), temperature (20–50 °C), and storage conditions (0–90 days) and no difference in SERS signal was observed.^[143] A major advantage of these stability tests and SERS substrates, is that most have been tested over a significant period. Those which can retain their stability for up to 90 days would be more realistic for a commercialized product. Additionally, some have also considered the effects of external influences, complex environments, and real-life conditions, which ultimately improve their potential for in-field storage and implementation.

8.5. Portability

The increased commercial availability of portable Raman spectrometers has further advanced the on-site potential for SERS as an in-field test for mycotoxins. This is an obvious advantage over confirmatory techniques such as LC-MS/MS where instrumentation is restricted to the laboratory. In addition to portability, it is important for these devices to be user-friendly, rapid, affordable, and reliable. Typically, in the past the performance of portable instruments has been poor compared to their laboratory counterpart. However, in recent years technology companies have focused on improving their hardware, spectral range, and resolution. Nowadays, some portable devices can rival the sensitivities of benchtop equivalents whilst, maintaining their in-field usability, simplicity for non-spectroscopists, optical stability, and rapid results (either as quantitative values or qualitative decisions; yes/no, pass/fail, etc.). Portable instruments are designed to allow the spectrometer to be taken to the sample and not vice versa thus, a result can be delivered at the point of need, which is extremely valuable for the end-user in terms of cost and time.^[38]

Furthermore, algorithms for processing spectral information are commonly incorporated into the design and operation of portable devices, which also benefit the analysis of complex mixtures, quantitative analysis, and/or decision making. Some can also be combined with cloud-based spectral libraries for identification and quantification, which might be particularly useful when trying to decipher mixtures or low-level contamination. However, taking advantage of machine learning and spectral databases also requires a stable internet or Wi-Fi connec-

tion on-site, which may not be feasible in all locations such as, resource limited environments or within developing countries. Whilst most techniques are initially developed in a laboratory using a benchtop instrument, it would be beneficial in the future if the same techniques could be transferred and reproduced using handheld or portable spectrometers.

Several publications have reported using portable Raman spectrometers to detect mycotoxins within a food or feed matrix (Table 5). Those which do report portable applications commonly employ handheld Raman spectrometers combined with a 785 nm laser. For example, Chen et al. described a solution-based aptasensor for the detection of ZEN in beer and wine. The sensor consists of Fe₃O₄@Au MNPs modified with sulfhydryl (SH)-ZEN complementary DNA as capture probes (Fe₃O₄@Au MNP–cDNA) and Au@Ag core–shell nanoparticles modified with DTNB Raman reporter and SH-ZEN aptamer as reporter probes (Au@DTNB@Ag CS-Apt). Based on the inversely proportional relationship, the LOD of the sensor could be determined as 1 ng kg⁻¹ and recoveries ranged between 96% and 111% using a portable SPLD-RAMAN-785-Q spectrometer with a 785 nm laser (Hangzhou SPL photonics).^[118] This laser is a popular choice due to cost-efficiency, availability, high-quality, and the compromise between Raman scattering intensity and fluorescence suppression. However, 532 and 633 nm lasers have also been reported for some benchtop applications. The choice will ultimately depend on availability, cost, the choice of SERS substrate employed and its corresponding excitation wavelength. Ultimately, conducting analysis using portable devices is a step in the right direction, however it is still common for these handheld analyses to take place within a laboratory, which defeats the purpose of the spectrometer's intended design. Portable spectrometers have been exploited in a laboratory setting to detect ZEN,^[100,118] OTA,^[77,100] AFs,^[70,71,99,100,106,136,138] DON,^[100,116] FB₁,^[100,147] and T-2.^[100] Several of these techniques also incorporate molecular binders and chemometrics or machine learning (as discussed previously) to facilitate binding and detection.

8.6. Sample Preparation

A major limitation for on-site implementation is the need for sample preparation prior to analysis. Sample preparation is challenging for most spectroscopy techniques including IR, which requires the removal of water from the sample. For SERS, it is difficult to perform analysis or detect trace levels of contamination without performing an extraction. Those who have attempted to detect mycotoxins on the surface of agricultural products have suffered from poor sensitivity, with detection limits not able to meet the EU regulations for human consumption or animal feed for example, DON in oats.^[116] Therefore, to improve detection limits more stringent sample preparation steps are normally required to remove the toxin from the matrix. To extract residues an extraction solvent (e.g., 60% MeOH) is typically added to a ground sample, followed by sonification and/or centrifugation for a short time (usually <60 min).^[49,70,136] The supernatant or extract will be removed and mixed or dried onto the SERS substrate prior to analysis. In addition to solvent-based extractions, the release of mycotoxins from food or feed matrices has also been conducted by exploring specific extraction procedures including,

SLM extraction to remove OTA from white and red wine,^[145] LLE to remove OTA from wine and wheat,^[73] SPE to remove AOH and PAT from apple juice^[119] and QuEChERS extraction to remove AFB₁ residues from grain.^[71] However, some notable drawbacks include interferences from non-targeted compounds and reduced sensitivities. Also, many procedures are traditionally too complex and the use of toxic chemicals, such as chloroform or dichloromethane would not be suitable for on-site extractions due to health, safety, and environmental concerns.

The main obstacles for transferring SERS techniques outside of the laboratory are normally in relation to sample handling procedures. First, conducting these procedures on-site may be challenging for some industry sectors depending on the facilities required and the availability of equipment. Second, the release of solvents into the atmosphere is often not well received by industry. However, completely removing extractions and some level of laboratory practice seems an unlikely option for SERS. Using fewer toxic chemicals, those which are more environmentally friendly or aqueous extraction procedures on the other hand, may be a more feasible option. Nonetheless, a solution is essential if the technique is ever to be successfully implemented on-site. Ultimately, the movement of any analytical technique from the laboratory to in-field will require some level of compromise. If we consider the commercialized rapid tests, which are already available for the in-field testing of food and feed, similar procedures, reagents, and equipment are required to perform these tests, as would be required for an on-site SERS test. LFTs and ELISAs are readily available for mycotoxin detection, however the sample still needs to be prepared, extracted using solvent and/or water mixture before conducting the test and acquiring the result. Currently, LFTs would be the most favored option by industry due to their simplicity, fewer procedural steps, rapidity, and low-cost. Although used frequently, ELISA-based tests may be less popular due to antibody cross-reactivity, lengthy procedures, and the level of skill required by the end user to conduct the tests.^[92] As mentioned previously, SERS has many advantages and holds great potential as a read-out technique over these current assays on the market. Additionally, due to the high level of selectivity that can be achieved using SERS, identifying potential cross-reactivities may also be more likely using SERS, than other colorimetric approaches.

8.7. Time to Analysis

For SERS the reported time to analysis often only includes the total assay time, but the time taken to fabricate metallic nanosubstrates and nanoprobables should also be considered, especially when substrate stability is an issue. For example, Ma et al. fabricated a Au and Ag nanodumbbell assembly with inter-nanogap after an overnight incubation at 37 °C.^[81] Similarly, Shao et al. described the preparation of a SERS-active aptasensor after hybridizing two nanoprobables for 14 h.^[89] Additionally, Li et al. functionalized hairpin DNA onto gold-coated glass slides over 12 h to perform an SERS-based aptasensor.^[96] The authors highlight that most of these complex operations such as chip functionalization, SERS tag preparation, and aptamer hybridization with complementary DNA can be pre-completed in the laboratory, with only sample adding and washing steps required for analyte detection.

This may be true for all procedures which entail lengthy nanomaterial preparation steps; thus, one solution would be to transport and store the substrates on-site ready for use. However, each component would require lengthy tests to confirm stability, storage conditions and impact of environment (i.e., light, temperature, humidity, etc.). Any reagent that is a component or part of a potential on-site test or assay would also be subjected to the same validation steps prior to becoming a commercialized product and would not be accepted onto the commercial market without passing these stringent tests. However, reducing the need to prepare SERS substrates on a frequent basis would be an obvious time and cost saving benefit for the developers and end-users of the SERS tests.

In addition, the total analysis time will determine whether the SERS procedure is likely to be considered as a routine test. Whilst some procedures may be too long to benefit from in-field use, some may ultimately improve the analysis of samples in an industry setting, due to the turnaround time required to send samples to the laboratory for confirmatory analysis. Most SERS methodologies report an analysis time between 2 and 24 h. For example, Rodriguez et al. performed two incubations totaling 24 h before detecting DON and OTA using PAA and FON.^[111] Thus, the likelihood for this technique to be implemented on-site is less, than those reporting shorter turnaround times. Additionally, Chen et al. employed a pre-etched nanocluster to detect AFB₁ in peanut oil. However, the substrate is prepared over 13 h, etched with HNO₃ for 25 min to expose functional groups, and soaked in AFB₁ sample solution for 10 h before analysis.^[106] Furthermore, AOH was detected by Hahm et al. after a 12-h incubation using Ag-embedded Si NPs.^[85] However, the incubation must also be performed at a set temperature of 25 °C. Therefore, implementing the test on-site may not be an option for countries with humid or subtropical climates, unless control measures are in place. Also, Huang et al. reported a 10.5 h procedure using a “turn-on” mode SERS aptasensor to determine OTA standards.^[114] On the other hand, Feng et al. reported a 50 min extraction followed by a 2 h incubation with a AgNP-porous anodized aluminum (PAA) membrane to detect AFB₁ in walnut.^[138] Additionally, AFB₁ was detected by Wu et al. after incubating MXenes nanosheets bound to aptamer modified AuNP dimers with sample solution for only 1 h.^[141] It is difficult to imagine how several of these techniques could ever be considered as “rapid.” For mycotoxin applications, perhaps those which can achieve a result within 1–2 h using SERS, should only be considered as truly rapid.^[138,141] However, some areas of the food sector may still benefit or improve their current methods of testing with analysis times of up to 24 h, as it can take several days or sometimes weeks to receive confirmatory results from a laboratory, but what is deemed as an acceptable time will ultimately depend on the end-user.

In this section, opinions on the development and validation of SERS methodologies, both from a scientific and industry perspective have been discussed. The current situation highlights that validation including sensitivity, selectivity, reproducibility, substrate stability, portability, sample preparation, and time to analysis is often prioritized differently throughout the literature. During the critical review process this raised several questions for real applications. 1) Should sensitivity be the main priority of validation, or should reaching regulated limits be considered sensitive enough? 2) Why is selectivity, matrix detection, substrate

stability or portability not considered important during validation? 3) Can a method with an analysis time of >2 h really be considered as “rapid”? 4) Will we ever get to the stage where in-field validation is routine for SERS? Additionally, these sections intend to inform industry of the advantages and potential of SERS over other commercially available tests for mycotoxin detection (e.g., LFAs and ELISAs) and make them aware of the validation parameters which must be provided. It will be important to benchmark these parameters against these available technologies in the future if SERS is ever going to compete.

9. Conclusion and Future Perspectives

This review has focused on the SERS methodologies developed for the detection of mycotoxins over the past decade. Many papers have demonstrated the great potential of SERS to detect mycotoxins in various food and feed matrices however, none of these methods have reached the level of development or validation required for implementation as screening tests for routine analysis. To improve this situation, three categories have been suggested as a guide to follow when developing and validating a SERS methodology. The aim of this guide is to encourage the development of techniques which are feasible for in-field use, and to ensure that crucial parameters including stability, portability, and sample preparation are not overlooked.

Category A: These techniques often provide straightforward procedures with high sensitivity in solvent conditions; however, a major drawback is that these methods have not established their feasibility for determining mycotoxins in a food or feed matrix. The most simplistic techniques often suffer from matrix effects and reduced sensitivities. As these interferences have not been evaluated these methods can only be considered proof of concept techniques. Full validation of these methods is required within a real sample and should be the next step for these techniques to enhance their practicality and potential for commercialization.

Category B: These techniques have made a step toward commercialization by validating their methods in real matrices; however, some sample preparation issues may remain. For example, spiking supernatant after performing an extraction is not a typical on-site procedure. Whilst the spiking of blank samples can often be used to replicate naturally contaminated food and feed, these should not replace including naturally contaminated samples within the validation procedure. Additionally, the use of chlorinated extraction solvents would not be accepted by many for in-field use. Procedures should aim to reduce the use of solvents and replace them with water-based extractions (where applicable) to improve “green chemistry”. Very few methods report LODs in matrix conditions and are only mentioned in solvent (i.e., standards) thus, have no real correlation to the European regulatory limits for food and feed, which should be addressed.

Category C: These techniques have further improved their practicality for real sample analysis by analysing naturally contaminated samples and/or using portable Raman spectrometers. However, sensitivities of these methods often cannot meet regulatory limits and validation, or repeatability measurements (e.g., CV, RSD, or measurement uncertainty) have not been reported. Therefore, improvements to detection limits in real

samples and selectivity when faced with non-targeted compounds still need to be addressed. Substrate stability in different environmental conditions should be addressed to ensure that the materials can be stored and applied in real life settings. If validation has been completed within a laboratory setting and all parameters (including those mentioned in Category B) have been achieved using a portable instrument, in-field validation is the next step to be conducted by these techniques.

To summarize, the fabrication of SERS substrates plays a fundamental role in the sensitivity, selectivity, reproducibility, feasibility in matrix, and stability of the nanomaterials. It is ultimately the most important step for developing any successful SERS method. Colloidal particles are highly stable in solution but provide weaker SERS enhancement. Anisotropic nanoparticles (e.g., AuNS) can provide phenomenal SERS enhancement due to their unique shape and size. Dual metallic nanomaterials or core-shell structures are also known to improve sensitivities over Au or Ag alone, thus a combination of sizes, shapes, and compositions of nanomaterials may be the key for SERS-based mycotoxin detection, particularly for those mycotoxins with extremely low regulatory limits (e.g., AFs). Recognition elements (e.g., aptamers, antibodies) can be produced relatively cheap and not only improve the specificity of the procedure, but can play a pivotal role in improving the stability of nanomaterials. Aptamers are more straightforward to immobilize onto metallic substrates and have higher stability than antibodies, but can suffer more from matrix interferences. If the techniques are to be implemented on-site, shelf-life, storage, and transportation of aptamer-based substrates may be less problematic.

To visualize SERS as a commercialized in-field test for the routine analysis of mycotoxins it may include several components: i) a test kit containing fabricated nanosubstrates and extraction solutions, ii) a handheld Raman spectrometer for analysis, iii) chemometrics built into the software held on the instrument to decipher complex matrices and multiple contaminants, and iv) a database stored in a cloud-based system containing the unique spectral information of mycotoxins, which the obtained sample spectra can be compared to. Several essential steps would also be required before any test becomes a commercialized product: i) the stability and storage conditions of the SERS nanosubstrates should be confirmed for real life scenarios (e.g., light, pH, temperature); ii) the applicability of SERS-based tests should be assessed in a range of naturally contaminated food and feed matrices to ascertain suitability; and iii) full on-site validation would be required to ensure the rapid test is fit for purpose within different environments. To date none of the techniques mentioned in this review have performed validation outside of the laboratory and this would be the next progressive step for those which have already developed SERS tests using portable devices and/or have performed validation using naturally contaminated samples. Additionally, machine learning algorithms for example, RF, SVM, ANN, and CNN and data fusion techniques are yet to be reported for SERS and may be a future focus to improve accuracy and reliability of measurements and model predictions.

Overall, the validation of SERS methodologies in order of priority has been to improve the 1) sensitivity and reproducibility for detecting mycotoxins in solvent or aqueous environments,

2) selectivity of the developed assays in the presence of interfering mycotoxins or contaminants, 3) feasibility in real food and/or feed samples, 4) stability of SERS substrates in a range of different environmental conditions, and 5) transferability of developed methodologies to portable spectrometers. Further advancements to nanomaterial design will ultimately continue to push LODs and sensitivities to even lower levels. Although sensitivity is a fundamental parameter, perhaps further advancements in this area would not be most beneficial. Numerous methods with detection limits down to ppt and ppq have been developed using a vast array of nanomaterials. These sensitivities are low enough to meet the EU regulations for any regulated mycotoxin. Perhaps the future focus should be on improving the commercialization potential and real-life applications of these SERS technologies. If the technique is sensitive enough to meet regulatory limits in a naturally contaminated sample, perhaps the next focus should be to improve substrate stability, reduce production costs, improve portability, and simplify sample preparation procedures, rather than developing complex procedures which may be too sensitive and sophisticated to have purpose in the real world.

Acknowledgements

The authors would like to thank Dr. Joost Nelis for the fruitful discussions and valuable suggestions during the initial stages of manuscript preparation. The authors N.L., S.F., R.K., and C.T.E. would like to acknowledge funding from several institutions. First, this research was created as part of the European Union's Horizon 2020 research and innovation program under Grant Agreement No. 101016444 (PHOTONFOOD). Second, this work was conducted as part of a research project of the Austrian Competence Centre for Feed and Food Quality, Safety and Innovation (FFoQSI). The COMET-K1 competence centre FFoQSI is funded by the Austrian ministries BMVIT and BMDW and the Austrian provinces Niederösterreich, Upper Austria, and Vienna within the scope of COMET—Competence Centers for Excellent Technologies. Third, the authors N.L., C.C., S.A.H., and C.T.E. would like to acknowledge the funding provided as part of the Horizon Europe Framework Programme Horizon-CL6-2021-FARM2FORK-01 grant agreement under Project No. 101059813 (HOLiFOOD).

Conflict of Interest

The authors declare no conflict of interest.

Author Contributions

Natasha Logan: investigation, conceptualization, methodology, writing – original draft, writing – review and editing. Cuong Cao: conceptualization, methodology, writing – review and editing. Stephen Freitag: writing – review and editing. Simon A. Haughey: writing – review and editing. Rudolf Krska: conceptualization, funding acquisition, writing – review and editing. Christopher T. Elliott: conceptualization, funding acquisition, writing – review and editing, supervision.

Keywords

nanotechnology, surface-enhanced Raman spectroscopy, nanofabrication, mycotoxins, agri-food applications

Received: September 18, 2023

Revised: December 20, 2023

Published online:

- [1] H. S. Hussein, J. M. Brasel, *Toxicology* **2001**, 167, 101.
- [2] L. M. Juraschek, A. Kappenberg, W. Amelung, *Sci. Total Environ.* **2022**, 814, 152425.
- [3] J. C. Frisvad, U. Thrane, R. A. Samson, J. I. Pitt, *Advances in Food Mycology*, Springer US, Boston, MA **2006**.
- [4] M. Eskola, G. Kos, C. T. Elliott, J. Hajslová, S. Mayar, R. Krska, *Crit. Rev. Food Sci. Nutr.* **2020**, 60, 2773.
- [5] R. Krska, A. Molinelli, *Anal. Bioanal. Chem.* **2007**, 387, 145.
- [6] S. Luo, H. Du, H. Kebede, Y. Liu, F. Xing, *Food Control* **2021**, 127, 108120.
- [7] C. Gruber-Dorninger, T. Jenkins, G. Schatzmayr, *Toxins* **2019**, 11, 375.
- [8] D. P. Bebber, M. A. T. Ramotowski, S. J. Gurr, *Nat. Clim. Change* **2013**, 3, 985.
- [9] R. Krska, M. Eskola, C. T. Elliott, *Toxin-Free Food? Health Risks and Benefits of Our Food*, Picus Verlag, Vienna, Austria **2023**.
- [10] EFSA CONTAM Panel (EFSA Panel on Contaminants in the Food Chain). EFSA CONTAM Panel (EFSA Panel on Contaminants in the Food Chain). *Scientific opinion Risk assessment of aflatoxins in food* EFSA Journal, EFSA, Parma, Italy, **2020**, 18, 112.
- [11] S. Smaoui, T. D'Amore, M. Tarapoulouzi, S. Agriopoulou, T. Varzakas, *Microorganisms* **2023**, 11, 2614.
- [12] M. Eskola, C. T. Elliott, J. Hajslová, D. Steiner, R. Krska, *Crit. Rev. Food Sci. Nutr.* **2020**, 60, 1890.
- [13] R. S. Chhaya, J. O'Brien, E. Cummins, *Trends Food Sci. Technol.* **2021**, 126, 126.
- [14] R. Bhat, R. V. Rai, A. A. Karim, *Compr. Rev. Food Sci. Food Saf.* **2010**, 9, 57.
- [15] M. Leite, A. Freitas, A. S. Silva, J. Barbosa, F. Ramos, *Trends Food Sci. Technol.* **2021**, 115, 307.
- [16] F. Cheli, D. Battaglia, R. Gallo, V. Dell'Orto, *Food Control* **2014**, 37, 315.
- [17] S. Agriopoulou, E. Stamatelopoulou, T. Varzakas, *Foods* **2020**, 9, 518.
- [18] D. Kizis, A.-E. Vichou, P. I. Natskoulis, *Sustainability* **2021**, 13, 2537
- [19] A. Malachová, M. Stránská, M. Václavíková, C. T. Elliott, C. Black, J. Meneely, J. Hajslová, C. N. Ezekiel, R. Schuhmacher, R. Krska, *Anal. Bioanal. Chem.* **2018**, 410, 801.
- [20] M. Sulyok, D. Stadler, D. Steiner, R. Krska, *Anal. Bioanal. Chem.* **2020**, 412, 2607.
- [21] S. Agriopoulou, E. Stamatelopoulou, T. Varzakas, *Foods* **2020**, 9, 518.
- [22] D. Bueno, G. Istambouli, R. Muñoz, J. L. Marty, *Appl. Spectrosc. Rev.* **2015**, 50, 728.
- [23] S. Freitag, M. Sulyok, N. Logan, C. T. Elliott, R. Krska, *Compr. Rev. Food Sci. Food Saf.* **2022**, 21, 5199.
- [24] C. Dachoupan Sirisomboon, R. Putthang, P. Sirisomboon, *Food Control* **2013**, 33, 207.
- [25] M. J. Stasiewicz, T. D. O. Falade, M. Mutuma, S. K. Mutiga, J. J. W. Harvey, G. Fox, T. C. Pearson, J. W. Muthomi, R. J. Nelson, *Food Control* **2017**, 78, 203.
- [26] L. M. Kandpal, S. Lee, M. S. Kim, H. Bae, B.-K. Cho, *Food Control* **2015**, 51, 171.
- [27] A. Femenias, F. Gatiús, A. J. Ramos, V. Sanchis, S. Marín, *Food Chem.* **2021**, 341, 128206.
- [28] D. Heperkan, E. Gökmen, *J. AOAC Int.* **2016**, 99, 899.
- [29] Y. Yang, Y. Zhang, C. He, M. Xie, H. Luo, Y. Wang, J. Zhang, *Int. J. Food Sci. Technol.* **2018**, 53, 2386.
- [30] N. Berardo, V. Pisacane, P. Battilani, A. Scandolara, A. Pietri, A. Marocco, *J. Agric. Food Chem.* **2005**, 53, 8128.
- [31] X. Cheng, A. Vella, M. J. Stasiewicz, *Food Control* **2019**, 98, 253.
- [32] G. Kos, H. Lohninger, R. Krska, *Anal. Chem.* **2003**, 75, 1211.
- [33] F. Shen, Q. Wu, X. Shao, Q. Zhang, *Int. J. Food Sci. Technol.* **2018**, 55, 1175.

- [34] A. De Girolamo, C. von Holst, M. Cortese, S. Cervellieri, M. Pascale, F. Longobardi, L. Catucci, A. C. R. Porricelli, V. Lippolis, *Food Chem.* **2019**, *282*, 95.
- [35] Z. Guo, M. Wang, J. Wu, F. Tao, Q. Chen, Q. Wang, Q. Ouyang, J. Shi, X. Zou, *Food Chem.* **2019**, *286*, 282.
- [36] A. E. Grow, L. L. Wood, J. L. Claycomb, P. A. Thompson, *J. Microbiol. Methods* **2003**, *53*, 221.
- [37] H. Yao, Z. Hruska, R. Kincaid, R. Brown, T. Cleveland, D. Bhatnagar, *Food Addit. Contam.: Part A* **2010**, *27*, 701.
- [38] R. A. Crocombe, *Appl. Spectrosc.* **2018**, *72*, 1701.
- [39] L. Sual, IR Versus Raman – The Advantages and Disadvantages, <https://www.azooptics.com/Article.aspx?ArticleID=1291> **2019**, (accessed: August 2023).
- [40] M. Lin, *The Application of Surface-Enhanced Raman Spectroscopy to Identify and Quantify Chemical Adulterants or Contaminants in Foods*, **2010**, in Handbook of Vibrational Spectroscopy (eds J. M. Chalmers and P. R. Griffiths), John Wiley & Sons, Chichester, England, UK, **2018**, pp. 649–662.
- [41] C. Levasseur-Garcia, *Infrared Spectroscopy Applied to Identification and Detection of Microorganisms and Their Metabolites on Cereals (Corn, Wheat, and Barley) in Agricultural Science*, IntechOpen, London, UK **2012**, Ch. 9, pp. 185–196.
- [42] X. Wu, S. Gao, J.-S. Wang, H. Wang, Y.-W. Huang, Y. Zhao, *Analyst* **2012**, *137*, 4226.
- [43] L. Smeesters, W. Meulebroeck, S. Raeymaekers, H. Thienpont, *Food Control* **2015**, *51*, 408.
- [44] B. C. Galarreta, M. Tabatabaei, V. Guieu, E. Peyrin, F. Lagugné-Labarthe, *Anal. Bioanal. Chem.* **2013**, *405*, 1613.
- [45] M. Schmidt-Heydt, B. Cramer, I. Graf, S. Lerch, H.-U. Humpf, R. Geisen, *Toxins* **2012**, *4*, 1535.
- [46] J. Keller, D. Moldenhauer, L. Byrne, H. Haase, U. Resch-Genger, M. Koch, *Toxins* **2018**, *10*, 538.
- [47] K. M. Lee, T. J. Herrman, *Food Bioprocess Technol.* **2016**, *9*, 588.
- [48] M. Solfrizzo, A. De Girolamo, A. Visconti, *Food Addit. Contam.* **2001**, *18*, 227.
- [49] J. Li, H. Yan, X. Tan, Z. Lu, H. Han, *Anal. Chem.* **2019**, *91*, 3885.
- [50] M. Muscarella, M. Iammarino, D. Nardiello, C. Palermo, D. Centonze, *Talanta* **2012**, *97*, 145.
- [51] D. K. Singh, E.-O. Ganbold, E.-M. Cho, K.-H. Cho, D. Kim, J. Choo, S. Kim, C. M. Lee, S. I. Yang, S.-W. Joo, *J. Hazard. Mater.* **2014**, *265*, 89.
- [52] M. Appell, L. C. Wang, W. B. Bosma, *J. Lumin.* **2017**, *188*, 551.
- [53] M. Appell, W. B. Bosma, *J. Lumin.* **2011**, *131*, 2330.
- [54] L. Wu, H. Yan, G. Li, X. Xu, L. Zhu, X. Chen, J. Wang, *Food Anal. Methods* **2019**, *12*, 1648.
- [55] S. Sadhasivam, O. Barda, V. Zakin, R. Reifen, E. Sionov, *Molecules* **2021**, *26*, 4545.
- [56] E. Fliszár-Nyúl, B. Lemli, S. Kunsági-Máté, L. Dellafora, C. Dall'Asta, G. Cruciani, G. Pethő, M. Poór, *Int. J. Mol. Sci.* **2019**, *20*, 2352.
- [57] T.-T. Pan, D.-W. Sun, H. Pu, Q. Wei, *J. Agric. Food Chem.* **2018**, *66*, 2180.
- [58] S. D. Harvey, M. E. Vucelick, R. N. Lee, B. W. Wright, *Forensic Sci. Int.* **2002**, *125*, 12.
- [59] Commission Regulation (EC) No. 1881/2006, *Setting Maximum Levels for Certain Contaminants in Foodstuffs*, European Union, Brussels, Belgium **2006**.
- [60] Commission Directive 2003/100/EC, *Amending Annex I to Directive 2002/32/EC of the European Parliament and of the Council on Undesirable Substances in Animal Feed*, European Union, Brussels, Belgium **2003**.
- [61] J. Langer, D. Jimenez de Aberasturi, J. Aizpuru, R. A. Alvarez-Puebla, B. Auguie, J. J. Baumberg, G. C. Bazan, S. E. J. Bell, A. Boisen, A. G. Brolo, J. Choo, D. Cialla-May, V. Deckert, L. Fabris, K. Faulds, F. J. Garcia de Abajo, R. Goodacre, D. Graham, A. J. Haes, C. L. Haynes, C. Huck, T. Itoh, M. Käll, J. Kneipp, N. A. Kotov, H. Kuang, E. C. Le Ru, H. K. Lee, J.-F. Li, X. Y. Ling, et al., *ACS Nano* **2020**, *14*, 28.
- [62] H. Wei, S. M. Hossein Abtahi, P. J. Vikesland, *Environ. Sci.: Nano* **2015**, *2*, 120.
- [63] P. Pal, A. Bonyár, M. Veres, L. Himics, L. Balázs, L. Juhász, I. Csarnovics, *Sens. Actuators, A* **2020**, *314*, 112225.
- [64] C. Ziegler, A. Eychmüller, *J. Phys. Chem. C* **2011**, *115*, 4502.
- [65] J.-E. Park, Y. Lee, J.-M. Nam, *Nano Lett.* **2018**, *18*, 6475.
- [66] Q. Li, X. Zhuo, S. Li, Q. Ruan, Q.-H. Xu, J. Wang, *Adv. Opt. Mater.* **2015**, *3*, 801.
- [67] C. Kuttner, M. Mayer, M. Dulle, A. Moscoso, J. M. López-Romero, S. Förster, A. Fery, J. Pérez-Juste, R. Contreras-Cáceres, *ACS Appl. Mater. Interfaces* **2018**, *10*, 11152.
- [68] J. R. G. Navarro, D. Manchon, F. Lerouge, N. P. Blanchard, S. Marotte, Y. Leverrier, J. Marvel, F. Chaput, G. Micouin, A.-M. Gabudean, A. Mosset, E. Cottancin, P. L. Baldeck, K. Kamada, S. Parola, *Nanotechnology* **2012**, *23*, 465602.
- [69] B. Peng, G. Li, D. Li, S. Dodson, Q. Zhang, J. Zhang, Y. H. Lee, H. V. Demir, X. Y. Ling, Q. Xiong, *ACS Nano* **2013**, *7*, 5993.
- [70] L.-L. Qu, Q. Jia, C. Liu, W. Wang, L. Duan, G. Yang, C.-Q. Han, H. Li, *J. Chromatogr. A* **2018**, *1579*, 115.
- [71] S.-H. Liu, B.-Y. Wen, J.-S. Lin, Z.-W. Yang, S.-Y. Luo, J.-F. Li, *Appl. Spectrosc.* **2020**, *74*, 1365.
- [72] K.-M. Lee, T. J. Herrman, Y. Bisrat, S. C. Murray, *J. Agric. Food Chem.* **2014**, *62*, 4466.
- [73] L. M. Rojas, Y. Qu, L. He, *Talanta* **2021**, *224*, 121792.
- [74] N. Logan, J. Lou-Franco, C. Elliotta, C. Cao, *Environ. Sci.: Nano* **2021**, *8*, 2718.
- [75] W. A. Tegegne, M. L. Mekonnen, A. B. Beyene, W.-N. Su, B.-J. Hwang, *Spectrochim. Acta, Part A* **2020**, *229*, 117940.
- [76] Y. Kang, H.-X. Gu, X. Zhang, *Anal. Methods* **2019**, *11*, 5142.
- [77] Y. Hernández, L. K. Lagos, B. C. Galarreta, *Sens. Bio-sens. Res.* **2020**, *28*, 100331.
- [78] A. Li, L. Tang, D. Song, S. Song, W. Ma, L. Xu, H. Kuang, X. Wu, L. Liu, X. Chen, C. Xu, *Nanoscale* **2016**, *8*, 1873.
- [79] A. Foti, C. D'Andrea, V. Villari, N. Micali, M. Donato, B. Fazio, O. Maragò, R. Gillibert, M. Lamy de la Chapelle, P. Gucciardi, *Materials* **2018**, *11*, 440.
- [80] D. He, Z. Wu, B. Cui, E. Xu, *Microchim. Acta* **2020**, *187*, 215.
- [81] X. Ma, B. Shao, Z. Wang, *Anal. Chim. Acta* **2021**, *1188*, 339189.
- [82] Y. Zhao, Y. Yang, Y. Luo, X. Yang, M. Li, Q. Song, *ACS Appl. Mater. Interfaces* **2015**, *7*, 21780.
- [83] J. Ko, C. Lee, J. Choo, *J. Hazard. Mater.* **2015**, *285*, 11.
- [84] C. Song, B. Yang, Y. Yang, L. Wang, *Sci. China: Chem.* **2016**, *59*, 16.
- [85] E. Hahn, Y.-H. Kim, X.-H. Pham, B.-H. Jun, *Sensors* **2020**, *20*, 3523.
- [86] R. Chen, S. Li, Y. Sun, B. Huo, Y. Xia, Y. Qin, S. Li, B. Shi, D. He, J. Liang, Z. Gao, *Microchim. Acta* **2021**, *188*, 281.
- [87] Q. Chen, M. Yang, X. Yang, H. Li, Z. Guo, M. H. Rahma, *Spectrochim. Acta, Part A* **2018**, *189*, 147.
- [88] D. Song, R. Yang, S. Fang, Y. Liu, F. Long, A. Zhu, *Microchim. Acta* **2018**, *185*, 491.
- [89] B. Shao, X. Ma, S. Zhao, Y. Lv, X. Hun, H. Wang, Z. Wang, *Anal. Chim. Acta* **2018**, *1033*, 165.
- [90] H. He, D.-W. Sun, H. Pu, L. Huang, *Food Chem.* **2020**, *324*, 126832.
- [91] A. Shiohara, Y. Wang, L. M. Liz-Marzán, *J. Photochem. Photobiol., C* **2014**, *21*, 2.
- [92] Z. Xiaoyan, L. Ruiyi, W. Xiaofei, L. Zaijun, *Anal. Methods* **2014**, *6*, 2862.
- [93] V. M. Szlag, S. Jung, R. S. Rodriguez, M. Bourgeois, S. Bryson, G. C. Schatz, T. M. Reineke, C. L. Haynes, *Anal. Chem.* **2018**, *90*, 13409.
- [94] V. M. Szlag, R. S. Rodriguez, S. Jung, M. R. Bourgeois, S. Bryson, A. Purchel, G. C. Schatz, C. L. Haynes, T. M. Reineke, *Mol. Syst. Des. Eng.* **2019**, *4*, 1019.

- [95] F. Y. H. Kutsanedzie, A. A. Agyekum, V. Annavaram, Q. Chen, *Food Chem.* **2020**, *315*, 126231.
- [96] Q. Li, Z. Lu, X. Tan, X. Xiao, P. Wang, L. Wu, K. Shao, W. Yin, H. Han, *Biosens. Bioelectron.* **2017**, *97*, 59.
- [97] Y. Li, Q. Chen, X. Xu, Y. Jin, Y. Wang, L. Zhang, W. Yang, L. He, X. Feng, Y. Chen, *Sens. Actuators, B* **2018**, *266*, 115.
- [98] X. Yan, W. Zhu, Y. Wang, Y. Wang, D. Kong, M. Li, *Chemosensors* **2023**, *11*, 22.
- [99] H. Wang, M. Liu, Y. Zhang, H. Zhao, W. Lu, T. Lin, P. Zhang, D. Zheng, *Molecules* **2022**, *27*, 5280.
- [100] W. Zhang, S. Tang, Y. Jin, C. Yang, L. He, J. Wang, Y. Chen, *J. Hazard. Mater.* **2020**, *393*, 122348.
- [101] C. W. Fang, C. Wei, M. Xu, Y. Yuan, R. Gua, J. Yao, *RSC Adv.* **2016**, *6*, 61325.
- [102] M. Yang, G. Liu, H. M. Mehedi, Q. Ouyang, Q. Chen, *Anal. Chim. Acta* **2017**, *986*, 122.
- [103] J. Sun, W. Li, X. Zhu, S. Jiao, Y. Chang, S. Wang, S. Dai, R. Xu, M. Dou, Q. Li, J. Li, *J. Agric. Food Chem.* **2021**, *69*, 11494.
- [104] R. Chen, H. Wang, C. Sun, Y. Zhao, Y. He, M. S. Nisar, W. Wei, H. Kang, X. Xie, C. Du, Q. Luo, L. Yang, X. Tang, B. Xiong, *Talanta* **2023**, *258*, 124401.
- [105] H. He, D.-W. Sun, H. Pu, Z. Wu, *Talanta* **2023**, *253*, 123962.
- [106] Q. Chen, T. Jiao, M. Yang, H. Li, W. Ahmad, M. M. Hassan, Z. Guo, S. Ali, *Spectrochim. Acta, Part A* **2020**, *239*, 118411.
- [107] E.-O. Ganbold, C. M. Lee, E.-M. Cho, S. J. Son, S. Kim, S.-W. Joo, S. I. Yang, *Anal. Methods* **2014**, *6*, 3573.
- [108] X. Jing, L. Chang, L. Shi, X. Liu, Y. Zhao, W. Zhang, *ACS Appl. Bio Mater.* **2020**, *3*, 2385.
- [109] D. Huang, J. Chen, L. Ding, L. Guo, P. Kannan, F. Luo, B. Qiu, Z. Lin, *Anal. Chim. Acta* **2020**, *1110*, 56.
- [110] Y. Ding, H. Shang, X. Wang, L. Chen, *Analyst* **2020**, *145*, 6079.
- [111] R. S. Rodriguez, V. M. Szlag, T. M. Reineke, C. L. Haynes, *Mater. Adv.* **2020**, *1*, 3256.
- [112] M. Li, H. Wang, X. Yu, X. Jia, C. Zhu, J. Liu, F. Zhang, Z. Chen, M. Yan, Q. Yang, *Analyst* **2022**, *147*, 2215.
- [113] Z. Wu, D. He, B. Cui, Z. Jin, E. Xu, C. Yuan, P. Liu, Y. Fang, Q. Chai, *Microchim. Acta* **2020**, *187*, 495.
- [114] X.-B. Huang, S.-H. Wu, H.-C. Hu, J.-J. Sun, *ACS Sens.* **2020**, *5*, 2636.
- [115] S. S. Jiao, X. Hu, H. Li, J. Yang, X. Wen, S. Wang, M. Pan, *Sens. Actuators, B* **2022**, *355*, 131245.
- [116] J. Yuan, C. Sun, X. Guo, T. Yang, H. Wang, S. Fu, C. Li, H. Yang, *Food Chem.* **2017**, *221*, 797.
- [117] J. Liu, Y. Hu, G. Zhu, X. Zhou, L. Jia, T. Zhang, *J. Agric. Food Chem.* **2014**, *62*, 8325.
- [118] R. Chen, Y. Sun, B. Huo, Z. Mao, X. Wang, S. Li, R. Lu, S. Li, J. Liang, Z. Gao, *Anal. Chim. Acta* **2021**, *1180*, 338888.
- [119] Z. Guo, P. Chen, M. Wang, M. Zuo, H. R. El-Seedi, Q. Chen, J. Shi, X. Zou, *LWT* **2021**, *152*, 112333.
- [120] R. Sharma, K. V. Ragavan, M. S. Thakur, K. S. M. S. Raghavarao, *Biosens. Bioelectron.* **2015**, *74*, 612.
- [121] R. Stiufuluc, C. Iacovita, C. M. Lucaci, G. Stiufuluc, A. G. Dutu, C. Braescu, N. Leopold, *Nanoscale Res. Lett.* **2013**, *8*, 47.
- [122] K.-T. Yong, Y. Sahoo, M. T. Swihart, P. N. Prasad, *Colloids Surf. A* **2006**, *290*, 89.
- [123] H.-M. Kim, S. Jeong, E. Hahm, J. Kim, M. G. Cha, K.-M. Kim, H. Kang, S. Kyeong, X.-H. Pham, Y.-S. Lee, D. H. Jeong, B.-H. Jun, *J. Ind. Eng. Chem.* **2016**, *33*, 22.
- [124] J.-H. Kim, J.-S. Kim, H. Choi, S.-M. Lee, B.-H. Jun, K.-N. Yu, E. Kuk, Y.-K. Kim, D. H. Jeong, M.-H. Cho, Y.-S. Lee, *Anal. Chem.* **2006**, *78*, 6967.
- [125] A. I. Pérez-Jiménez, D. Lyu, Z. Lu, G. Liu, B. Ren, *Chem. Sci.* **2020**, *11*, 4563.
- [126] X.-H. Pham, M. Lee, S. Shim, S. Jeong, H.-M. Kim, E. Hahm, S. H. Lee, Y.-S. Lee, D. H. Jeong, B.-H. Jun, *RSC Adv.* **2017**, *7*, 7015.
- [127] Q. Tong, W. Wang, Y. Fan, L. Dong, *TrAC, Trends Anal. Chem.* **2018**, *106*, 246.
- [128] D. Song, R. Yang, F. Long, A. Zhu, *J. Environ. Sci.* **2019**, *80*, 14.
- [129] T. J. Merkel, K. P. Herlihy, J. Nunes, R. M. Orgel, J. P. Rolland, J. M. DeSimone, *Langmuir* **2010**, *26*, 13086.
- [130] S. A. Nafiu, A. M. Ajeebi, H. S. Alghamdi, A. Aziz, M. N. Shaikh, *Asian J. Org. Chem.* **2023**, *12*, 202300051.
- [131] R. Bukasov, A. Sultangazyev, Z. Kunushpayeva, A. Rapikov, D. Dossym, *Int. J. Mol. Sci.* **2023**, *24*, 5578.
- [132] C. Wang, B. Liu, X. Dou, *Sens. Actuators, B* **2016**, *231*, 357.
- [133] M. S. Schmidt, J. Hübner, A. Boisen, *Adv. Mater.* **2012**, *24*, OP11.
- [134] P. Chen, C. Li, X. Ma, Z. Wang, Y. Zhang, *Food Control* **2022**, *134*, 108748.
- [135] N. M. Santhosh, V. Shvalya, M. Modic, N. Hojnik, J. Zavašnik, J. Olenik, M. Košiček, G. Filipič, I. Abdulhalim, U. Cvelbar, *Small* **2021**, *17*, 2103677.
- [136] B. Lin, P. Kannan, B. Qiu, Z. Lin, L. Guo, *Food Chem.* **2020**, *307*, 125528.
- [137] X. Wang, S.-G. Park, J. Ko, X. Xiao, V. Giannini, S. A. Maier, D.-H. Kim, J. Choo, *Small* **2018**, *14*, 1801623.
- [138] Y. Feng, L. He, L. Wang, R. Mo, C. Zhou, P. Hong, C. Li, *Nanomaterials* **2020**, *10*, 1000.
- [139] T. Meng, M. Shi, Y. Guo, H. Wang, N. Fu, Z. Liu, B. Huang, C. Lei, X. Su, B. Peng, Z. Deng, *Sens. Actuators, B* **2022**, *354*, 131097.
- [140] S. Zheng, C. Wang, J. Li, W. Wang, Q. Yu, C. Wang, S. Wang, *Chem. Eng. J.* **2022**, *448*, 137760.
- [141] Z. H. Wu, D.-W. Sun, H. P. Q. Wei, X. Lin, *Food Chem.* **2022**, *372*, 131293.
- [142] Z. Wu, D.-W. Sun, H. Pu, Q. Wei, *Talanta* **2023**, *253*, 124027.
- [143] F. Zhang, W. Ke, L. Shi, H. Liu, Y. Zhao, *Anal. Chem.* **2019**, *91*, 11812.
- [144] R. Gillibert, M. N. Triba, M. Lamy De La Chapelle, *Analyst* **2018**, *143*, 339.
- [145] S. Rostami, K. Zór, D. S. Zhai, M. Viehrig, L. Morelli, A. Mehdi, J. Smedsgaard, T. Rindzevicius, A. Boisen, *Food Control* **2020**, *113*, 107183.
- [146] Q. Liu, K. Vanmol, S. Lycke, J. V. Erps, P. Vandenabeele, H. Thienpont, H. Ottevaere, *RSC Adv.* **2020**, *10*, 14274.
- [147] O. Guselnikova, P. Postnikov, R. Elashnikov, E. Miliutina, V. Svorcik, O. Lyutakov, *Anal. Chim. Acta* **2019**, *1068*, 70.
- [148] Y. Zhu, L. Wu, H. Yan, Z. Lu, W. Yin, H. Han, *Anal. Chim. Acta* **2020**, *1107*, 111.
- [149] A. A. Tseng, Kuan Chen, C. D. Chen, K. J. Ma, *IEEE Trans. Electron. Packag. Manuf.* **2003**, *26*, 141.
- [150] B. C. Galarreta, E. Harté, N. Marquestaut, P. R. Norton, F. Lagugné-Labarthe, *Phys. Chem. Chem. Phys.* **2010**, *12*, 6810.
- [151] Y. Kalachyova, D. Mares, O. Lyutakov, M. Kostejn, L. Lapcak, V. Švorčík, *J. Phys. Chem. C* **2015**, *119*, 9506.
- [152] O. Guselnikova, P. Postnikov, Y. Kalachyova, Z. Kolska, M. Libansky, J. Zima, V. Svorcik, O. Lyutakov, *ChemNanoMat* **2017**, *3*, 135.
- [153] Z. Huang, G. C.-P. Tsui, Y. Deng, C.-Y. Tang, *Nanotechnol. Rev.* **2020**, *9*, 1118.
- [154] M. A. Abaddi, L. Sasso, M. Dimaki, W. E. Svendsen, *Microelectron. Eng.* **2012**, *98*, 378.
- [155] A. Jaiswal, C. K. Rastogi, S. Rani, G. P. Singh, S. Saxena, S. Shukla, *iScience* **2023**, *26*, 106374.
- [156] H. Kwon, S. H. Lee, J. K. Kim, *Nanoscale Res. Lett.* **2015**, *10*, 369.
- [157] K. Totsu, K. Fujishiro, S. Tanaka, M. Esashi, *Sens. Actuators A Phys.* **2006**, *130–131*, 387.
- [158] Z. Huang, G. Meng, Q. Huang, Y. Yang, C. Zhu, C. Tang, *Adv. Mater.* **2010**, *22*, 4136.
- [159] K. Wu, T. Rindzevicius, M. S. Schmidt, K. B. Mogensen, A. Hakonen, A. Boisen, *J. Phys. Chem. C* **2015**, *119*, 2053.
- [160] N. Santhosh, G. Filipic, E. Tatarova, O. Baranov, H. Kondo, M. Sekine, M. Hori, K. Ostrikov, U. Cvelbar, *Micromachines* **2018**, *9*, 565.

- [161] W. Lee, R. Ji, U. Gösele, K. Nielsch, *Nat. Mater.* **2006**, *5*, 741.
- [162] A. Jiříčková, O. Jankovský, Z. Sofer, D. Sedmidubský, *Materials* **2022**, *15*, 920.
- [163] X. Chen, Z. Qu, Z. Liu, G. Ren, *ACS Omega* **2022**, *7*, 23503.
- [164] R. Chowdhury, D., C. Singh, A. Paul, *RSC Adv.* **2014**, *4*, 15138.
- [165] D. C. Marcano, D. V. Kosynkin, J. M. Berlin, A. Sinitskii, Z. Sun, A. Slesarev, L. B. Alemany, W. Lu, J. M. Tour, *ACS Nano* **2010**, *4*, 4806.
- [166] E. M. Deemer, P. K. Paul, F. S. Manciu, C. E. Botez, D. R. Hodges, Z. Landis, T. Akter, E. Castro, R. R. Chianelli, *Mater. Sci. Eng., B* **2017**, *224*, 150.
- [167] D. Chen, H. Feng, J. Li, *Chem. Rev.* **2012**, *112*, 6027.
- [168] N. K. Chaudhari, H. Jin, B. Kim, D. San Baek, S. H. Joo, K. Lee, *J. Mater. Chem. A* **2017**, *5*, 24564.
- [169] M. Naguib, M. Kurtoglu, V. Presser, J. Lu, J. Niu, M. Heon, L. Hultman, Y. Gogotsi, M. W. Barsoum, *Adv. Mater.* **2011**, *23*, 4248.
- [170] R. M. Ronchi, J. T. Arantes, S. F. Santos, *Ceram. Int.* **2019**, *45*, 18167.
- [171] Y. Gogotsi, B. Anasori, *ACS Nano* **2019**, *13*, 8491.
- [172] V. Thiviyanathan, D. G. Gorenstein, *Proteomics: Clin. Appl.* **2012**, *6*, 563.
- [173] M. Li, S. K. Cushing, N. Wu, *Analyst* **2015**, *140*, 386.
- [174] C. Kolm, I. Cervenka, U. J. Aschl, N. Baumann, S. Jakwerth, R. Krška, R. L. Mach, R. Sommer, M. C. DeRosa, A. K. T. Kirschner, A. H. Farnleitner, G. H. Reischer, *Sci. Rep.* **2020**, *10*, 20917.
- [175] Y. Wang, X. Bai, W. Wen, X. Zhang, S. Wang, *ACS Appl. Mater. Interfaces* **2015**, *7*, 18872.
- [176] Y. Huang, S. Zhao, Z.-F. Chen, M. Shi, J. Chen, H. Liang, *Chem. Commun.* **2012**, *48*, 11877.
- [177] S. Lara, A. Perez-Potti, *Biosensors* **2018**, *8*, 104.
- [178] A. Bossi, F. Bonini, A. P. F. Turner, S. A. Piletsky, *Biosens. Bioelectron.* **2007**, *22*, 1131.
- [179] F. Ahmad, M. M. Salem-Bekhit, F. Khan, S. Alshehri, A. Khan, M. M. Ghoneim, H.-F. Wu, E. I. Taha, I. Elbagory, *Nanomaterials* **2022**, *12*, 1333.
- [180] D. P. dos Santos, M. M. Sena, M. R. Almeida, I. O. Mazali, A. C. Olivieri, J. E. L. Villa, *Anal. Bioanal. Chem.* **2023**, *415*, 3945.
- [181] K. H. Esbensen, P. Geladi, *J. Chemom.* **2010**, *24*, 168.
- [182] Y. Sun, H. Tang, X. Zou, G. Meng, N. Wu, *Curr. Opin. Food Sci.* **2022**, *47*, 100910.
- [183] Y. Xu, P. Zhong, A. Jiang, X. Shen, X. Li, Z. Xu, Y. Shen, Y. Sun, H. Lei, *TrAC, Trends Anal. Chem.* **2020**, *131*, 116017.
- [184] P. Galvin-King, S. A. Haughey, C. T. Elliott, *Food Control* **2018**, *88*, 85.
- [185] N. M. Ralbovsky, I. K. Lednev, *Spectrochim. Acta, Part A* **2019**, *219*, 463.
- [186] R. González-Domínguez, A. Sayago, Á. Fernández-Recamales, *Foods* **2022**, *11*, 3940.
- [187] C. Muehlethaler, G. Massonnet, P. Esseiva, *Forensic Sci. Int.* **2011**, *209*, 173.
- [188] L. A. Berrueta, R. M. Alonso-Salces, K. Héberger, *J. Chromatogr. A* **2007**, *1158*, 196.
- [189] P. Yu, M. Y. Low, W. Zhou, *Trends Food Sci. Technol.* **2018**, *71*, 202.
- [190] M. Muniz-Miranda, F. Muniz-Miranda, M. C. Menziani, A. Pedone, *Molecules* **2023**, *28*, 573.
- [191] B. Pacholczyk-Sienicka, G. Ciepiewski, Ł. Albrecht, *Molecules* **2021**, *26*, 382.
- [192] S. K. Vashist, J. H. T. Luong, *Bioanalytical Requirements and Regulatory Guidelines for Immunoassays* in Handbook of Immunoassay Technologies (Eds: S. K. Vashist, J. H. T. Luong), Academic Press, Cambridge, Massachusetts, USA **2018**, pp. 81–95.
- [193] W. Zhao, M. A. Brook, Y. Li, *ChemBioChem* **2008**, *9*, 2363.
- [194] J. Vessman, R. I. Stefan, J. F. Van Staden, K. Danzer, W. Lindner, D. T. Burns, A. Fajgelj, H. Müller, *Pure Appl. Chem.* **2001**, *73*, 1391.



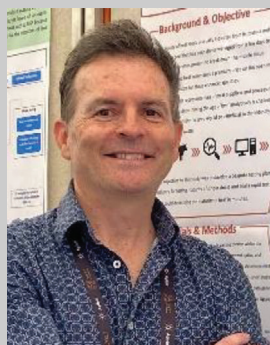
Natasha Logan is a research fellow at the Institute for Global Food Security, Queen's University Belfast. She holds a B.Sc. in food quality, safety and nutrition, an M.Phil. in food safety and biotechnology, and a Ph.D. in applied nanotechnology. During her Ph.D. she focused on developing novel colorimetric and SERS technologies to detect mercury contamination in environmental samples. Her current research interests are in the synthesis and fabrication of nanomaterials, development of SERS technologies for the detection of chemical contaminants in food and feed, and exploiting chemometrics and machine learning for agri-food applications.



Cuong Cao holds a reader position and leads the Advanced Micro- and Nanotechnology Lab (AMINO) at the Institute for Global Food Security (IGFS), School of Biological Sciences (SBS), Queen's University of Belfast (QUB). He has over 15 years of research experience in the synthesis, fabrication, and characterization of plasmonic and catalytic nanostructures, advanced biosensing platforms, and integrated point-of-care analysis to address issues in infectious diseases, food safety, and environmental pollution.



Stephan Freitag is a senior scientist at the University of Natural Resources and Life Sciences, Vienna. He holds an M.Sc. in biotechnology from the University of Applied Sciences in Tulln and a Ph.D. in technical chemistry from the Technical University of Vienna. During his Ph.D. he focused on the development of novel mid-infrared sensing schemes. His current research includes the development of rapid and green methods for mycotoxin screening using mid and near-infrared spectroscopy as well as chemometrics.



Simon A. Haughey is a senior research fellow in Agri-Food Contaminants within IGFS and manager of the ASSET Technology Centre. He has a B.Sc. (Hons) in Pure and Applied Chemistry and a Ph.D. in Organic Chemistry. He is currently the project leader for research into the development of spectroscopic “fingerprinting” techniques, e.g., Raman spectroscopy, FT-IR, NIRS, and HSI, coupled with chemometrics, to detect fraud/adulteration for food and feed commodities. He is a Chartered Chemist (CCChem), and Fellow of the Royal Society of Chemistry (FRSC).



Rudolf Krska is a professor of analytical chemistry and head of the Institute of Bioanalytics and Agro-Metabolomics at the University of Natural Resources and Life Sciences, Vienna. He also leads the strategic research of Austrian's Competence Centre for Food and Feed Safety and he holds a position as jointly appointed professor at Queen's University Belfast. Moreover, he is the president of the Austrian Society of Analytical Chemistry and Honorary Member of the Royal Irish Academy. Krska is one of the most prestigious researchers in the area of mycotoxins and food safety.



Christopher T. Elliott Ph.D., FRSC, FRSB, MRIA, OBE, is a Professor of Food Safety and a founder of the Institute for Global Food Security at Queen's University Belfast. He was appointed the ASEAN Professor for Global Food Security in 2022 and is based at Thammasat University in Thailand. Chris has led numerous research projects worldwide in relation to the detection and control of agricultural, food and environmental contaminants.